UNIVERSIDAD POLITÉCNICA DE MADRID

ESCUELA TÉCNICA SUPERIOR DE

INGENIEROS DE CAMINOS, CANALES Y PUERTOS

Highly Sensitive Smart Sensor for Early Fire Warning Detection

DOCTORAL THESIS

Submitted for the degree of Doctor by:

Xiaolu Li

Ingeniero de Materiales

Madrid, 2023

UNIVERSIDAD POLITÉCNICA DE MADRID
Escuela Técnica Superior De Ingenieros de Caminos, Canales y Puertos

Doctoral Degree in Engineering of Structures, Foundations and Materials

Highly Sensitive Smart Sensor for Early Fire Warning Detection

DOCTORAL THESIS

Submitted for the degree of Doctor by:

Xiaolu Li
Ingeniero de Materiales

Under the supervision of:
Dr. De-Yi Wang

Madrid, 2023

Title: Highly Sensitive Smart Sensor for Early Fire Warning Detection

Author: Xiaolu Li

Doctoral Programme: Doctoral Degree in Engineering of Structures, Foundations and Materials

Thesis Supervision:

Dr. De-Yi Wang, Senior Researcher/Research Program Leader, Supervisor

External Reviewers:

Thesis Defense Committee:

Thesis Defense Date:

ACKNOWLEDGEMENTS

As I started to write this section, I could not believe that the four-year doctoral study would come to an end. Looking back at the past four years, precious memories flash before my eyes like a movie. Even if the four years cover the entire pandemic environment, life here is still colorful, fulfilling, and incredible.

First, I would like to sincerely thank my supervisor Dr. De-Yi Wang, who offered me an opportunity to start my doctoral study in Spain. He provides me with professional guidance on academic research and kindly encourages me in my study and daily life during the whole study. He always has a rigorous attitude, comprehensive consideration, clear logic, and realistic working, which sets me an excellent example. I remember all his guidance and advice, including the experiments, presentation, life, etc., which will benefit me all my life. More importantly, these four-year studies cover the pandemic, from the initial outbreak to the gradual return to everyday life. He offers me a lot of psychological counseling that enables me to live and study more positively and optimistically.

I would like to show a special thanks to Dr. Xiuqin Zhang, who always supports me with encouragement, care, and consolation that helps me to go thought a hard time.

Our HPPN group is a lovely and cheerful research group; everyone is like a family member to me. I am incredibly grateful to each member of the HPPN group who helpfully provided me with assistance and companionship throughout my study at IMDEA Materials Institute. I appreciate Dr. José Sánchez del Río Sáez, who helped me a lot on the experimental design. So that I can carry out my doctoral project smoothly. In addition, my faithful gratitude goes to Dr. Jing Zhang, Dr. Lu Zhang, Dr. Yanyan Duan, Dr. Rongkun Jian, Dr. Zhuban Shao, Dr. Xiaosui Chen, Dr. Chengshou Zhao, Dr. Antonio Vázquez-López, Dr. Pedro Luis de Hoyos Martínez, Dr. Raquel Sánchez Díaz, Dr. Guang-Zhong Yin, Dr. Abdulmalik Yusuf, Dr. Can Fu, Ms. Jimena de la Vega, Ms. Wen An, Mr. Xiang Ao, Mr. Junchen Xiao, Ms. Mingyang Zhang, Ms. Meihui Zhou, Ms. Xiaoli Xu, Ms. Jie Xu, Ms. Qi Chen, Mr. Jose Hobson, Mr. Juan León Ramos, Ms. Burcu Özdemir, other group members for their kind help. Moreover, I sincerely thank the technician group in IMDEA for their strong support of characterization and testing. Most importantly, I sincerely thank the China Scholarship Council which provides financial support for all my Ph.D. studies.

Finally, thanks are given to my parents and younger brother for their profound love, unreasonable support, and endless tolerance, making me more motivated for my studies.

Appreciate and cherish every moment in my life!

Xiaolu Li

June, 2023

RESUMEN

Los peligros de incendio se manifiestan en pérdidas de bienes, víctimas, daños ecológicos, etc., que amenazan gravemente la supervivencia y el desarrollo de los seres humanos. Actualmente, se utilizan varias medidas para controlar los riesgos de incendio, estas mediciones se dividen en estrategias pasivas de control de incendios que incluyen la adición de retardantes de llama, y estrategias activas de control de incendios que contienen alerta temprana de incendios y gestión de extinción de incendios.

Los sensores de alerta temprana de incendios son una estrategia eficaz. Trabajan principalmente monitorizando y respondiendo a las principales características del proceso de combustión en sus primeras etapas, generando más tiempo disponible más tiempo disponible para tomar medidas oportunas antes de la propagación del fuego para lograr un manejo eficiente del fuego. Este enfoque de control de incendios presenta una ventaja destacada para mitigar los riesgos de incendio. Recientemente, se han avanzado en sensores de alerta temprana de incendios y su desarrollo aún está en curso. Con el objetivo de una mayor optimización, en esta tesis se fabrican diferentes sensores de advertencia de incendios para lograr una advertencia inteligente de incendios a baja temperatura, que muestra la sensibilidad, incluida la temperatura de respuesta, el tiempo de respuesta y la transmisión inteligente de mensajes detectados. Específicamente, estos desarrollos de sistemas de alerta de incendios están presentes en los sensores de alerta temprana de incendios basados en óxido de grafeno (GO) (Capítulo 3), en los sensores de alerta temprana de incendios basados en papel de celulosa (CP) (Capítulo 4), y explora más a fondo el sensor de alerta temprana de incendios de baja temperatura reutilizado en diversas condiciones de humedad (Capítulo 5).

En el capítulo 3, se propone un novedoso sensor de incendios termosensible basado en una película P/Si-GO mediante tecnología capa por capa. Este sensor de alerta temprana de incendios logra una respuesta ultrarrápida en 1 s a una temperatura baja de 250 °C o en un incendio real. Curiosamente, la cooperación de un sistema de comunicación inalámbrico inteligente hecho a medida permite que este sensor muestre mensajes de advertencia en múltiples pantallas de computadora locales y de largo alcance a distancias de hasta 20 km del área objetivo del incendio. Además, la solución funcional prediseñada funciona como un nano-revestimiento de advertencia de incendios envuelto en una espuma de poliuretano flexible, lo que indica la viabilidad del nano-

revestimiento de advertencia de incendios. Con respecto a la limitación de la reducción térmica de GO a baja temperatura, se espera que se introduzca un MXene conductor como puente para preparar otro sensor de advertencia de incendios basado en GO modificado con MXene. Este sensor implementa una alerta de baja temperatura a 250 ºC en 1 segundo y se combina con un pequeño dispositivo de conversión de señal inalámbrico de diseño propio para mejorar su inteligencia. Además, la transmisión de la señal de advertencia contiene el mensaje de advertencia en un monitor de computadora y un valor preciso de luminosidad del fuego en tiempo real en un monitor de computadora local y remoto a través del sensor de luminosidad asociado.

En el capítulo 4, se aplica el sustrato CP para preparar sensores de advertencia de incendios que son prometedores para la protección contra incendios en interiores. En detalle, se fabrica una novedosa alarma contra incendios utilizando CP retardante de llama cargado con GO y MXene. Debido al excelente efecto de conmutación de resistencia eléctrica dependiente de la temperatura del GO, el papel modificado actúa como un aislante eléctrico a temperatura ambiente y se vuelve conductor de electricidad a altas temperaturas. La introducción de MXene conductivo mejora la velocidad de detección de incendios, lo que genera una advertencia de incendio por baja temperatura de 2 s, que en primer lugar se calcula mediante una técnica novedosa y cuantificable. Además, el sensor de alarma contra incendios diseñado está acoplado a una interfaz de comunicación inalámbrica para transmitir convenientemente señales de incendio "PELIGRO DE FUEGO" a una pantalla de cristal líquido de forma remota. Para lograr el equilibrio entre flexibilidad y retardo de llama, un sistema de advertencia de incendios basado en CP funcional y flexible producido mediante una técnica simple de recubrimiento por inmersión proporciona flexibilidad, advertencia rápida de baja temperatura y una novedosa capacidad de conversión de señal inalámbrica local y remota. El sistema de alerta de incendios propuesto cumple con el requisito crítico de una alerta rápida de baja temperatura, presentando mensajes de advertencia en 2 s por debajo de 250 ºC y con buenas propiedades mecánicas. Además, los datos de luminosidad y temperatura recopilados se envían a ordenadores locales y remotos mediante conversión inalámbrica. Este papel de alarma contra incendios inteligente diseñado es prometedor como papel tapiz de advertencia de incendios para el interior de casas sin sacrificar la decoración.

En el capítulo 5, se propone un sensor basado en CS modificado con sales utilizando un método

de ensamblaje fácil que responde a temperaturas aún más bajas, especialmente aquellas causadas por electrodomésticos. Este sensor responde rápidamente a una temperatura baja de 50 °C y a una llama en 2 s. Además, este sensor se reutiliza para advertir de peligro 17 veces, lo que resulta en una mayor practicidad. Adicionalmente, este sensor tiene una respuesta sensible a la humedad relativa humedad relativa superior al 50 % a 50 °C y 75 °C debido a su sensibilidad a la humedad, lo que mejora la capacidad de este sensor de alerta temprana de incendios que funciona en diversas condiciones de humedad. La propiedad especial proporciona una aplicación potencial en ambientes hostiles.

ABSTRACT

Fire hazards are manifested in property loss, casualties, ecological damage, etc., which seriously threaten the survival and development of human beings. Various measurements are utilized to mitigate the caused harm. Briefly, these measurements are divided into passive fire-control strategies, including the addition of flame retardants, and active fire-control strategies containing early fire warning and fire-fight management.

Early fire-warning sensors are one efficient strategy. They mainly work by monitoring and response to the features of combustion behavior in the early stage, which earns more available time to take timely action before fire propagation to achieve efficient fire management. This fire-control approach presents a salient advantage in mitigating fire hazards. Early fire warning sensors have recently been advanced, and their development is still ongoing. Aiming for further optimization, different fire-warning sensors are fabricated in this thesis to achieve smart low-temperature fire warnings, showing sensitivity in response temperature, response time, and intelligent transmission of detected messages. Specifically, these developments of fire-waring sensors are present in the graphene oxide (GO) -based early fire-warning sensors (Chapter 3), cellulose paper (CP) -based early fire-warning sensors (Chapter 4), and further explores the reused low-temperature early fire-warning sensor under various humidity condition (Chapter 5).

In chapter 3, a novel early thermo-sensitive fire sensor based on P/Si-GO film by layer-by-layer technology is proposed. This early fire-warning sensor achieves an ultrafast response within 1 s at a low temperature of 250 °C or an actual fire. Intriguingly, the cooperation of an intelligent custom-made wireless communication system allows this sensor to show warning messages on multiple local and long-range computer screens at distances up to 20 km from the target fire area. Furthermore, the pre-designed functional solution works as fire-warning nano-coating wrapped into a flexible polyurethane foam, indicating the feasibility of fire-warning nano-coating. Concerning the limitation of thermal reduction of GO at low temperatures, conductive MXene expected as a bridge is introduced to prepare another MXene-modified GO-based fire-warning sensor. This sensor implements a low-temperature alert at 250 ºC within 1 s and is coupled with a small self-designed wireless signal conversion device to improve its intelligence. Moreover, the warning signal

transmission contains the warning message on a computer monitor and precise real-time fire luminosity value on a local and a remote computer monitor via the associated luminosity sensor.

In chapter 4, CP substrate is applied to prepare fire-warning sensors promising for indoor fireproofing. In detail, a novel fire alarm is fabricated by using flame-retardant CP loaded with GO and MXene. Owing to the excellent temperature-dependent electrical resistance switching effect of GO, the modified paper acts as an electrical insulator at room temperature and becomes electrically conductive at high temperatures. Introducing conductive MXene enhances the fire detection speed, leading to a low-temperature fire warning of 2 s, which is first calculated by a novel and quantifiable technique. Moreover, the designed fire alarm sensor is coupled to a wireless communication interface to conveniently transmit fire signals “FIRE DANGER” to a liquid crystal display screen remotely. For achieving the balance between flexibility and flame retardancy, one flexible functional CP-based fire-warning system produced via a simple dip-coating technique provides flexibility, rapid low-temperature warning, and a novel local and remote wireless signal conversion capability. The proposed fire-warning system meets the critical requirement of a fast low-temperature warning, presenting warning messages within 2 s under 250 ºC and mechanical properties. Moreover, the luminosity and temperature data collected is sent to local and remote computers by wireless conversion. These designed smart fire alarm papers are promising for fire-warning wallpaper for interior houses without sacrificing decoration.

In chapter 5, a salts-modified CS-based sensor is proposed using a facile assembling method responding to further lower temperatures, especially those caused by household electric appliances. This sensor responds quickly to a low temperature of 50 °C and a flame within 2 s. In addition, this sensor is reused to warn of danger 17 times, resulting in improved practicality. Furthermore, this sensor responds to relative humidity above 50 % at 50 °C and 75 °C sensitively due to its humid sensitivity, improving this early fire warning sensor's ability to work under various humidity conditions. The particular property provides a potential application in harsh environments, especially on rainy days. The comparison between different salts-modified CS films is carried out to elucidate the mechanism of the formation of electric current under the joint driven by temperature and humidity. Moreover, real-time temperature and relative humidity monitoring can be achieved with a wireless transmission section. This design shows a promising approach for multifunctional

CS-based sensors and paves a path to developing a new generation of smart fire-warning detectors.

Contents

ABBREVIATIONS

Polymers and compounds	
GO	Graphene oxide
RGO	Reduced graphene oxide
ETS	2-(Diphenylphosphino) ethyltriethoxysilane
DMF	N, N-dimethylformamide solution
PU	Polyurethane foam
FPU	Flexible polyurethane foam
MAX	Ti_3AlC_2 powder
LiF	Lithium fluoride powder
HCl	Hydrochloric acid solution
PTS	Phenyltrimethoxysilane
PA	Phytic acid
MXene	Titanium carbide, Ti_3C_2
CP	Cellulose paper
MTM	Trimethoxymethylsilane
PEO	poly(ethylene oxide)
NaCl	Sodium chloride
CS	Chitosan
NH_4Cl	Ammonium chloride
$CaCl_2$	Calcium chloride
P	Phosphorus
Si	Silicon
Al	Aluminum
CO	Carbon monoxide

CO_2	Carbon dioxide
Characterization technique	
FTIR	Fourier transform infrared spectroscopy
XRD	X-ray diffraction spectroscopy
SEM	Scanning electron microscopy
TEM	Transmission electron microscopy
EDS	Energy dispersive X-Ray spectroscopy
MCC	Micro combustion calorimeter
DSC	Differential scanning calorimeter
TGA	Thermogravimetric analysis
DMA	Dynamic mechanical analysis
Raman	Raman spectroscopy
HRR	Heat release rate
pHRR	Peak heat release rate
LBL	Layer-by-layer assembly
IOT	Internet of Things
TTN	The Things of Network
TTS	The Things of Stack

LIST OF SCHEMES

LIST OF FIGURES

LIST OF TABLES

CHAPTER 1

Introduction

"There is no such thing as a great talent without great willpower."

- Honoré de Balzac

1.1 Background and motivation of the study

Fire, as a worldwide phenomenon, has achieved long-term development and contributed to developing human civilization [1]. Fires affect global ecosystem patterns, economic situations, and life of human beings [2-5]. However, everything has two sides. Once a fire breaks out of control, the caused hazards are immeasurable, involving life and property safety, ecology, environment, and other aspects. In recent years, huge fire hazards have happened, such as the Notre Dame Cathedral fire, the months of bushfires in Australia, and the California fires in the United States. These fire hazards give rise to massive losses, casualties, and ecological damage, pointing out the current imperfect capability to control fires even though the coexistence between humans and fire has been for a long time [1, 6, 7]. In addition, these fire hazards also give us a warning - improving the efficiency of fire management is still an ongoing challenge.

To improve the efficiency of fire-control strategies, a deeper understanding of the combustion behavior should be carried out. The combustion of materials is a complicated process accompanied by multiplex physical and chemical reactions [8, 9]. In general, the occurrence of fires requires three vital factors: heat source, oxygen, and fuel [8, 10]. Once materials are exposed to a heat resource, the thermal pyrolysis of materials happens in the air environment. It gradually evolves into violent combustion of fire propagation, causing severe fire hazards [8-11].

During the whole combustion processing, the temperature change is one typical character. Temperature can gradually rise with increased burning time, as shown in **Scheme 1-1**. According to the curve, the combustion process is divided into three stages: the ignition stage, the fire developing and developed stage, and the decay stage [12]. At each stage, fire-control strategies are employed. The current fire measurements are classified into three categories: early fire-warning systems [13-

15], adding flame retardants [16-20], and firefighting [21-24]. In detail, early fire-warning systems are mainly used to monitor and respond to abnormal behavior in the ignition stage, emphasizing that the warning happens before a severe fire outbreak [14]. In addition, flame retardancy can slow down fire propagation by decreasing combustion's heat and gas release. Furthermore, fire control management related to firefighting can be implemented due to the extremely fast fires spread into a fire-developing stage of the combustion process. However, specific fire damage is unavoidable at that combustion stage. In summary, the mentioned fire-control ways can mitigate fire hazards to varying degrees.

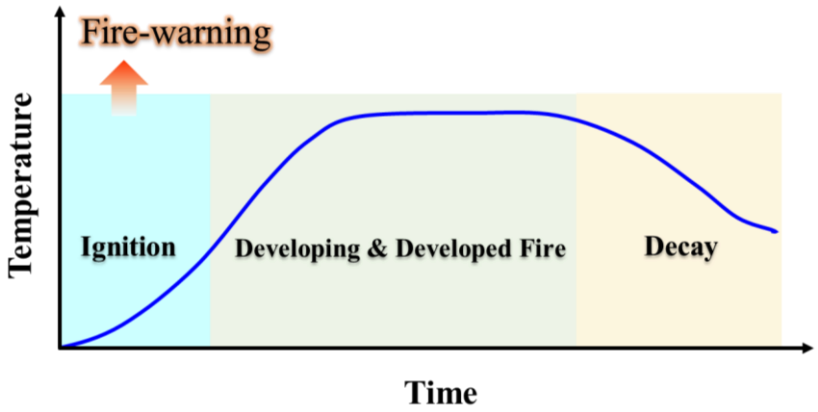

Scheme 1-1 Temperature change with burning time during combustion process.

Comparatively, if timely fire-control strategies are taken during the ignition stage of the combustion, the large-scale fire propagation could be suppressed. This strategy supports people to earn more evacuation time and reduce casualties and losses. In consideration of this advantage, the early fire alarm has become a research focus. After the development of recent years, much research about fire-warning systems has been reported. The according statistics are described in **Fig. 1-1** [14]. Most current fire alarms provide early warning to alert the public to the approaching fire hazards. However, there are still deficiencies in the direction of sensitivity and intelligence. Based on what is mentioned above, optimizing fire-warning systems is expected to develop a new generation of smart low-temperature fire-warning systems, which express response temperatures, response time, and signal transmission. Theoretically, the high-sensitivity property of early fire-warning systems requires them to respond to a low temperature and quickly transmit the detected signal to the public. Considering these motivations, different smart early fire-warning systems are elucidated in the following chapters.

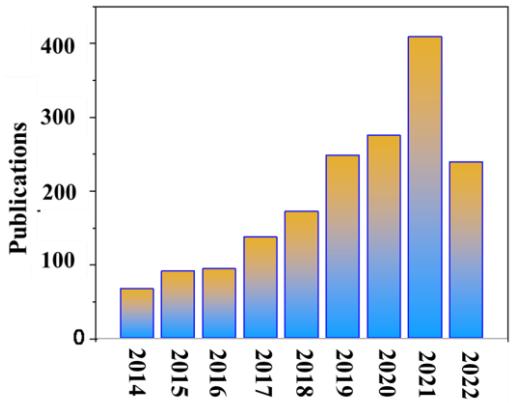

Fig. 1-1 The statistics of publication on early fire-warning systems in recent years.

1.2 Combustion behavior

As shown in **Fig. 1-2**, a brief schematic diagram is used to understand the combustion process, which can facilitate us to implement fire detection measures better. Combustion of materials is an intense and complex thermal oxidation reaction, accompanied by physical and chemical processes, characterized by blazing flames, glowing, severe smoke, heat, infrared or ultraviolet light radiation, or gases [11, 25]. When exposed to an external heat source, materials will undergo thermal degradation or pyrolysis, producing different kinds of volatiles of non-combustible gases, combustible gases, and liquid products. Then, combustible and liquid products are mixed with air, especially the oxygen in the air, which can further promote the flame developing to drive combustion behavior under the cooperation with high enough temperature [10, 11, 26].

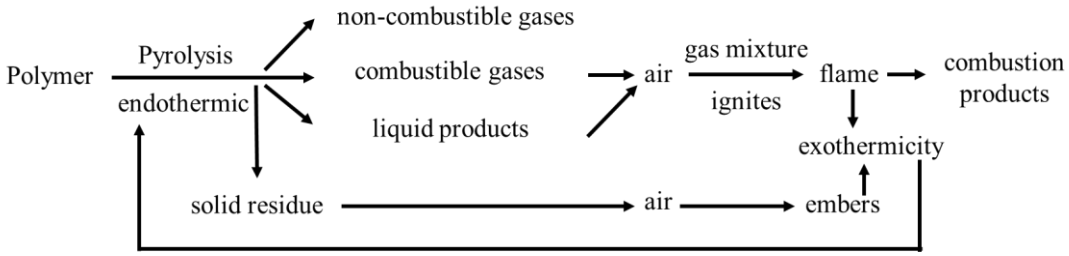

Fig. 1-2 Schematic illustration of the combustion process of polymer [27].

There are three foremost steps of heating, thermal decomposition or pyrolysis, and ignition to initiate the combustion behavior of material [11, 27]. Among them, pyrolysis is an endothermic process, which requires lots of energy for the dissociation energies of any bonds to be broken and other activation energies of the pyrolysis process [11]. For distinctive materials, the decomposition temperatures show differences within a specific range because of their structural distinctions. In

Table 1.1, the decomposition temperatures, flash ignition, and auto-ignition for some common materials are listed. According to this information, most materials start to degrade when the temperature reaches a temperature of more than 300 °C, which is strongly associated with the property of combustion of materials [27]. This provides an essential parameter for designing early fire-warning systems.

Table 1-1 Thermal decomposition and ignition temperatures determined by ASTM D 1929 for some common materials.

Materials	**Decomposition temperature/ºC**	**Flash ignition temperature/ºC**	**Auto-ignition temperature/ºC**
Poly(methyl methacrylate)	170 - 300	300	450
Cellulose / cotton	280 - 380	210	400
Low-density polyethylene	340 - 440	340	350
Polyoxymethylene	-	375	-
Nylon	-	420	-
Polypropylene	330 - 410	350 - 370	390 - 410
Polyvinyl chloride	200 - 300	390	455
Polycarbonate	-	520	380
Polystyrene	300 - 400	345 - 360	490

Once pyrolysis begins, more fuels are formed, producing a supply of flames. The pyrolysis rate increases, and flames spread across the polymer surface [11]. In general, the flame spread is related to the combustion heat of materials. As long as the critical heat flux, thermal response parameters, and gasification materials are sufficient for pyrolysis and forward movement of the flame, the flame spreads rapidly across the surface [27]. When the flame reaches the surface of the polymer, it will be easier to react with oxygen, resulting in a more intense combustion behavior.

Furthermore, the fire propagation is high-speed once combustion occurs, illustrated by the flame diffusion reactions in hydrocarbons, as shown in **Fig. 1-3**. The vital step in the process is the chain branching step propagated by the highly reactive hydrogen or hydroxyl radicals. This leads to a high velocity on the flame front, further causing rapid flame to spread. Furthermore, fire

propagation is highly dependent on the physical state of the burning materials. When the materials are thin, it is difficult to cool down the surface by transferring heat to the inside part of the materials. Thus, materials would be burned quickly without any non-melting and shrinkage. The extreme fire propagation again emphasizes the significance of highly efficient fire management.

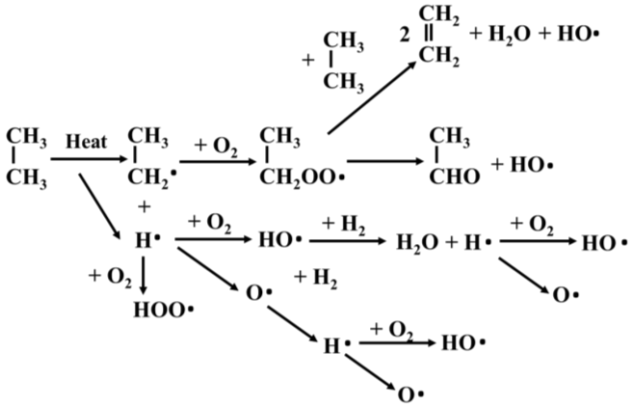

Fig. 1-3 Free radical generation during the combustion of ethane [28].

As previously stated, many characteristics are produced during the complicated burning process of materials. All these characteristics can be used to reflect the combustion behavior. By monitoring these characteristics, fire-detecting technology emerges as a highly effective strategy and has achieved long-term development. As described in **Fig. 1-4**, fire sensors emerged in the nineteenth century, and more diverse fire-detecting systems evolved over time. These sensors comprise typical smoke sensors, CO gas sensors, UV-IR gas sensors, infrared sensors, thermal infrared imaging, flame detectors, sound sensors, and thermos-sensitive sensors [29]. Briefly, the characteristics detected from combustion include heat, gas, flame, smoke, and others. Correspondingly, it is divided into two types: typical commercial fire early warning sensors (smoke alarms, gas sensors, flame sensors) and heat-sensitive sensors. Detailed descriptions will be given in the following chapters.

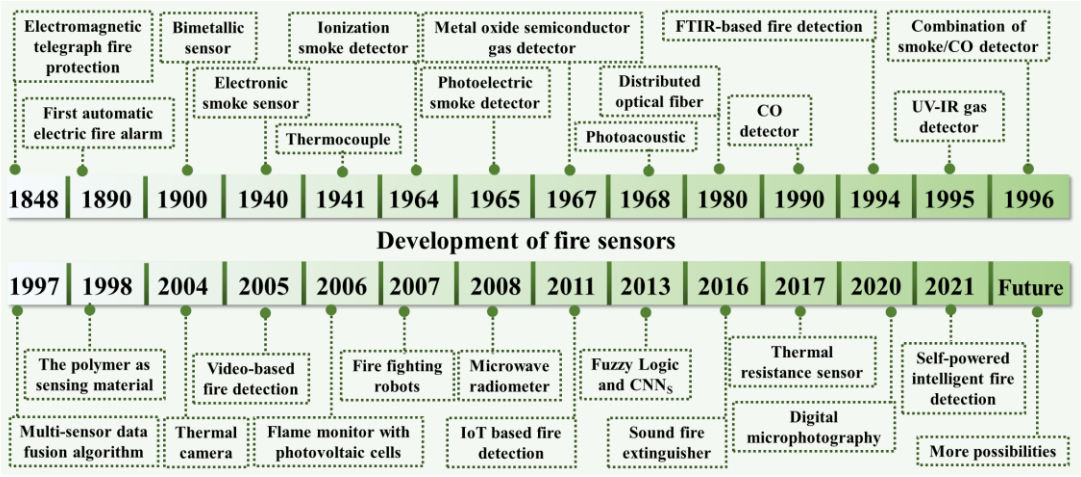

Fig. 1-4 A brief timeline for developing fire detectors [30].

1.3 Typical commercial fire-warning sensors

1.3.1 Smoke sensors

As early as the nineteenth century, smoke sensors emerged. In the subsequent development, smoke sensors have been continuously researched, manufactured, and advanced under the intelligence technology's drive, gradually developing towards commercialization. Smoke sensors are used in commercial applications and are essential in homes, offices, schools, hospitals, and industrial places [25, 31, 32]. Up to now, smoke sensors have become one of the most demanded products in the home security alarm market.

The smoke sensors mainly detect smoke emission, a typical feature in combustion processing, and respond to the potential fire situation. Rapid smoke detection does a favor in putting the fires effectively to escape successfully. When a light beam or electromagnetic radiation passes through the interface of particles, produced smoke can be detected. In general, the concentration, volume, and size of smoke are applied as parameters for smoke detection. The structure and composition of produced smoke generated by the collection of solid particles, liquid particles, and gas particles are distinct for different fire hazards. Smoke sensors must be able to respond to smoke and combustion, which contains non-visual technology and visual technology that will be clearly described below.

a). Non-Visual Smoke Detection

When the smoke accumulation reaches a certain amount, smoke detectors can carry out an alarm to show danger by monitoring the generated smoke during combustion. Based on the detection

principle and information collection type, common non-visual smoke sensors are classified into ionic smoke sensors, photoelectric smoke sensors, fame sensors, *etc*. Generally speaking, the customary smoke sensors are ionic and photoelectric, widely applied in various applications [33].

Ionic smoke sensors with stable and reliable operation, invented around 1900, are an advanced technology for efficient fire management [34]. They are installed in many places, such as factories, office buildings, hospitals, museums, and other places, to provide warning to mitigate fire hazards. Typically, ionic smoke sensors have an ion cavity and a radiation source. When smoke particles enter the ion cavity, the ionization current can change. This is attributed to the adsorption effect on the ions in the cavity. Subsequently, the ionization current is further analyzed to reflect the smoke concentration to judge whether the fires will occur. However, ionic smoke sensors have high requirements for environmental humidity, cleanliness, and maintenance, leading to limited usage to a certain degree.

Photoelectric smoke detectors generally consist of a photoelectric cavity and a receiver. Under normal circumstances, the receiver has no optical signal because of the unique angle between the tube and the receiver. When a fire happens, the generated smoke particles can enter the photoelectric cavity. The scattered light will then be formed, and the receiver can receive the light signal and convert it into a corresponding electrical signal. After processing the electrical signal, these results are compared with the set threshold to check whether a fire warning occurs.

Moreover, the detection principle of photoelectric smoke sensors is based on the scattering effect of infrared light. As depicted in **Scheme 1-2**, smoke sensors work primarily on the emission or scattering of infrared light. Photoelectric conversion devices can detect infrared or scattered infrared light and convert them into an electrical signal. The changes in electrical signal are closely related to the produced smoke concentration. Then, the electrical signal will be processed using amplification, integral comparison, and algorithm to get the final value, which can be compared to the set threshold. If this value exceeds the threshold of smoke alarms, an early warning signal will be sent for local fire warning. In summary, photoelectric smoke sensors exhibit the advantages of high reliability, long-time usage, wind resistance, moisture resistance, and electromagnetic interference resistance.

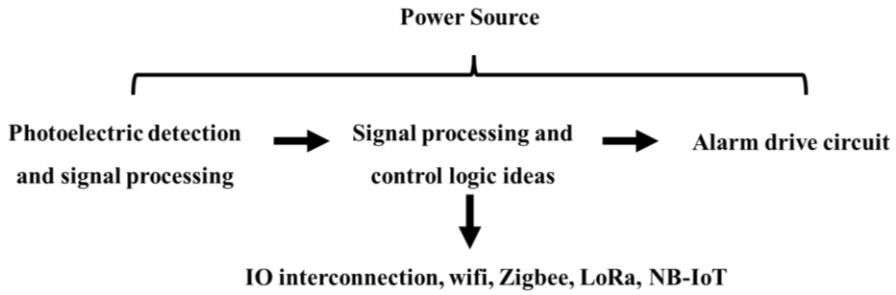

Scheme 1-2 A brief illustration of gas detection.

b). Visual Smoke Detection

In general, the fast and accurate algorithm is closely related to the sensitivity of smoke detectors. With the rapid mechanical and image-processing development, smoke detection algorithms based on video images have received considerable attention. Definitely, video images of fires can be collected through video cameras, cameras, and other equipment [35-37]. Afterward, all the recorded information is input into the computer for subsequent processing. Principally, it is difficult for computers to process these visible images directly. So, how to digitize visual images to digital data is necessary.

Usually, smoke detection based on computer vision images mainly includes five steps: acquisition of smoke video, preprocessing stage, feature extraction, classification recognition, and final alarm [30].

The corresponding process illustration is shown in **Fig. 1-5**. First, the collected smoke videos about fires are re-processed using digital image processing technology and correlation algorithms to figure out the areas of smoke and suspected areas of fire smoke [35, 38]. This stage is the most vital step comparatively. How to extract the accurate regions of smoke is the key to the fulfillment of the warning. Because of the processed results, the visual and dynamic features of the candidate smoke regions are analyzed carefully to extract the salient features of smoke. Subsequently, the extracted features are input into the classifier for identification to determine whether it is smoke. Once smoke is detected, the alarm will be triggered to realize the alert.

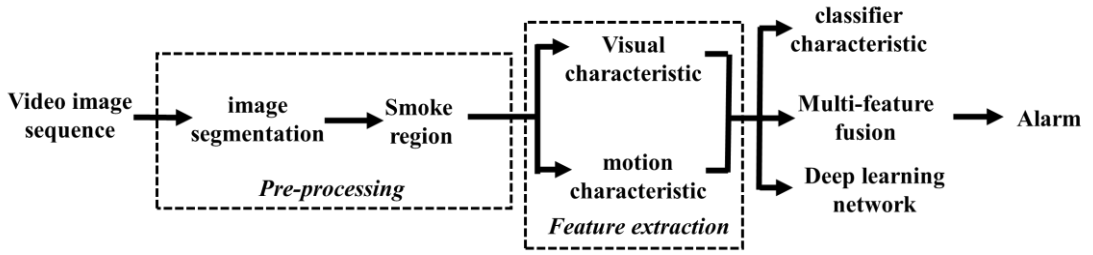

Fig. 1-5 Detection steps of smoke sensors based on video images [27].

In the preprocessing stage, the acquired image can be segmented into multiple objects and regions to reduce the computational difficulty. Among these existing image segmentation methods, the threshold segmentation technique is an efficient technique. Usually, the implementation of threshold segmentation techniques primarily depends on image color and motion-based segmentation techniques. For image color segmentation technology, it is important to distinguish real smoke from the suspected smoke regions by the color difference. According to the collected smoke images in different fire scenes, different color space models are applied to segment the collected images to acquire the target area. Moreover, for motion-based segmentation technology, the motion parameters and more visual features of the target smoke area are obtained via background subtraction, image difference, or optical flow segmentation.

In general, the motion characteristics of common smoke contain irregular texture and shape changes. The changes in static and dynamic features of smoke during the combustion process can be employed to extract the smoke. These changes of smoke features present in smoke color, texture, profile, shape, *etc*., [35, 39-42]. Among them, the color change is a significant visual change of smoke features. However, color monitoring is easily affected by severe environmental situations, leading to increased difficulty in detection accuracy. In addition, the texture change of smoke can be recorded by statistical methods and spectral methods that need a large amount of calculation. Moreover, using the directional gradient histogram to describe the gradient strength of the local area of the image can eliminate the interference of illumination and leaves in the process of smoke recognition. Furthermore, the smoke trajectory has the characteristics of low frequency, smooth streamlines, straight lines, etc., which can also be carried out for feature extraction.

After the extraction of smoke features, classification and recognition are employed by these methods of classifier recognition, multi-feature fusion detection, comparison of different detection

algorithms, and network models. Classifier identification mainly formulates a data set through the extracted smoke-related features and divides the feature data set into a training set and a test set according to a particular method. According to the test results, it is judged whether the output of the classifier is smoke. Currently, the classifiers are used in smoke sensors mainly based on video images, including neural networks and support vector machines. It isn't easy to accurately realize smoke detection with mere one feature. The extracted features of smoke can be organically combined to effectively improve the recognition rate of smoke. Furthermore, the learning network model represented by a convolutional neural network can automatically realize feature extraction of smoke that can better describe the essential characteristics of smoke.

Current smoke sensors can achieve efficient detection indoors or in small spaces. However, the timeliness is not satisfied if smoke sensors are put outdoors or in large areas, mainly caused by the complexity and diversity of large-scale environments. These can increase the difficulty of smoke extraction and detection, leading to the difficulty in obtaining accurate smoke detection in a short time. In summary, the current smoke sensors have the disadvantages of low smoke recognition ability, poor real-time performance, and high requirement of rapid smoke detection, resulting in a low smoke detection rate. To improve the smoke recognition rate, increasing the difficulty of calculation is necessary. Unfortunately, the complicated analysis will conversely cause poor real-time performance. In other words, this intricate calculation leads to a certain degree of false alarm rate and false negative rate for smoke sensors based on video images. In addition, some particular fire types- particularly slow burning or smoldering, fires-generate only a tiny amount of particulates, and these types of fires are generally difficult to detect using conventional fire detectors [43].

1.3.2 Gases sensors

Apart from smoke, different gases produced at various stages of combustion processing can also be detected objects to illustrate the potential fire information. Based on this situation, gas sensors are developed to diminish fire hazards [12, 44]. Broadly, gas sensors are fire-warning detectors or monitors operated on their principle [45]. Gas sensors are triggered when the accumulated gases during the combustion process reach the critical alarm threshold. They convert the detected information into electrical signals processed or interpreted by an instrument or computer, generating an alarm for fire safety measures.

Gas sensors are commonly utilized to detect gases that can reasonably predict fire evolution. Typically, the target gases contain the combustible products of CO, CO_2, H_2, O_2, H_2O, *etc.* during the entire combustion process [46, 47]. As a result of the diversity of generated gases, gas sensors come in various types: specific and multiple gas sensors. Specialized gas sensors detect the designated gas products and are activated when gas content reaches a setting threshold. While multiple gas sensors are available to measure multiple gas products, offering greater precision. Fundamentally, gas sensors detect changes in generated gases during combustion processing. Currently, gas sensors rely on technologies such as catalytic beads, acoustics, infrared rays, gas chromatography, semiconductors, calorimetric systems, photoionization, electrochemistry, and optics. A comparison to a reference of "good air component" is made to indicate potential fire danger.

Two commonly detected gases are CO and CO_2. Correspondingly, the frequently used gas sensors are CO sensors and CO_2 sensors. Primarily, much CO_2 is released during a fire hazard [30, 48]. Additionally, the generated harmful gases of CO and hydrogen cyanide during intense burning can react with O_2 to product CO_2 [49]. The reaction leads to gradual changes in both O_2 and CO concentrations, showing the combustion state. Especially in detecting O_2, a decrease in content can demonstrate the smoldering behavior, a phenomenon often challenging for smoke sensors to detect.

Furthermore, the manufactured gases are strongly correlated with the speed of burning. Slow-burning fires produce substantial CO and CO_2, whereas rapid burning conditions lead to much CO_2 and H_2O. The presence of these gases in detection can convey the combustion situation. On account of the diverse fire sources, the composition of gases produced during combustion varies significantly. Contrastively, CO gas sensors exhibit higher reliability and universality in different fire scenarios. Two kinds of gas sensors exist wet electrolyte and non-dispersive infrared absorption (NDIR). Wet electrolyte-based gas sensors are compact, cost-effective, and versatile, often employed with smoke and/or heat sensors.

Moreover, these gas sensors are advantageous in detecting smoldering phenomena, yet their drawback lies in a short service life, necessitating frequent replacement [29]. NDIR gas sensors leverage the radiation energy emitted by most flames within the IR region, with a CO_2 peak at about 4.3 μm, which is caused by the combustion of various materials, as depicted in **Fig. 1-6** [29]. In addition, these NDIR gas sensors are large, complicated, high-cost, and have long-time usage. NDIR

CO sensors are mainly applied to monitor fire hazards in coal mills, conveyors, and silos. When using gas detectors, they are strategically set up at one or more positions to collect gases. Subsequently, the collected gases undergo further analysis via NDIR to assess the possible fire incidents.

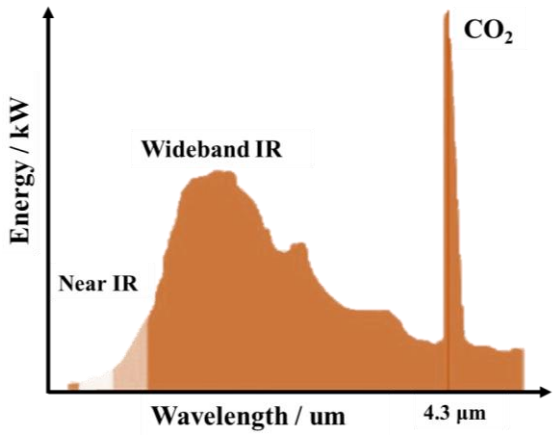

Fig. 1-6 Spectrum distribution of light emitted by flames [29].

To summarize, CO gas sensors typically operate at room temperature and demand a relatively low power source to achieve fire warning. CO gas sensor has an edge over smoke sensors in detecting tiny smoldering. Nonetheless, whether these gas sensors maintain equivalent sensitivity in fire detection needs to be further considered, especially under unique application scenarios, such as low temperature, high humidity, rainy days, and other challenging environments.

1.4 State of the art

1.4.1 Fire-warning mechanism

The conventional working mechanism for early fire-warning systems is diverse, with corresponding schematic descriptions depicted in **Scheme 1-3** [14]. In the electrical circuit, including the power supply, cables, warning lamp, and fire-warning samples, the electrical conductivity of warning samples changes under different temperature conditions. One is the transformation from insulation at room temperature to a conductive state after a high temperature or flame attack, which can trigger the warning lamp. The other one is the conductive-to-insulate change upon high temperatures or flame attack, leading to the disconnection of an electrical circuit. This is a simple and highly operational working principle to prepare early fire sensors, inspiring various fire alarms to be developed.

Moreover, thermal-induced optical changes are also applied for early fire-warning systems. The color, transmittance, shape, and other characteristics can also display differences when a high temperature or flame attacks warning materials. All the phenomena of combustion behavior can be used as a warning signal. From the perspective of usage, the working mechanism of fire-waring technology can be divided into two types: irreversible and reused, which will be explained in the following sections.

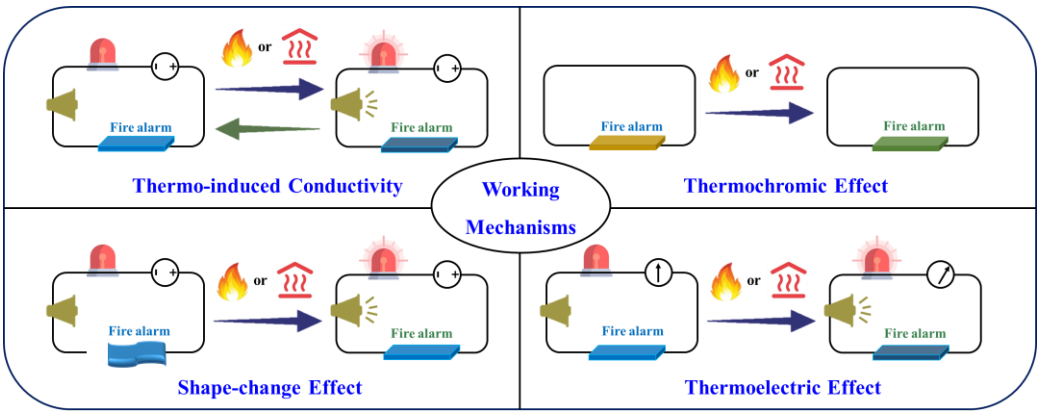

Scheme 1-3 Schematic illustration of different working mechanisms of early fire-warning systems.

a). Irreversible fire-warning mechanism - GO

The structure of GO

Since its emergence in 2004, graphene has become a typical two-dimensional material within the expansive carbon materials family [50]. Characteristically, graphene constitutes a signal-layer graphite sheet with one atom-sized thickness and a honeycomb structure formed by sp^2 hybridized carbon atoms, ensuring structural integrity and stability [51, 52]. Owning to its particular structure, graphene showcases excellent properties that comprise high charge carrier mobility, optical property, superior mechanical strength, superb thermal conductivity, *etc.* [53-57]. As a result, researchers from different fields express an attractive interest in graphene material. However, natural graphene is difficult to obtain in large quantities. In response, many methods have been explored to produce graphene-like material more conveniently and cost-efficiently. In the current techniques, the reduction of graphene oxide (GO) is one of the most dependable approaches [58].

GO is a well-known oxidized derivative form of graphene. Usually, GO is prepared through attacking graphite crystals with strong oxidizers, such as acid or alkali solution [53, 59]. After this oxidation treatment, some oxygen-containing groups are introduced into the graphite stacks.

Subsequently, sonication or mechanical stirring treatments are utilized to exfoliate oxidized graphite to obtain the final GO nanosheets. As shown in **Fig. 1-7**, GO still displays the graphene-like layered structure even after the strong oxidation treatment [50, 53, 60].

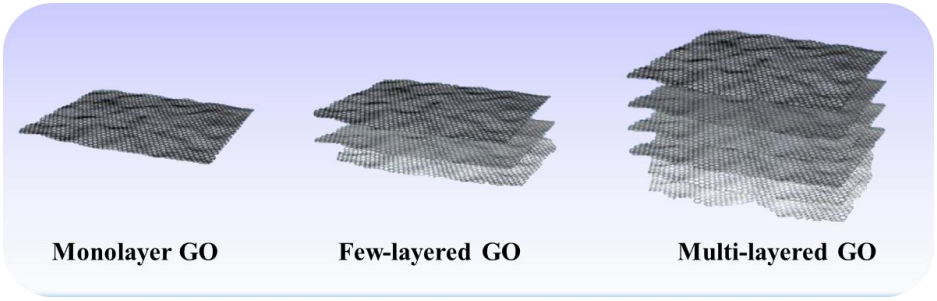

Fig. 1-7 the schematic illustration of monolayer, few-layered and multi-layered GO.

The investigation of the structural model of GO has been developed better to understand the effect of oxidation treatment on GO structure. However, no exact atomic structure model of GO has been proposed until now due to the complexity of the oxidation process, even though considerable efforts have been made toward structural investigation for a long time [51, 61, 62]. In accordance with the current reported structural models, one chemical structural model of GO is commonly accepted. As presented in **Fig. 1-8**, GO comprises randomly sized planar graphene-like aromatic patches spaced by sp3-hybridized carbons modified by hydroxyl groups, epoxy groups, and carboxyl groups [59]. The content of oxygen-containing groups and dimensions of nanosheets are linked to the intricate oxidation degree. Through ultrasonic treatment during exfoliation, graphite generally tends to yield GO with smaller and uneven nanosheet sizes.

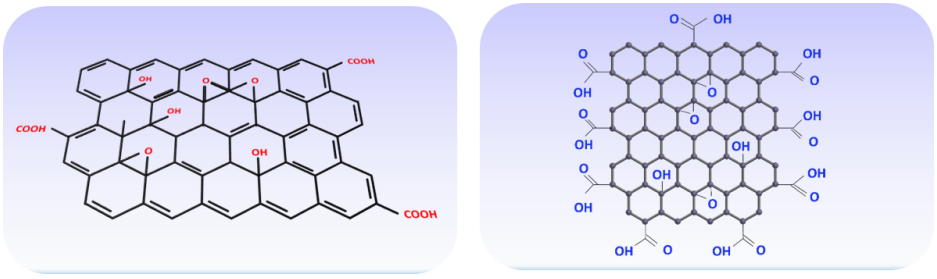

Fig. 1-8 the schematic illustration of the molecular structure of GO.

According to the preparation process of GO described above, the structure of GO is not perfect enough due to the oxidation exfoliation procedure, compared with the highly conjugated structure of pristine graphene. The distinctive structure of GO endows it with remarkable performance. Specifically, GO demonstrates chemical stability, a large specific surface area, excellent physical

and electrical properties, electro-chemistry, optical properties, *etc.*, using promising applications [57, 63-66].

Amphiphilic property of GO

After the synthesis of GO by intense oxidation treatment, diverse oxygen forms consisting of out-of-plane epoxide and hydroxyl species and edge functional groups of carboxyl, carbonyls, hydroxyl groups, and in-plane ether-like species are introduced. These intricate oxygen groups of GO result in unique surface functionalization characteristics. A notable property is the amphiphilicity of GO, allowing GO to dissolve into water and organic solutions to produce large quantities of stable solutions at low costs. This characteristic improves the processability of GO and addresses a limitation posed by graphene, which is often challenging to incorporate as an additive in the fabrication of nanocomposite materials [53].

The carboxyl groups located at the periphery of GO exhibit ionization, renders them negatively charged in an aqueous solution. In addition, the structural disruption and changed layer distance resulting from the oxidization treatment greatly diminish the attractive interactions between GO layers. This reduction in interactions facilitates effortless dispersion across different solvents, as illustrated in **Fig. 1-9** [59]. Furthermore, ionization generates a compelling electrostatic force that ensures the stable distribution of GO nanosheets in water, yielding a well-defined suspension. This heightened dispersion capability facilitates the mixing between GO and other materials.

Compared with the carbon atoms within graphene, the carbon atoms in GO encompass sp^2-hybridized carbon atoms that constitute the original honeycomb lattice structure and sp^3-hybridized carbon atoms with functional groups. For the surface of GO, the areas with the sp^2-hybridized carbon atoms are viewed as unoxidized regions, while the areas containing the sp^3-hybridized carbon atoms is deemed oxidized region. The proportion between oxidized area and unoxidized region serves as an indicator of the functionalized degree of GO. The degree of surface functionalization significantly affects the solubility of GO in water. Additionally, unlike the strong in-plane π-π interactions in graphene, the π-π interactions between GO nanosheets become weak, leading to a ready fabrication of GO-based materials with various microstructures.

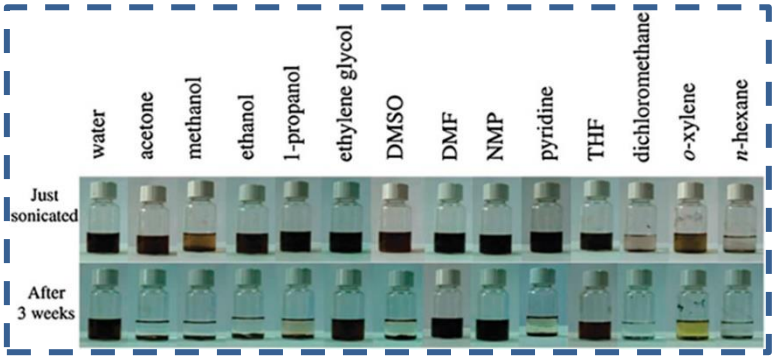

Fig. 1-9 the dispersion of GO in water and other chemistries [59].

Self-assemble performance of GO

Moreover, GO also exhibits excellent self-assembly properties owing to the amphiphilic properties of GO and its unique surface chemical properties. These attributes enable the construction of diverse GO-based materials with distinct nanostructures, such as films, hydrogels, hollow spheres, particles, *etc*. The self-assemble phenomenon of GO lies in the self-concentration process on various interfaces. As the self-assembly proceeds, GO nanosheets move upward. Consequently, all the nanoflakes are captured and stabilized on the interface after solvent evaporation, forming the macroscopic GO film through intricate nano-covalent interactions [53].

The self-assemble phenomenon of GO can be realized across different interfaces that consist of liquid-air interface, liquid-liquid interface, and liquid-solid interface. By contract, the liquid-air interface, comprising the ambient atmosphere as the gas phase and a GO suspension as the liquid phase, serves as a particularly effective platform to achieve GO self-assembly. As shown in the schematic illustration in **Fig. 1-10**, GO nanosheets can migrate across the interfaces while concurrently decreasing the surface tension of the GO suspension, aiding in the formation of GO-based films. In addition, GO's amphiphilicity and surface chemical activity are considered pivotal contributors to self-assembly between liquid-air interfaces. Three standard techniques are employed for interfacial self-assembly: the Langmuir-Blodgett self-assembly, evaporation-induced self-assembly at the 2D interface, and evaporation-induced self-assembly at the 3D interface. Comparatively, the Langmuir-Blodgett self-assembly approach is particularly efficient in preparing the GO with controllable thickness [53].

Depending on the above-mentioned unique property, GO-based materials with different microstructures and morphologies can be obtained by tuning these interfaces.

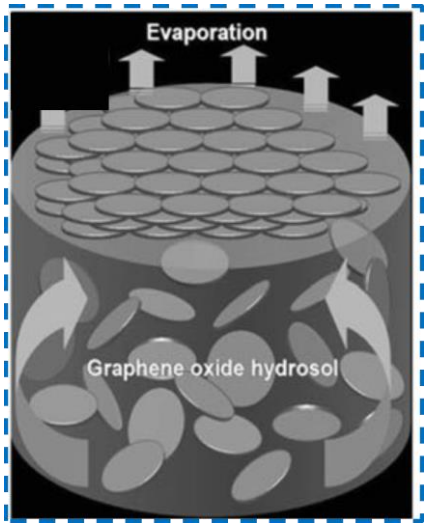

Fig. 1-10 the scheme of a GO suspension-air interfacial self-assembly [53].

Thermo-sensitive property of GO

GO also showcases thermal instability and chemical activity, rendering it susceptible to thermal disproportionation or reduction by specific agents, producing a chemically modified graphene known as reduced graphene oxide (RGO) [59, 67-69]. RGO has a similar structure to graphene and presents some semblable properties, such as thermal conductivity, electrical conductivity, mechanical properties, specific surface area, morphology, and solubility [65]. Therefore, implementing GO reduction is extremely important for getting identical performance with graphene.

Broadly, GO is an electrical insulator because of the disruption of its regular sp^2 network formed during oxidation processing. To restore the regular sp^2 network, the oxygen-containing groups of GO need to be removed by reduction reaction. In essence, the aim of the reduction of GO is to eliminate the oxygen-containing groups on the GO structure to restore the regular honeycomb network. Presently, the standard approaches of chemical reduction [70], electrochemical reduction, and thermal reduction are adopted to obtain RGO materials. Chemical reduction agents include hydrazine, alkaline chemicals, amino compounds, hydrohalic acids, sulfur compounds, hydroxyl compounds, metal hydrides, lively metals, *etc*. In comparison, the thermal reduction approach for producing RGO is more straightforward, safer, and economically viable [71, 72]. Based on what is mentioned above, thermal treatment proves the capability to transfer insulative GO into conductive RGO, showing its thermal-sensitivity, which can broaden its potential practical applications [73].

Under the thermal attack, GO undergoes a sudden temperature change, generating water vapor,

CO, and CO_2. These gases create air pressure between the layers of GO nanosheets. The existence of pressure plays a pivotal role in the removal of oxygen-containing groups of GO [74-76]. This implies that the produced pressure is strongly linked to reduction temperatures. Generally, a higher degree of thermal shock gives rise to a more efficient reduction of GO.

Numerous studies have been conducted to explore the thermal reduction processing of GO until now. Bagri *et al*. reported a molecular dynamics simulation study on the structural evolution of GO during heating treatment, revealing the conversion of the hydroxyl and epoxy groups in the initial structure into carbonyl and ether groups by thermal annealing [70]. However, due to the thermodynamic stability of carbonyl and ether groups, they persist within the GO structure to hinder the complete reduction. Thus, it is difficult to thoroughly remove all the oxygen-containing groups from GO to achieve a complete structural restoration, as the scheme illustration presented in **Fig. 1-11** [60]. Most RGO retain residual oxygen-containing functional groups, which offer steric hindrance and prevent restacking.

On the other hand, this indicates the structural defects of RGO, which gives rise to the performance disparity between graphene and RGO. Moreover, a dual-path mechanism for the thermal reduction of GO caused by oxygen coverage is also elucidated [68]. Furthermore, a theoretical analysis of thermal reduction in GO has also been carried out to shed light on the relationship between the reduction temperature and the content of oxygen-containing groups [69]. Specifically, the critical dissociation temperatures for hydroxyl groups are around 650 °C, while the initial reduction temperature of carboxyl groups falls within the 100 -150 °C range. Conversely, carbonyl groups show comparatively more excellent stability.

The studies underscore the significance of the reduction in temperatures. These thermal reduction temperatures are closely associated with the RGO quality, shown in the carbon weight ratio and lattice defects of RGO. Optimal reduction temperatures of GO produce fewer lattice defects in the structure of GO, which is favorable for an exceptional structure. Except for the structural defects, the thermal reduction of GO causes additional challenges that consist of substantial weight loss, material volume expansion, and nanosheet stacking. Both these issues need to be further investigated. Among these issues, the stacking of GO nanosheets is mainly attributed to the enhanced π-π interaction between layers aroused by the restoration of the sp^2 network [53].

Similarly, this phenomenon disrupts the already microstructure of GO materials, negatively influencing applications such as adsorption, ion transport, catalysis, *etc*. These intricate factors collectively emphasize the need for thorough consideration in further research.

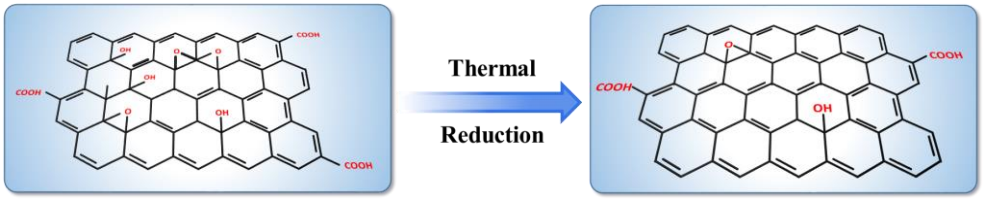

Fig. 1-11 Thermal reduction of GO to form RGO.

Based on the above description, GO can be thermally reduced to form RGO by utilizing its thermal-sensitive properties, even though some issues appear during the thermal reduction processing. The structural characteristics of RGO can be finely tuned through precise control over the extent of reduction, which will further affect the different properties of RGO.

b). Irreversible fire-warning mechanism - MXene

In addition to GO material, two-dimensional MXene has recently become an attractive candidate for fire-warning systems. MXene is produced by exfoliating MAX in hydrofluoric acid at room temperature. Typically, MAX is carbides and nitrides with a $M_{n+1}AX_n$ formula, where n = 1, 2, or 3, M represents a transition metal, A denotes an A-group element from group 13 and group 14, X is C or N from laminated structures characterized by anisotropic properties [77]. Comparatively, A-group atoms are the most reactive due to their weak bound. There are more than 60 types of MAX [78]. In specific scenarios, the M and A-group elements can be extracted from the MAX structure to form a carbide-derived carbon with distinctive properties [79].

Herein, MAX of Ti_3AlC_2 is chosen as the raw materials for MXene after the extraction of Al. Importantly, remarkable performances of MXene that consist of high metallic conductivity, substantial negative surface charge, hydrophilicity, *etc*., showcase the advantage in diverse research areas [80], as depicted in **Fig. 1-12**.

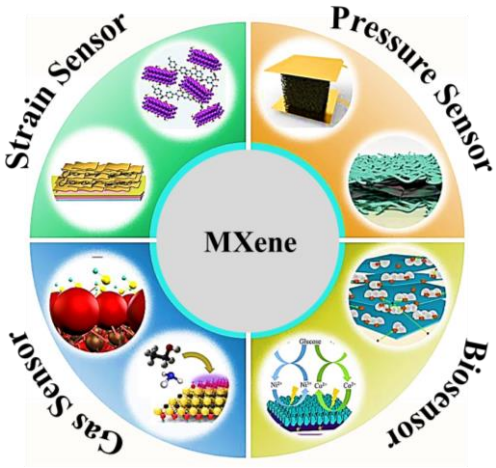

Fig. 1-12 Schematic description of the structure and application of MXene.

The excellent thermoelectric effect of MXene makes it a promising candidate for various electrical applications. Thermoelectric materials are a novel class of energy substances that can directly realize the mutual transfer of heat and electric energy without other external energy sources. Specifically, when a particular temperature distinction exists between the two ends of a material, an electric current will appear, which is attributed to the Seebeck effect. Conversely, when the electric current passes through the thermoelectric material, there will be a directional flow of heat, resulting in a thermal difference between the two ends of the material. This phenomenon is known as the Peltier effect, shown in the schematic description from **Fig. 1-13**. This character of MXene exemplifies its potential role in advancing early fire-warning systems.

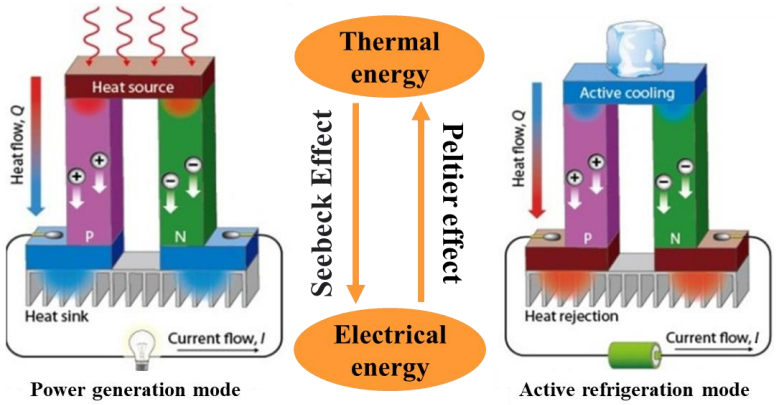

Fig. 1-13 Schematic illustration of the thermoelectric effect of MXene.

c). Reused fire-warning mechanism - CS

Apart from the above-mentioned operational principles employed in early fire-warning systems, developing alternative working mechanisms is imperative to enable the utilization of these systems

in diverse and complex scenarios. Chitosan (CS) might be a promising candidate for advancing early fire-warning systems.

CS is one chitin product sourced from a wide range of origins. It is easy to obtain from seafood such as shrimp, crab, and shellfish, as well as from the cell walls of lower organisms such as seaweed, fungi, and yeast [81-83]. CS is the only alkaline polysaccharide rich in C and N elements. Its molecular framework is built upon glucose units adorned with amino groups. The CS structure contains amino and hydroxyl groups, as presented in **Fig. 1-14**. It is relatively active and can be modified, activated, and cross-linked. Specifically, the active amino group in the CS molecule can be acidified into salts. In contrast, introducing carboxyl groups permits the replacement of synthetic side chains such as ammonium salt, mixed ether, *etc*. These CS-based derivatives have water solubility, alcohol solvent, organic solubility, and surface activity.

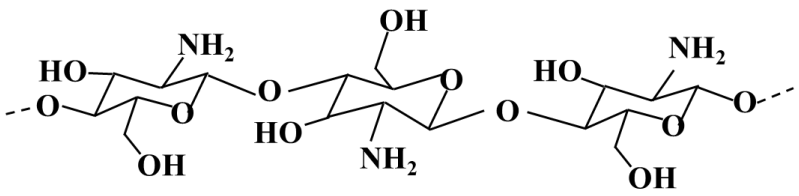

Fig. 1-14 Schematic illustration of CS structure.

The solubility of CS material is associated with the surrounding pH value. When the pH exceeds 5, CS completely dissolves in an acidic solution to form a relatively viscous liquid. This is attributed to the protonation of the amino group. If it is under alkalization treatment, CS ca be used for a gel and precipitate. In addition, the hydroxyl and amino groups in CS materials have coordination and chelation functions. These hydroxyl and amino groups in CS material can be cross-linked and grafted with cross-linking agents for network polymers.

Moreover, the amino groups within CS materials can establish complexes with transition metal ions, subsequently undergoing cross-linking with suitable agents. This imparts a template agent's memory and selective adsorption properties [84]. Furthermore, CS can be acylated under suitable conditions to prepare water-soluble compounds with low-carbon numbers and high-carbon hydrophobic derivatives. CS stands as a positively charged cationic polymer that forms polyelectrolyte complexes.

CS possesses exceptional biological safety, biodegradability, and biocompatibility. It

demonstrates antibacterial, non-toxic, tasteless, and gentle on the skin, making it an invaluable component in agriculture, light industry, medicine, tissue engineering, and environmental protection, as depicted in **Fig. 1-15**.

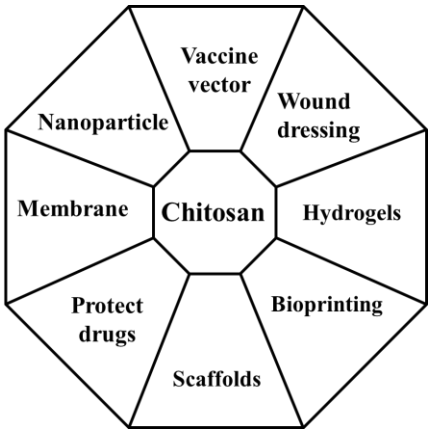

Fig. 1-15 Potential applications of CS material [81].

Moreover, CS presents the fascinating temperature-sensitive property to form an electric current. This phenomenon arises from the mobility of free charges within CS, which can jump between different sites under the influence of elevated temperatures and a power supply. This feature holds promise in various applications and serves as a source of inspiration for developing early fire-warning systems.

1.4.2 Thermo-sensitive fire-warning sensors

GO-assisted fire-warning sensors

GO has been primarily viewed as a preferred candidate for early fire alarms because of its thermally unstable chemical activity. It can produce conductive RGO after experiencing reduced treatment and exothermic disproportionation reaction [53]. In addition, the unique amphiphilic of GO can achieve functionalized hybrid carbon materials with various performances [53].

On the basis of the superiority of GO, varied early GO-based fire sensors are reported [85-97]. Eco-friendly paper is one of the substrates. As shown in **Fig. 1-16**, a smart fire-warning wallpaper produced by the modification of hydroxyapatite nanowires (HNs) and polydopamine-modified GO (PGO) utilizes the conversion of electrical conductivity of GO for warning. With the temperature increasing, GO becomes conductive to trigger the warning lamp and warning buzzer at 126.9 ℃ for alert [98]. Moreover, a kind of wood pulp paper (WPP) coated by phenoxycyclophosphazene-

functionalized graphene oxide (FGO) and chitosan-functionalized carbon nanotubes (CNTs) can also implement early warning in several seconds by using GO's sensitivity to temperatures [99].

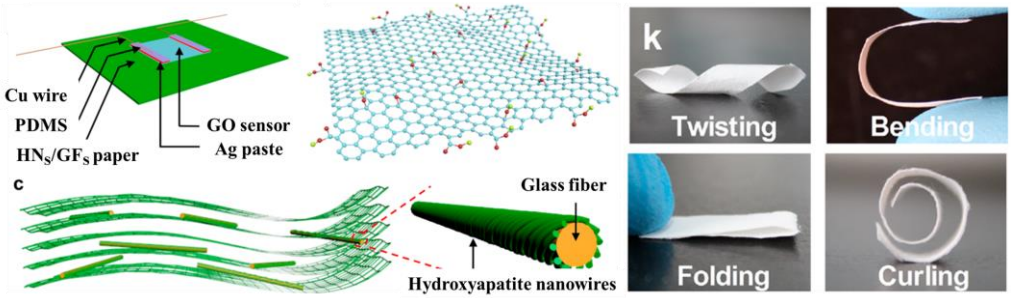

Fig. 1-16 Schematic fabricating process and micro-structure of fire alarm wallpaper, GO structure with rich oxygen-containing groups, and glass fiber paper with multilayered structure.

Besides the environmental paper, a variety of GO-based film materials are fabricated as fire alarms. Broadly, GO-based films are caused by self-assembly phenomena at interfaces of mixture solution that are attributed to GO's amphiphilicity and surface chemistry [53]. A GO-based composite film with synergetic benefit from 3-methacryloxypropyltrimethoxysilane (MPMS) and L-ascorbic acid (LAA) shows an ultrafast early warning response within 7 s at 300 ℃ (**Fig. 1-17** (a)) [100]. Another hydrophobic sisal cellulose microcrystal film is also described as a fire sensor. This composite film is co-modified by graphene nanosheets (GN), soy protein isolate (SPI), sisal cellulose microcrystals (MSF-g-COOH), and citric acid (CA) with improved flame retardancy, exhibiting sensitive response capability after being burned [101].

Benefiting from the self-assembly ability of GO, a multi-functional mixture solution is pre-designed to be wrapped into different substrates by typical dip-coating or evaporation methods. This simple, low-cost sample preparation method displays universality to various substrate materials, such as wood black, PU foam, cotton fabric, polystyrene resin (PR), etc. For instance, Wu et al. reported hierarchical fire-warning coatings created by GO and silicone structures that can be covered onto PR, wood block, cotton, and PU foam [102]. As depicted in **Fig. 1-17** (b), the surfaces of flammable materials with a warning layer become black. This resulting coating can improve combustible substrates' flame resistance and provide a warning signal in 2 - 3 s.

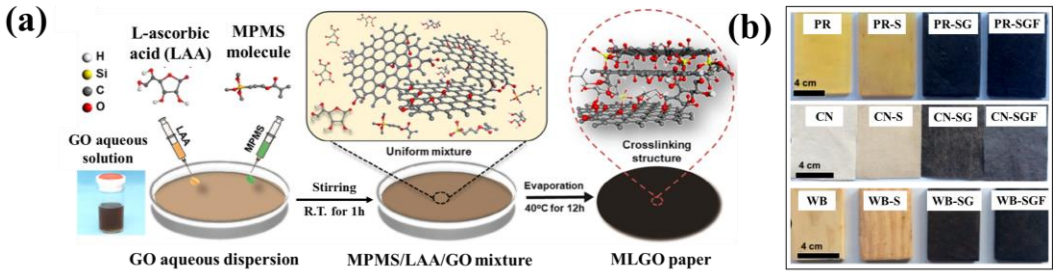

Fig. 1-17 (a) Schematic illustration of MPMS/LAA co-modified GO (MLGO) paper, MLGO paper. (b) photographs of the fire-warning coatings on the surface for different flammable materials: PR, CN, and WB.

Apart from the above fire-warning films, there is another kind of warning layer decorated on the surface of PU foam. The pre-designed water-soluble solution containing hybrid ammonium polyphosphate (APP), silane, and GO can be wrapped on the PU surface for an early fire sensor (**Fig. 1-18** (a)). By exploiting GO's electrical conductivity, these special hybrid coatings can respond to flame within only 2 s and a high temperature of 300 ℃ at 11.2 s [103]. Other melamine-formaldehyde (MF) sponges are also used as an early warning substrate (**Fig. 1-18** (b)). Hydrophobic, reversible compressibility and flame-retardant properties have been improved in one multi-functional GO wide-ribbon (GOWR) wrapped MF sponges. Under a fire attack, this alarm is triggered with an ultrafast alarm response of 2 s [104].

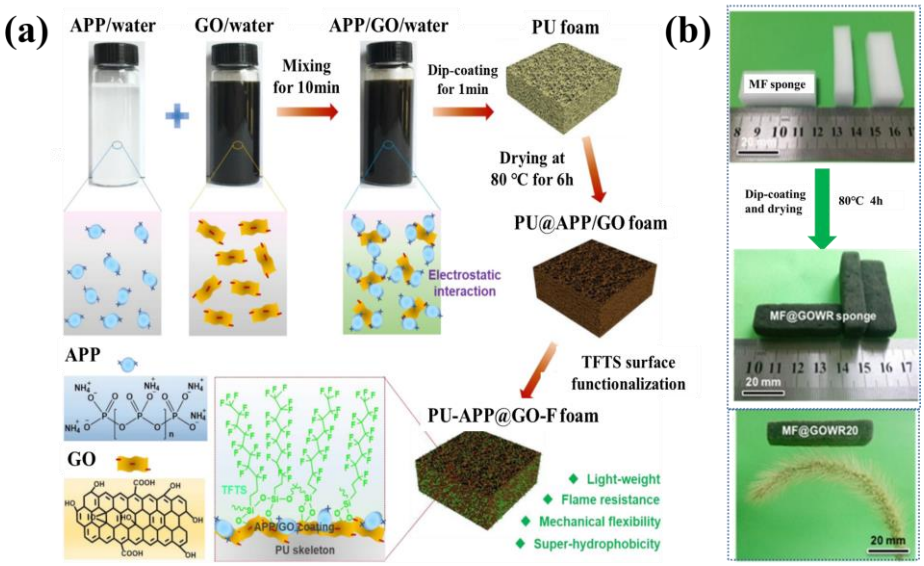

Fig. 1-18 (a) Detailed preparation process of water-based hybrid APP and GO mixture solution coated on the surface of PU foam. (b) Pictures of pure MF and MF@GOWR sponges via dip-coating way; image of MF@GOWR20 to show lightweight feature.

As mentioned in the fire alarms in the previous section, a variety of GO-assisted early fire alarms on different flammable materials are proposed [105]. Nonetheless, GO-based early fire sensors are not exempt from limitations in application. They still have some challenging parts that need to be advanced. Firstly, they cannot be used repeatedly or detect fire revival due to the irreversibility nature of the GO reduction. Secondly, GO-based fire sensors require an external power source to generate an electrical signal [106-108], which will cause inconvenience in operation, ultimately limiting the large-scale application [109].

Semiconductor-based fire-warning sensors

Except for GO, other materials have been proposed for fire detection and thermal sensing, containing semiconductors, conjugated polymers, carbon-based nanomaterials, sulfides, and nanohybrids [110, 111]. Traditionally, different semiconductors have been carried out for fire detection by utilizing the characteristic of conductivity changes with temperatures. Several semiconductors, such as Metal Oxides (MOs) or CNT, are known for gas sensing [112, 113]. These semiconductor materials have recently been considered for thermosensitive early fire sensors [114-116]. Their working principle is similar to the previously discussed GO-based fire-warning systems by means of electrical resistance change upon heating or burning exposure.

There is a growing demand for flexible fire alarms that can be integrated into flexible fabric products or used directly as functional fabric products, such as textiles, CF, or polypropylene (PP). Semiconductors arise as a potential candidate for fire alarms with the motivation of their excellent sensor characteristics in terms of sensitivity and response/recovery time observed in gas-detecting sensors [113], temperature, or pH sensors [117], as well as their easy implementation within these substrates. The combination of semiconductors and polymers offers notable advantages since this allows the creation of low-cost, large scale and multi-functional sensors. Concerning fire sensing, different semiconductors have been considered for enhancing thermosensitive properties to achieve sensitive temperature detection, including different MOs such as Fe_3O_4 [110], ZnO [117], SnO_2, etc. [118]. A sandwich-like fire alarm fabric (Ag@Fe_3O_4-MS) based on 1D-Fe_3O_4 nanowire arrays and fish-scale-like silver sheets, designed by in situ layer-by-layer assemblies on the surface of PP nonwoven fabric is provided [110]. Ag@Fe_3O_4-MS is an electrical insulator under room conditions and turns into a conductor when exposed to flame or to an increase in temperature (below 100 ºC).

This structure shows a rapid response time of 2 s and is reliable repeatability with at least 15 min alarm time in the flame [110].

Carbon-based allotropies, alongside GO, have also been considered for thermosensitive fire alarms due to several temperature-induced phenomena that can serve as objects to be detected, such as material volume expansion, magnetic susceptibility change, and resistance exchange. As a representative of carbon-based materials, CNT can be employed to prepare an early fire-warning system by monitoring environmental temperature changes [112]. The chitosan/montmorillonite/CNT composite aerogel (CCA) is assembled and shown in **Fig. 1-19** (a) [119]. In particular, the employed amino-functionalized CNT (A-CNT) can provide CCA with high electrical resistance (sharp decrease with increasing temperature), high mechanical strength (to create resistant aerogel), and tubular structure (which acts as an exposed pathway to fire). The combination with carboxymethyl chitosan (CCS) can be a promising substitute for traditional friendly flame retardants due to the abundance of hydroxyl groups and amino groups, endows CCS aerogel with excellent charring capability and thermal insulation. This early fire-warning system can realize a short response time (~ 0.25 s) and resist a high-temperature flame up to 1200 °C as observed in **Fig. 1-19** (b).

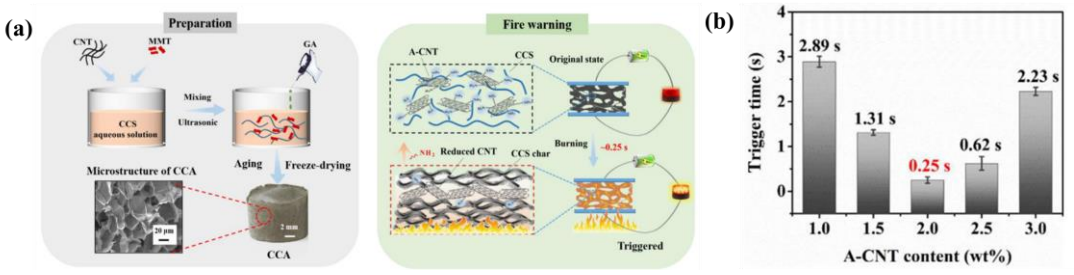

Fig. 1-19 (a) Fire alarms based on semiconductor materials. Design strategy for CCA. a Preparation route, supersensitive fire-warning capability, and mechanism of CCA; (b) Fire-warning trigger time of CCA with different A-CNT content.

Another carbon-based carbon black (CB) material for fire sensors has been proposed. It is a novel flame-retardant coating including CB nanoparticles (denoted as CB@KF) blended with polyvinylalcohol (PVA) and CNT over CF to assemble a fire-warning sensor (CB@KF-CF) [109]. In **Fig. 1-20** (a), the synthesis and behavior of a fire alarm under fire are summarized. This coating provides excellent flame retardancy for fire sensors because of its carbonization properties. CB@KF-CF exhibits an alarm time under flame in 4 s and at a temperature of 350 ºC in 8 s, as

observed from the screenshots in **Fig. 1-20** (b). The shell of CB@KF at a high temperature begins to degrade, which generates some phosphoric acid and polyphosphoric acid to promote the carbonization of CB@KF and dehydration of the substrate. The formation of a highly connected char layer, with a high degree of graphitization, can join the CNT and carbonized CB@KF to form a continuous and conductive network to trigger the fire-warning system.

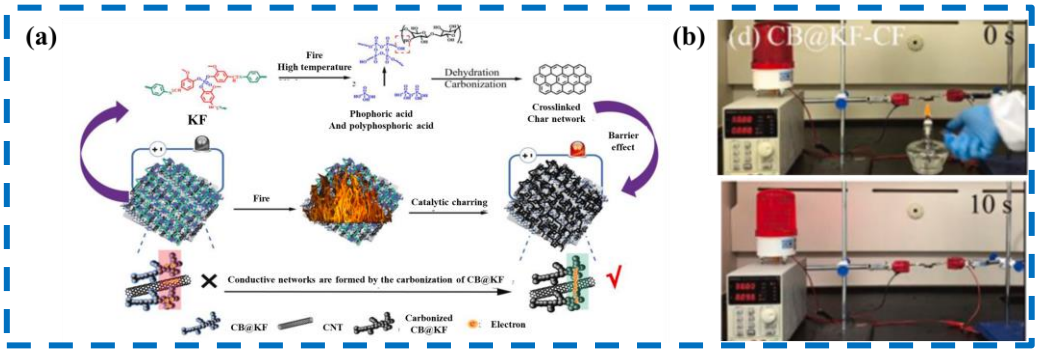

Fig. 1-20 (a) Schematic flame-warning mechanism of CB@KF-CF. (b) Simulated fire-warning process CB@KF-CF.

Transition metal carbides ($Ti_3C_2T_x$, MXene) have attracted increasing interest in many applications because of their large specific surface areas, favorable electrochemical properties, and excellent strengths [120]. Recently, some MXene-based fire-warning systems have been proposed, as they possess fantastic flame-retardant effects accompanied by their high electrical conductivity. Therefore, special attention has been paid to this particular subset of materials. A fire-warning system based on PEG or polyvinyl pyrrolidone (PVP) decorated with MXene has been reported [121]. Under flame, the electron excitation of the titanium network can trigger a resistance transition from an insulating state to a conductive state, showing an ultrafast fire response. Due to silane functionalization, the coatings are reusable and weather-resistant, which is fundamental for outdoor applications of sensors. Although MXene-based fire-warning systems have been proposed based on an electrical resistance mechanism, their combination with other materials has also opened the door for other triggering mechanisms based on voltage generation due to the thermoelectric effect.

1.4.3 Thermochromic-based fire-warning sensors

Not only the resistance and the generation of a voltage but also color changes can be applied as possible outputs under the presence of temperature changes. Actually, some materials that display a shift in color under different temperatures or heat accumulation are referred to as thermochromic

materials.

For instance, the color change can respond to temperature changes owing to the particular changes in the molecular structure. An example is presented by Zhao et al. [122]. After heating liquid metal microdroplets (LM)/polyborosiloxane elastomer (PBSE), benefiting from the tremendous thermal diffusion, the color quickly changed from black to pink at 55ºC (**Fig. 1-21** (b)). This color change caused by the structure demonstrates a significant advantage, especially as a low-temperature warning signal for a fire-warning sensor. The phthalonitriles could be transformed to phthalocyanine (Pcs) at about 180 °C, reflected in the color change at a temperature below the combustion temperatures [123]. The earlier fire warning component (EWC), based on spray-coated phthalonitriles that can transform to Pcs, shows a precise color conversion from white to green with increasing temperature, as observed in **Fig. 1-21** (a). An intelligent image recognition algorithm is employed to detect the color change, which can display a warning signal within 20 s at 275 °C and 3s under a real fire. This setup is based on the apparent color change to green with temperature, which is observed clearly by the changes in the FTIR spectra. With the increase of these characteristic modes, the algorithm can change from a 0 to 1 status to display a warning signal.

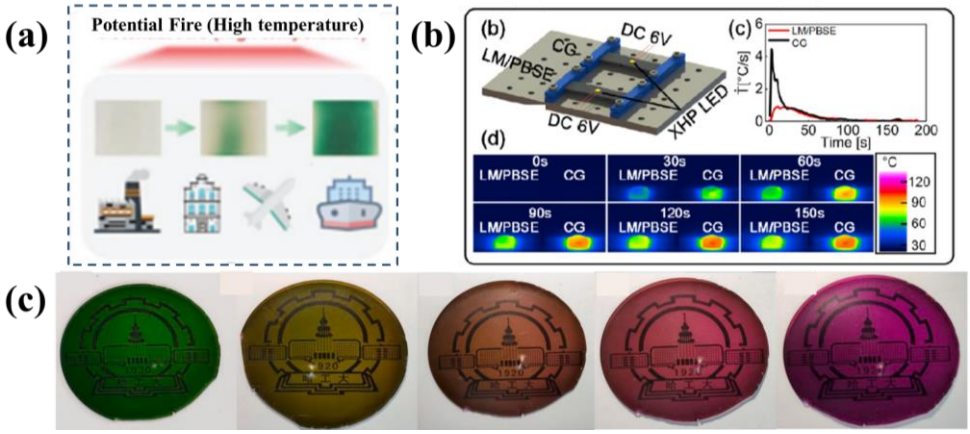

Fig. 1-21 (a) The fabrication of EWC, its color change process, and the potential fire simulation experiments at 275 °C and (fire alarm remote monitoring). (b) The thermal camouflage and thermal dissipation behavior of the LM/PBSE. (c) The color changes of the PMF material at different temperatures.

As presented in **Fig. 1-21** (c), A kind of reversible thermochromic POSS(Polyhedral Oligomeric Silsesquioxane)-metal films (PMFs) with variable ratio of POSS and metal salt $Cr(NO_3)_3 \cdot 9H_2O$ has been developed recently [124]. Due to the temperature increase, ligands such

as H_2O and NO_3^- are decomposed and released, causing the color change, which is recovered by capturing water molecules from the air and the subsequent re-coordination with PMFs. Thermochromic-based fire-warning systems are in an early stage of development, although they offer an alternative method to detect a fire at an early stage.

1.4.4 Shape change-based fire-warning sensors

Shape memory polymers are polymers whose shape can be either permanent or temporary, which can be switched under different circumstances, such as polymer phase transition or changed temperature. Jia et al. [125] fabricated an OFF-to-ON shape memory polymer that can respond to fire due to the cross-linked polycaprolactone network and shape memory. This shows from non-conductive at low to conductive at high temperatures. The device's electric current changes during these shape transformations and can be monitored, as observed in **Fig. 1-22** (a). The sample can be either in the initial state, stretched state, or shape-restored form. Only in the extended state the LED lamp can be turned on to indicate warning danger [126]. In addition, one MXene-based thermoplastic polyurethane (SMPU) fire alarm system is fabricated, which can reveal superior fire retardancy and rapid self-extinguishing performance [127]. This SMPU/MXene paper is rolled up initially. However, the sample becomes flat after heating to form a conductive pathway within 10 s, leading to a trigger to a warning responsive sensor that is observed in **Fig. 1-22** (b).

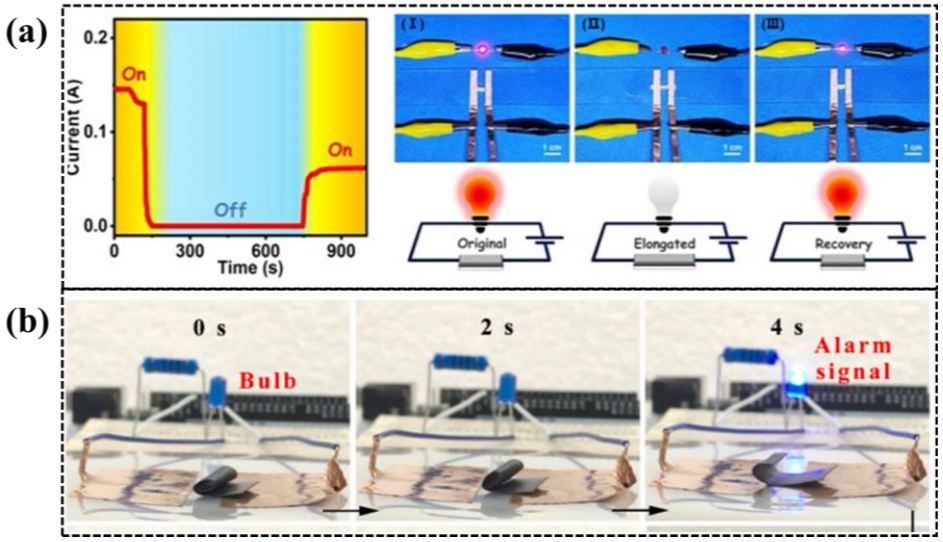

Fig. 1-22 (a) Real-time monitoring of current changes during stretching and shape recovery process via float device and electrochemical workstation at a given voltage of 0.1 V. Using LED indicators to evaluate sample conductivity in its initial state, stretched state, and shape-restored state. (b) The shape recovery process of rolled-up SMPU/MXene paper and the application as a fire-warning sensor.

1.4.5 Thermoelectric-aid fire-warning sensors

Thermoelectric (TE) materials have the ability to transform thermal energy into electricity because of the Seebeck effect, providing an alternative mechanism for fabricating an early fire-warning system by converting thermal energy into a voltage to activate a fire alarm during the pre-combustion stage [128]. Traditional TE materials account for solid inorganic semiconductors (Bi, Te, Se, and their based alloys [129, 130]), which benefit from excellent TE performance. However, these materials are typically expensive, scarce, toxic, and lack flexibility. Recently, ionic conductors, such as liquid and gel ionic conductors, have emerged as an alternative TE material due to their high thermopower [131]. Furthermore, conductive polymers (CPs) are also promising TE materials. In particular, PEDOT: PSS (poly(3,4-ethylenedioxythiophene): polystyrene sulfonate) based composites have demonstrated their high potential as TE material [129, 132-134]. To obtain a higher voltage output, TE materials are often combined in arrays containing p- and n-type TE materials to create thermoelectric generators (TEG), and some systems even work without external power supply [135, 136]. It is worth mentioning that one of the main advantages is the good reversibility of TE-based fire-warning sensor, resulting in the multiple usage for assembled fire-warning sensor, especially compared with the irreversible reduction of GO-based systems.

An instance is discussed to understand the TE-based fire-warning systems in practice better. In **Fig. 1-23**, the left section of the PI/MXene (polyimide/MXene) composite is heated (the hot side) as compared with the opposite side, which is often left at room temperature [106]. The difference in temperature triggers a voltage because of the Seebeck effect, whose magnitude depends on the temperature gradient as observed in the graph in **Fig. 1-23**. Therefore, in the practical case of a fire, the temperature difference of material caused by a real fire can generate a voltage warning signal, which could trigger a fire-warning system [107]. This alarm could be communicated wireless, which has been particularly interesting recently with the IoT development [137]. Fortunately, the applications of TE-based early fire-warning sensors have been proposed as wearable sensors to protect humans [136], detect forest fires [128], or as part of personal protective equipment for firefighters' clothing [107].

TE-based fire alarms have been implemented over the last two years. Wu and co-workers have used ionic liquids 1-ethyl-3-methyl- imidazolium acetate ([EMIm][Ac]), 1-ethyl-3-methylimi-

dazolium bis(trifluoromethylsulfony)imide ([EMIm][TFSI]) to assemble a paper-chip fire sensor, which can be triggered without external power under a flame attack [128]. However, the leakage of ionic liquids limits its further application. Additionally, driven by the excellent thermoelectric effect, the PI@MXene aerogel achieves the fire-warning within 5 s (**Fig. 1-23**) [106]. Owing to the lamellar structure of MXene nanosheets, PI@MXene exhibits fast self-extinguishing within 1 s after exposure to a flame, showing excellent flame retardancy. Both thermosensitive and strain sensors based on poly(3,4-ethylenedioxythiophene) polystyrenesulfonate (PEDOT: PSS)/ CNT / waterborne polyurethane (WPU) have been proposed [136]. PEDOT: PSS acts as a conductive binder of CNT when the composite is stretched. Surprisingly, this sensor shows a quick voltage rise response (~0.7 s) to a slight temperature difference of 5 K. The composite films can maintain stable TE performance after washing 1000 times and withstand repeated bending and stretching.

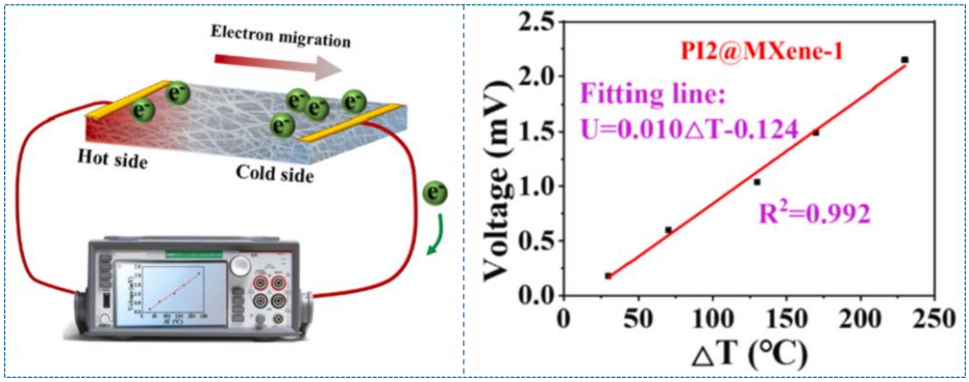

Fig. 1-23 Typical relevant TE-based early fire-warning sensors: the schematic diagram of a PI@MXene sensor and the liner fitting curve of corresponding voltage vs temperature difference.

Current trends in TE materials are in synchrony with the emergence of new technologies, such as the IoT or artificial intelligence (AI), which has led to a growing interest in wearable thermoelectric generators (WTEGs) and self-powered materials (maintenance-free power sources) [133, 136, 138]. Many applications revolve around the idea of using human body heat and strain to monitor physical signals generated by real-time human activities [136, 139], by creating fibers-based devices into woven yarns and clothing [140], and even for face masks [130].

An interesting TE-based fire-warning sensor has created a special nanocoating by combining a dermis-mimicking TE layer and an epidermis-mimicking flame retardant (FR) layer (**Fig. 1-24**) [108]. This imitates the human skin, where the dermis can detect temperature changes and send an

electrical signal to the brain. At the same time, the dermis layer is also a fire-resistant layer to protect the composite. The dermis-mimicking layer comprises the combination of silver selenide (Ag_2Se) nanorod, silver nanowire (AgNW), and polyvinyl butyral (PVB), which are spray coated over a substrate. In contrast, the epidermis-mimicking FR layer is constituted by epoxy silane-modified MMT and carboxymethyl chitosan (CCS). This fire-warning sensor presents excellent fire-warning ability within 2 s. In addition, it can trigger the fire-warning device within 2.8 s when it is re-burned and accurately measured temperature between 100 ºC - 300 ºC, displaying output voltages within the mV range. Moreover, Zeng et al. also employ a TE layer based on MXene and an FR layer composed of MMT nanosheet and 2-ureido-4[1H]-pyrimidinone-containing cellulose (UPC) via layer-by-layer assembly, which can display great alarming ability [141]. More importantly, the combined action of the hydrogen bond interactions attributed to UPC exhibits self-healing properties that can recover from damage within 24h, showing the multifunction of this system.

Another advantage of TE-induced fire alarms is that they can harvest low-quality heat from industry waste, automobile exhaust, and other unexploited heat energies [128]. In fact, in the scenario of a fire, the vast quantity of energy produced could be recycled and utilized to promote fire suppression and pollution reduction [142]. Deng et al. have proposed the Waste Heat Recovery and Utilization System, which can achieve an efficiency of the average heat flow utilization of 58 % and produce up to 692 W. This kind of fire-energy harvesting can also be used at a home scale, as fire from wood is usually used in rural areas for cooking. Heating can be exploited for micro-scale power generation using thermoelectric generators [143].

Nonetheless, current TE-based early fire-warning systems face issues that need to be tackled, such as limited preparation methods, complex structural designs, lower operating voltages, strain instability, and limitation of interfacial engineering [136, 138]. Thus, further research needs to be conducted.

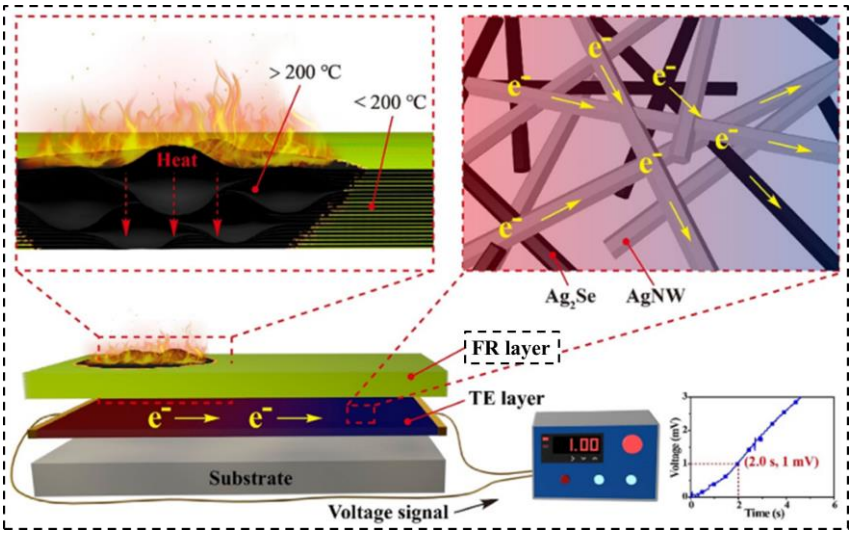

Fig. 1-24 Structural illustration of TE-based early fire-warning systems.

1.4.6 Triboelectric nanogenerator-based fire-warning sensors

An interest has been growing in triboelectric nanogenerators (TENGs) for early fire-warning systems. They have been utilized to harvest various forms of mechanical energy from the environment as a sustainable power supply [144]. The operation mechanism of TENGSs is based on the coupling effect of contact electrification and electrostatic induction [145]. A TENG usually comprises two tribo-materials, a positive and negative and electric contact, as observed in **Fig. 1-25** (a). The friction produced by an external force between these two surfaces causes the electrons to be transferred from positive to negative materials, creating an electron flow. This electrical current can be harvested and employed by connecting a TENG with an external circuit. One exciting feature for TENGs as fire-warning sensors is that they could gather other energy sources produced during a fire (wind and smoke) or human movement. Ideally, one main goal for TENGs is that they can be self-powered, i.e., capable of generating their electricity signal as a stimulus response.

One TENGs-based early fire-warning sensor is developed by combining TENGs and a thermosensitive sensor based on a polydopamine-modified GO-based sensor over hydroxyapatite nanowire paper [105]. The force applied by wind waves causes the contact between the copper electrode and a dielectric silicone sphere to generate a voltage signal. Next, the self-generating can switch LEDs on to achieve a warning under the exposure of a flame.

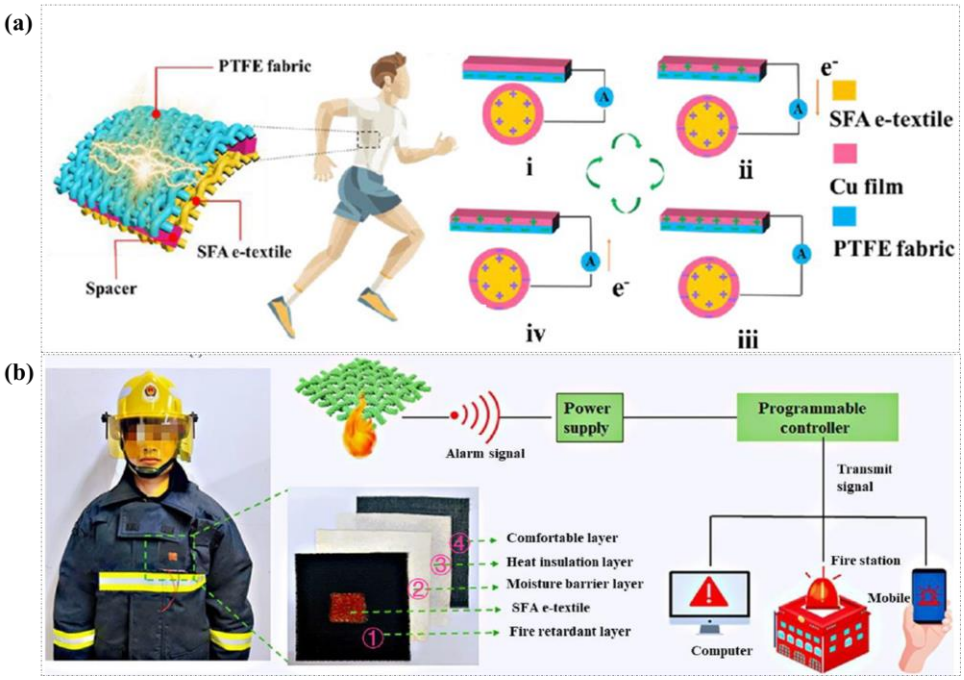

Fig. 1-25 (a) Basic electricity generation mechanism of the TENG by a vertical contact-separation mode. (b) Temperature-response resistance changes the behavior of the SFA e-textile under different temperatures, and the operating mode of the SFA e-textile as a fire alarm material in firefighting protection.

Hybrid energy harvesters, based on TENGs, provide a promising method for energy harvesting as well as fire sensing. Portable and wearable electronics are an emerging field due to the synergistic effect benefiting from the energy-producing during movement. Textiles can work as a substrate for self-powered wearable electronics, where vital research has been aimed toward wearable triboelectric nanogenerators [105]. He et al. have fabricated an ultralight self-powered fire alarm electronic textile (SFA e-textile) based on conductive aerogel fiber that comprises calcium alginate (CA), Fe_3O_4 nanoparticles (Fe_3O_4 NPs), and lightweight silver nanowires (AgNWs), which can work as the triboelectric positive material. The TENG is assembled with the interaction with a triboelectric-negative polytetrafluoroethylene (PTFE)-coated CF.

Interestingly, this e-textile allows a synergistic approach by obtaining accurate temperature monitoring and energy harvesting in firefighting clothing. SFA e-textile is integrated as an extra layer into firefighting protective clothing, and sensing different temperatures between 100 °C - 400 °C are repeatedly measured. This temperature detection can be transmitted, and an alarm sign could be triggered to protect the integrity of firefighters, as observed in **Fig. 1-25** (b). In addition, a

self-powered fire self-rescue location system is further established based on the SFA e-textile that can help rescuers search and rescue trapped firefighters in fire cases, as they can be identified in real-time.

1.5 Objectives of the thesis

Fire-warning sensors' development remains at the early stage, limiting available materials, sensitivity optimization, intelligence development, etc. The optimization of fire-warning sensors still faces a challenge. Therefore, this thesis aims to rationally design highly sensitive early fire-warning sensors with some advances, especially in terms of response temperature, response time, signal transmission, and sustainability. Specifically, the main objectives are as follows:

1) To design functionalized GO-based low-temperature early fire-warning sensors

2) To develop bio-based smart, highly efficient fire early warning sensors

3) To investigate the mechanism of low-temperature fire warning

4) To exploit a reusable bio-based smart early fire-warning sensor

CHAPTER 2

Materials and Experimental Techniques

"Imagination is more important than knowledge."

-Albert Einstein

2.1 Materials

GO powder was purchased from Changzhou Sixth Element Materials Technology Co. Ltd (China). Ti_3AlC_2 powder (MAX) was provided by Changchun Jilin 11 Technology Co., China. GO suspension was purchased from Grupo Antolin company. Modified carbon nanotube power (NH_4-CNT) was supplied by XFNANO Co., China. CS powder was provided by Fluorochem Ltd. The following chemicals were supplied by Sigma-Aldrich Chemical Co.: 2-(Diphenylphosphino) ethyltriethoxysilane (ETS), N, N-dimethylformamide solution (DMF, ACS reagent, 99.8%), Lithium fluoride powder (LiF), hydrochloric acid solution (HCl, ACS reagent, 37%), Phenyltrimethoxysilane (PTS), Phytic acid (PA) solution (50% (w/w) in water), hydrochloric acid (37%) (HCl), Trimethoxymethylsilane (MTM) solution, poly(ethylene oxide) (PEO), Sodium chloride (NaCl), ammonium chloride (NH_4Cl), calcium chloride ($CaCl_2$) powders, and Acetic acid solution (≥ 99 %). Cellulose paper was the common paper being covered on the table. Deionized water was obtained by the water purification system in the laboratory.

2.2 Experimental techniques

Fourier transformation infrared spectroscopy (FTIR)

FTIR spectrum from 400 cm^{-1} to 4000 cm^{-1} was collected using a Thermofisher Nicolet 5700 spectrometer with ATR mode (TA Instrument). The background spectra were recorded before measuring each specimen. The influence of background can be automatically deducted when every sample is tested. Software of OMNIC was utilized to analysis FTIR results.

X-ray diffraction spectroscopy (XRD)

XRD curves were obtained using the Philip X' Pert PRO diffractometer (Empyrean, PANalytical) with Cu Kα (λ=0.154 nm) radiation and Ni filter. The working voltage and current were 45 kV and

40 mA, respectively. Particles were crushed into the homogeneous powder before testing. The testing program with a scan angle range from 5°-70° was applied, and it took about 15 min for each test. Data-viewer software was used to convert the curves.

Atomic Force Microscope (AFM)

The surface roughness and performance of films were tested by AFM (XE-150) equipment. The sample is a square with a length of 1 cm. The film was scratched on the NSCRIPTOR DPN system in contact mode using an AFM tip. The chosen point was varied to control the force between the tip and the films. All the tests were employed at room temperature.

Scanning electron microscopy (SEM) and energy-dispersive X-ray spectroscopy (EDS)

SEM images were obtained by using equipment of EVO MA15 from Zeiss company. The working voltage and current were 5 kV and 0.69 nA, respectively. Insulating specimens were sprayed with a gold layer via a Sputting machine before SEM scanning. EDS element mapping was acquired by the collaborative using the instrument of EVO MA15 and dispersive X-ray spectra (EDS) (Oxford INCA 350).

Transmission electron microscopy (TEM)

TEM images were received by using transmission electron microscopy (Tecnai T20, FEI). The operation voltage and current were set based on the actual condition. Each specimen was dispersed in the organic solvent for a homogeneous solution under ultrasonic treatment before being dropped on the copper grid.

Differential scanning calorimeter (DSC)

DSC curves were obtained by using the Q200 instrument from the TA company. The measuring program was as follows: (1) heating from 30 ºC to 190 ºC at a rate of 10 ºC/min; (2) cooling from 190 ºC to 30 ºC at a rate of 10 ºC/min; (3) heating from 30 ºC to 200 ºC at a rate of 10 ºC/min. Each sample with about 5 mg was tested based on the mentioned program. TA software was applied to analysis the results.

Thermogravimetric analysis (TGA)

TGA curves were recorded using a Q50 instrument from a TA company under an air atmosphere or nitrogen environment. Approximate 5 mg of sample was measured according to the following

program: heating from 50 ºC to 750 ºC at a rate of 10 ºC/min.

Dynamic mechanical analysis (DMA)

Dynamic mechanical behavior and stress-strain curves of specimens were performed using a stretch model using a Q800 machine from TA company (USA). The sample size was around 15 mm × 5 mm × 0.2 mm. For dynamic mechanical behavior, each specimen was measured with a temperature rising from -120 ºC to 25 ºC at 2 ºC/min at a frequency of 1 Hz. For the tensile property, stress-strain curves of specimens were recorded at a rate of 0.1 N/min under room temperature. Each specimen was tested three times to check its stability.

Raman Spectroscopy

Raman spectra from 1000 cm^{-1} to 3500 cm^{-1} were acquired using the Raman microscopy system of Renishaw PLC with 50 mW. The laser with 532 nm wavelength was operated. Wire 4.1 software was applied to fit the peaks and calculate the area of the peaks.

Micro combustion calorimeter (MCC)

MCC results were recorded using MCC from the UK, FTT company (**Scheme 2-1** (a)). The working mechanism is mainly based on detecting oxygen consumption, described in **Scheme 2-1** (b). This machine's heating combustion for consuming 1 g of oxygen was fixed at about 13.1 KJ. The anaerobic thermal-degradation products were mixed with oxygen flow prior to conveying to the combustion furnace at 900 °C. Each specimen was tested three or four times under a nitrogen atmosphere. Combustion parameters about samples, especially the peak of heat release rate (HRR, W/g), were obtained by the software.

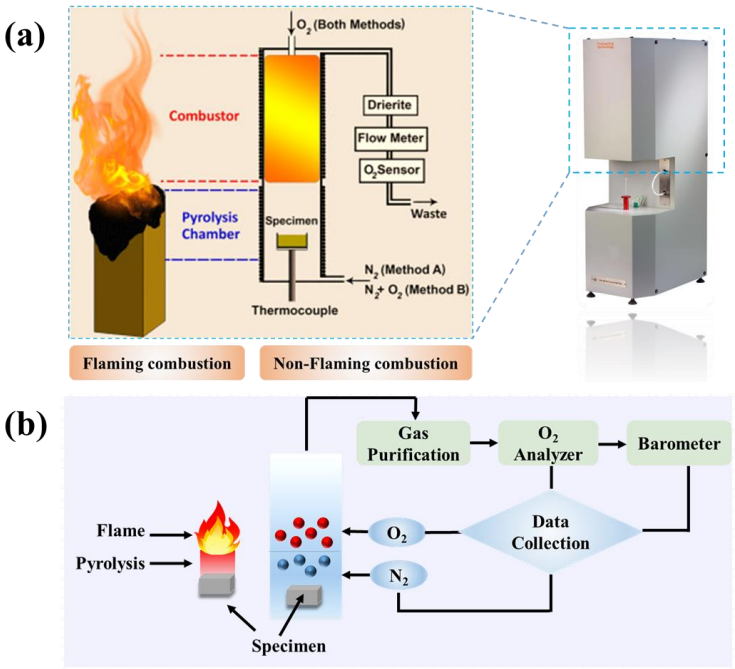

Scheme 2-1 (a) Description of core components of MCC;(b) Schematic description of MCC.

Electric resistance test

Electric resistance changes were made using a digital multimeter of model 3458A from Keysight Technologies Inc. Combined with an oven that controls temperatures, curves about electric resistance changes were obtained as a function of time. In addition, specimens' electric current changes were obtained by combining a digital multimeter and a low-noise current preamplifier of model SR570. Each sample's size tested in every system is consistent for this measurement.

Emission spectrum test

Light intensity changes of the warning lamp during the fire-warning process were detected using the connected electric pathway that includes an oven, an LED lamp, a power supply, a detector, and a computer (**Fig. 2-1**). The software of AvaSoft 8 was performed to analysis the results.

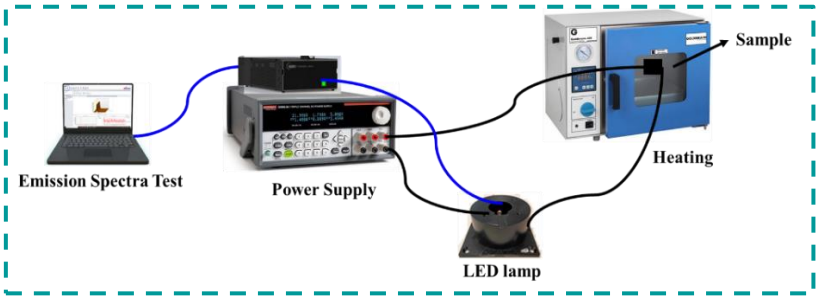

Fig. 2-1 Schematic emission spectrum test process for fire-warning samples.

X-ray Tomography technique

X-ray tomography (Nanotom 160NF, Phoenix, GE) technique was carried out to study the structural change of samples. The tomograms were collected at 90 kV and 80 μA conditions using a Mo target. The film sample was placed between two plastic sheets to fix the film better.

Suction filtration technique

Film-based specimens were prepared using the suction filtration technique, shown in **Fig. 2-2**. The filter paper is made of nylon membranes with a pore of 0.22 um and a diameter of 47 mm. In a specific system, the selected volume for each sample is identical to ensure the same thickness.

Fig. 2-2 Schematic illustration for suction filtration technique.

Signal transmission technique

The communication system here is an application based on the IoT, which will allow advising the fire danger by sending a message displayed on one of the IoT websites, particularly on the TTN website. The third and last output of the wireless transceiver R080A is connected to another wireless system based on the LoRA communication protocol. LoRA emitter is the MKRWan 1300 board programmed with the IDE Arduino interface. Once the LoRA emitter is activated by the third wireless receptor system R080A output, warning messages programmed in this LoRA emitter are sent periodically to the air, with time lapses of 2 seconds, depending on the number of bytes used in the message. Moreover, these messages are received by a gateway that could detect all the information coming out from the remote emitter and incorporate all the received information into the internet. The gateway is an RAK 2245 Raspberry Pi Hat coupled to a Raspberry PI 4 with a specific antenna typical of LoRA communications. RAK2245 is installed and programmed with the Raspberry Pi 4. It aims to collect messages to resend them to any Wi-Fi network so that information can be monitored in the TTS platform, which is the new update of the TTN network. LoRa emitters

can be separated 20 km long from the gateway in interurban areas, up to 200 km in regions without electromagnetic interference, and up to 1000 km in highly clean radio waves and open places such as Outer Space. As reported above, information can be visualized in any IoT platform, such as TTS, which aims to inform messages to the whole population for evacuation.

There are four stages to simulate wireless signal conversion described below:

(1) The detection of the conductivity change

The four-wire electrode method is used to measure the films' conductivity. First, the film is crabbed by two electrodes (power electrodes), separated 6 cm between them. Their other ends are connected to an electrical power source (PeakTech P6227). The other two clips wielded to the ends of another pair of cables work as electrodes and crab the same film. They are placed between the two power electrodes and are separated by 3 cm. These two electrodes work as sensing electrodes and measure the voltage and current flowing along with the samples.

(2) The activation of a wireless system

Sensing electrodes are connected with their opposite ends to the analogue inputs of a Data Acquisition system, which is designed with an Arduino ONE that plays the role of an ADC (analogue to digital converter) by activating (rising its voltage output from 0 V to 5 V) one of its digital outputs to HIGH state according to the voltage threshold programmed in the board. This activation is performed only when the voltage threshold reaches one fixed value or range of values. It's dependent on the sample's conductive state after being heated in a furnace or a flame. One of the analogue inputs of the ADC receives the input voltage from two sensing electrodes. Once the value reaches the voltage threshold, the digital output will change to the HIGH state. The voltage threshold is highly related to the film's conductivity, which depends on reducing the film in a furnace or under a flame. This means that the voltage threshold is based on the temperature the furnace or flame reaches. It allows activating one of the ADC outputs, rising its voltage from 0 V to 5 V (LOW->HIGH). The final voltage threshold is obtained by using the ADC conversion of 5 V to 1024 steps according to the following formula:

$$V_{threshold} = \frac{1024}{5V} x V_{selected}$$

Once $V_{threshold}$ is obtained, the LOW ADC output channel changes to the HIGH state,

increasing voltage to 5 V. This channel is connected to a Wi-Fi emitter that needs 5 V of electrical supply to send a remote activation signal to the Wi-Fi receptor.

(3) The Wireless receptor and the initiation of the sound/light alarm, the LCD, and the LoRA communication system

Once conductivity reaches the desired value, the wireless receptor will be active, and one of its output channels will supply 5 V and 70 mA to switch on the sound-light fire alarm. Furthermore, another output of the Wi-Fi receptor will provide voltage to a LoRA emitter programmed with IDE software. Once one of its inputs receives a characteristic threshold voltage, it will emit a message. In this setup, this threshold voltage is 5 V, corresponding to one of the Wi-Fi receptor outputs, which will be activated by the temperature of a furnace or a flame and the voltage programmed in the ADC (**Fig. 2-3**). As reported before, the LoRA emitter (MKWan 1300) can be separated from the LoRA receptor at distances up to 20 km from the emitter in interurban areas, has very low consumption, and signals are remotely transmitted.

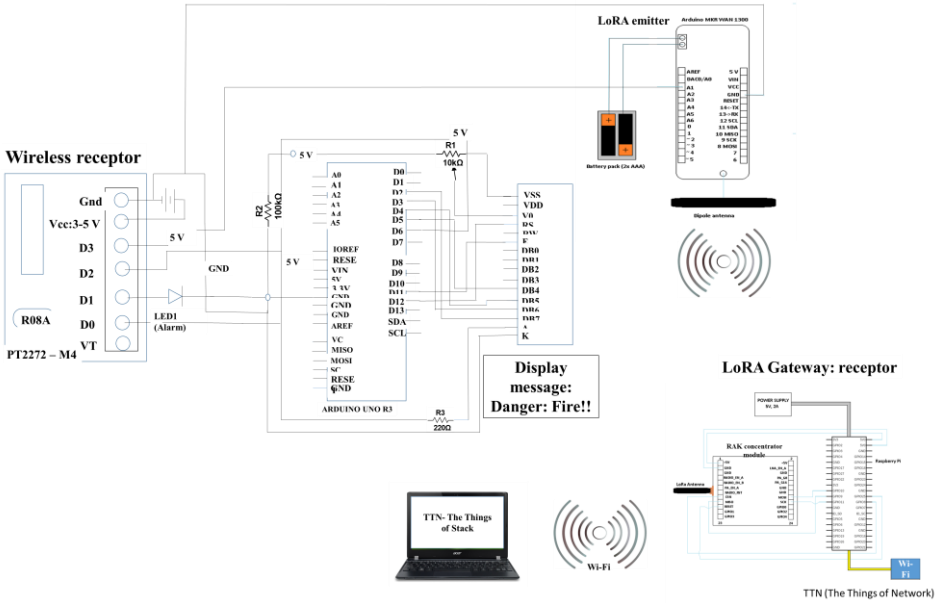

Fig. 2-3 Schematics of the reception modes: receptor R080A connected to the following devices: Arduino display, Sound and LED Alarm, LoRA emitter (MKWan 1300) and LoRA gateway receptor (RAK and Raspberry Pi) which is connected to the internet via WiFi.

(4) The LoRA receptor gateway

LoRA receptor is a gateway designed with an RAK 2245 Raspberry Pi Hat coupled to a Raspberry PI 4 board connected to the internet by Wi-Fi. This warning message can be read in any

of the LoRA IoT platforms, such as TTS, and any user can access a cell phone, a PC, or any electronic device connected to the internet by creating a TTN account in the TTN platform. Therefore, anyone worldwide with internet access may read the warning message. Herein, the warning message can be displayed simultaneously on the screen of the PC and multiple laptops, either the sound-light alarm switches on and beeps or the corresponding message displays in the LCD programmed with the open-source IDE software. This application is one of the most relevant implemented in the protection and security fields and uses high technology development in communications, electronics, information, and technology. It can be integrated with any IoT deployments where low-powered devices such as the LoRA emitters and gateways efficiently communicate with Internet-connected applications over long-range wireless connections.

Wireless conversion device design

With the aim of remote monitoring fire situations to better control fire, a novel wireless signal conversion and communication device has been designed to process the signal obtained from the fire warning system. The design is mainly based on communication between a Wi-Fi transmitter (**Fig. 2-4** (a)) and a Wi-Fi receptor (**Fig. 2-4** (b)). PeakTech P6227 is the electrical power supply. It's two outputs are used as force electrodes: the positive (Force＋) is connected to one side of the fire-warning paper, and the negative one (Force -) is placed opposite this electrode. Two sensing electrodes (Sense + and Sense -) are placed in the middle of the paper, such that there is no contact between force electrodes. In addition, the ending parts of two sense electrodes are connected to the Arduino's ground and analogue channel (i.e., A0), which is programmed according to the application used. A threshold is established according to the material's response temperature. A fire warning message would be sent by a Wi-Fi transmitter. The microcontroller of the Arduino board, used as an analog-to-digital converter (ADC), reads the changing voltage and converts its continuous magnitude to a number between 0 and 1023, equivalent to 0 V and 5 V.

Two voltage parameters supplied by the source and threshold or number of steps (voltage measured) for ADC should be considered. If a maximum number of 1023 is chosen, the temperature selected to activate the warning system would be the maximum measurable value for the voltage supply selected. Furthermore, because of the electrical noise existing in the board, the minimum number of steps corresponding to a minimum detection of voltage signal (maximum temperature)

is 270. In our configuration, the voltage of the power supply used is 5 V, and the number of steps is 870, corresponding to a voltage detected of $V = \frac{870x5V}{1023} = 4{,}27\ V$ and the response temperature.

The maximum distance between the Wi-Fi receptor and transmitter is approximately 2 km. The radio frequency signal is 433 MHz. Several receptor-transmitter units could be positioned at different distances and used as repeaters to obtain higher transmission distances. Communication between Wi-Fi modules and channels is the following: DataTi-> DataRi, with DataT the transmitter channel, data, the data received by the receptor, and i the number of channels going from 0 to 3. In addition, the receptor channel DataR0 is connected to an Arduino UNO with a Liquid crystal display (LCD) screen in this work, which shows "NORMAL" in normal state and "FIRE DANGER" (or any other message programmed) in abnormal temperatures. The LCD working principle is based on the Liquid Crystal Library, making it easier to configure and control the characters displayed on the screen without dealing with low-level basics of how it works.

Here, another threshold is programmed in the Arduino UNO board connected to the LCD. If the analog channel (i.e., A0) does not receive any signal, the message in the interface would be "NORMAL." However, if the threshold read by this channel is the maximum (1023, corresponding to a voltage of 5V), the message displayed will change to "FIRE DANGER."

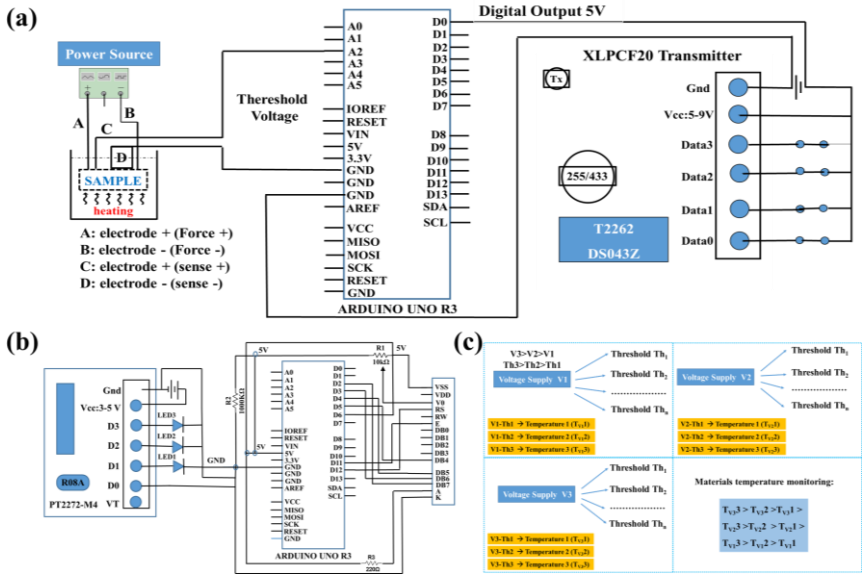

Fig. 2-4 (a) Schematics of Wi-Fi ADC-transmitter for receiving alarm messages and sending Wi-Fi signal. (b) Schematics of Wi-Fi receptor R080A and the Arduino connected to three LEDS and a LCD receiving above Wi-Fi signal for showing an alarm message on the screen. (c) Working process description of the fire warning system related to the threshold programmed in the ADC and voltage supply used.

A photoresistance sensor detection technique

Remote communications, an important part of signal transmission for fire alarm systems, play an essential role in warning effectiveness. An integrated self-designed wireless conversion device is developed for smart signal transmission. Firstly, the four-wire method detects the film's conductivity by measuring the voltage difference between two points and two electrodes. The sample's voltage drop is initially measured with the analog input channels of an Arduino UNO operating as a voltmeter. Once a fire happens, material conductivity increases to the voltage threshold programmed in Arduino. As a result, the voltage drops of the sample increases. Intriguingly, a brightness sensor simultaneously monitors fire-induced brightness change locally and remotely by the internet.

Wi-Fi Emitter XLPCF20 is activated once the film becomes more conductive. The remote signal is emitted and received by the Wi-Fi receptor R080A, which connects two electronic systems. One is a display programmed with Arduino, and the other is a LoRA emitter MKRWAN1300. When the sample's conductivity increases over the threshold, the LoRA emitter will send the same warning message to the internet. In addition, the RAK 2245 Raspberry Pi Hat connected to a Raspberry Pi 4 is a gateway to send messages remotely via Wi-Fi to the TTS platform website.

A photoresistance sensor is placed near the film to monitor the surrounding brightness. It allows the detection of real-time intelligence caused by the flame. The photoresistance sensor works based on the resistance change induced by light variation. If no light appears, this value is high and decreases with increased brightness. Theoretically, photoresistance precision is 0.1%, and its minimum value or sensitivity is 0.1%, as calculated in SI-2. The brightness range goes from 0% (no light) to 100% for high brightness. A very low percentage corresponds to a high voltage value (5 V in our case) measured by the Arduino Analog Digital Converter (ADC). On the contrary, when brightness becomes high, photoresistance becomes low, the electrical current becomes high, the voltage output of the ADC is near 0 steps, and the percentage is near 100 %. Moreover, flame brightness is monitored with a calibrated Avasphere 30-Irrad integrated sphere (Avantes), and a calibration curve of brightness vs. photoresistance signal is obtained.

A temperature sensor detection technique

Different devices contribute to communicating the data from the heat source to the final user. Both sensors - a photoresistor and a thermocouple - are placed close to the fire-warning paper to provide

a faster response. They are connected to a microcontroller, i.e., MKRWAN1300, to send the data they provided. The microcontroller's serial port is used to visualize the temperature and luminosity values locally utilizing a computer, while additional modules are added to the microcontroller for remote communication.

Specifically, an ESP8266 WiFi board is physically connected to the microcontroller for the luminosity data. The data is sent to the WiFi network by introducing the network SSID and password in the WiFi board through the microcontroller. Furthermore, an HTTP link is generated to enter the web to read luminosity values from any device with internet access. The local monitoring allows higher acquisition rates (> 1 Hz) compared to the ones detected remotely (1 Hz). It is important to note that both communication systems (local and remote) run at the same time.

For the temperature data, an Arduino MKRTherm shield is coupled into a LoRA emitter MKRWAN 1300; a wireless method shown in our previous works [15, 16, 53]. However, the MKRTherm module has never been used before for this LoRa application and with luminosity sensors. Temperature data is sent remotely to an RAK2245 Pi Hat concentrator, which operates as a gateway and receives all the packages emitted by the MKRWAN1300. The RAK is also connected to the WiFi network; data can be visualized in the TTS platform. Ubidots IoT software is programmed to be associated with TTS to plot the temperature line versus time. This protocol allows the emitter and receiver to be separated up to 20 - 30 km in interurban areas and 2 km in urban ones, depending on the electromagnetic pollution, increasing the transmission distance and drastically reducing the power consumption compared to other remote communication protocols. Based on the above working principle of this warning communication system, once the wallpaper situation changes caused by a flame, the luminosity and temperature are monitored, providing precise information to the operators about the potential danger.

A humidity sensor detection technique

The oven with controlled temperature and humidity is used here to simulate the humid environment. Environmental and film humidity are monitored when the film is wetted in the climatic chamber. In addition, real-time temperatures are also measured. This work integrates Wireless-Fidelity (Wi-Fi) and Long Range Radio (LoRa) communications for data transmission. Wi-Fi can transmit at high rates, reaching tens of meters at some hundreds of Hz when 2.5 or 5 GHz bands are used. Meanwhile,

LoRa, in the sub-GHz band, can send information at a few Hz but at 20 km distances from the emitter in interurban areas.

(1) Wi-Fi monitoring of environmental humidity and temperature

The Osoyoo Esp8266 Arduino Internet of Things (IoT) board monitors environmental humidity and temperature. DHT11 sensor is connected to the Esp8266 Wi-Fi shield attached to the main board to monitor temperature and humidity. This connection is performed between the D2 pin of the board and the S pin of the sensor, the same as Ground to Ground and 5V to the positive pin. Once the DHT11 library is installed with the IDE of Arduino, real-time temperatures and humidities measured by the DHT11 sensor inside the climatic chamber can be sent via Wi-Fi to the cloud. The IoT application utilizes an http link to visualize the detected temperatures and humidities via this link.

Furthermore, the Esp8266 board is directly connected to the computer through a USB port. Changes in temperature and humidity are recorded locally using the MegunoLink software and plotted as curves against time. These changes can be sent remotely using the Wi-Fi at the same time. Our previous works reported a similar connection [146, 147]. However, the detection of electric current for salt-modified CS-based films as fire-warning and humidity sensors has rarely been reported, especially when combined with LoRa (Leird and MKRWAN1300) simultaneously.

(2) LoRa monitoring of environmental humidity and temperature

Apart from the DHT11 sensor, the Seed Studio Grove moisture sensor is also employed. It is connected to an MKRWAN1300 LoRa emitter wrapped by films, which is associated with an MKR connector carrier and placed in the climatic chamber to monitor the humidity change of the film. However, no significant humidity change of CS-NaCl film is observed in the IoT LoRa interface (The Things of Stack). This might be associated with the limited water-holding capacity for CS-based films within a short-term test, which depends on the deacetylation degree of CS [148, 149].

The connection between the Seed Studio Grove and MKRWAN1300 LoRa emitter shows that the detected temperature and humidity values are sent under LoRa protocol to the open air. At the same time, the RAK2245 Pi Hat concentrator as a gateway receives the emitted data packages. In addition, the RAK2245 Pi Hat concentrator coupled to a Rasp-Berry PI can visualize detected information in the LoRa IoT platform (The Things Stack (TTS)) by providing the percentage of humidity values in the TTS platform.

Another new IoT LoRaWAN sub-GHz (868 MHz) named RS186 Sentrius sensor placed inside the climatic chamber allows monitoring humidity and temperature simultaneously under LoRa protocol. It transmits environmental temperature and humidity online and in situ every 10 s at long distances (20 km in interurban areas). Similarly, these physical magnitudes can be visualized on the internet via the TTS platform of any electronic device. Detected messages are monitored in the IoT http link remotely and locally using Megunolink and LoRa TTS measured from Sentrius sensor always coincide. These set-up measures offer a new pathway for potential functional sensors.

CHAPTER 3

Graphene oxide-based fire-warning sensors

"Life is like riding a bicycle. To keep your balance, you must keep moving."

-Albert Einstein

3.1 Tailored P/Si-decorated graphene oxide (GO)-based fire sensor

3.1.1 Introduction

Humans' deep knowledge of fire development gradually enables them to take various fire controls. However, despite many efforts, this capability to control fires is still imperfect [1]. As a result, controlling fire initiation and propagation is still a considerable challenge.

One available fireproof method is the fire-warning strategy [8, 14]. To implement reliable monitor and efficient regulation, highly sensitive fire alarms to monitor fire characterizations at the beginning of fire development are still under research. However, some studies are already reported [101, 114]. Most operate by detecting abnormal situations before a fire breaks out and sending alerts to the public through traditional information dissemination. The working process, working stability, and signal transmission are necessary for early fire alarms. According to these, Xu et al. reported a fire alarm based on melamine-formaldehyde sponges, which were wrapped by GO wide-ribbon compounded from unzipping carbon nanofibers, displaying a fast response of 33 s at 300 °C [104]. PU foam decorated with ammonium polyphosphate and GO and surface silane function was employed as a fire alarm with a response time of 11.2 s at 300 °C [103]. Apart from these studies, other fire-warning systems also respond quickly, but at or above the critical ignition temperature because ignition temperatures of most conventional flammable materials are around 300 °C - 500 °C [123, 150, 151]. There is still a risk for flame propagation that commonly occur within seconds when a fire is about to enter a full fire development stage [104, 152]. Hence, it is an urgent challenge to construct highly sensitive fire alarms that respond to temperatures below ignition temperatures (< 300 ° C), which would earn more evacuation time and minimize casualties and losses.

Internet technology has developed dramatically during the last few years. Most scientific fields demand online monitoring and sensing. For this reason, novel strategies related to internet technology have been proposed to detect fire. Traditional lamps and sounds used in fire-warning systems can transmit fire-warning signals to the public. However, this signal transmission can only detect fire and alert a small area near the target fire. More people can be guaranteed to take measures against fire disasters if large-scale warning signals can be transmitted. Until now, there has been little research on smart signal conversion. Therefore, the large-scale transmission of monitored fire signals through the internet is desirable. The wireless signal transmission part has been optimized to obtain a real-time warning message and is discussed in the following section.

Due to the advantages, LBL technology has been used to synthesize advanced materials, particularly in multi-functional films with nanometer-structural areas [153-157]. Firstly, the chemical component and structure of films are precisely controlled by a pre-designed solution, which allows the incorporation of other materials to generate one multi-functional film [153, 158]. Secondly, a mild and flexible preparation will create a functional layer on the substrate's surface or a large area of self-standing film. GO is widely known to be sensitive to temperature, making it an ideal candidate for temperature-based sensors, such as fire alarms [68, 71, 72, 159]. It is convenient to prepare multi-functional GO-based film by LBL because of its excellent dispersibility in water, film-forming ability, low-time consumption, and low damage to its inherent properties [50, 160, 161]. Therefore, the freestanding membrane with unique structures fabricated by LBL technology is highly promising in fire alarm applications.

According to the above description, a novel fire-warning film consisting of GO and flame retardant containing P and Si is investigated by the LBL strategy to develop a next-generation smart early fire sensor in this chapter.

3.1.2 Preparation and characterization of tailored-thickness fire-warning films

An aqueous GO suspension of 4 mg/ml was prepared for usage. ETS was diluted with DMF to prepare the homogeneous solution. These two solutions were mixed and continuously stirred for 0.5 h. Next, the GO@ETS-y films with tailored thickness are prepared by adjusting the pre-designed solution volume, where y means the different thickness, following the fabrication shown in **Scheme 3-1**. The detailed composition is shown in **Table 3-1**.

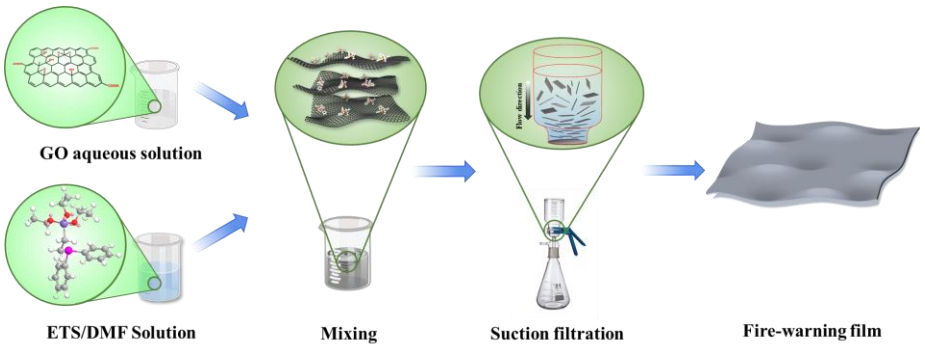

Scheme 3-1 The schematic fabrication process of the fire-warning film.

Table 3-1. Components of tailored-thickness fire-warning samples.

Samples	GO Concentration (mg/mL)	ETS Concentration (mg/mL)	Total Volume (mL)
GO@ETS-1	4	10	4
GO@ETS-2	4	10	8
GO@ETS-3	4	10	12

The introduction of ETS causes structural change. GO@ETS-y films with different solution volumes appear to have similar structural change trends. XRD, Raman, and SEM results of GO@ETS-y films are depicted in **Fig. 3-1**, confirming the increased layer thickness. Compared with the pristine GO paper, the diffraction peaks of GO@ETS-1, GO@ETS-2, and GO@ETS-3 shift to a low angle (**Fig. 3-1** (a)). The increased layer distances result from more intercalated ETS contents in GO flakes. Additionally, I_D/I_G values from Raman results agree with XRD results. There is no obvious difference in graphitization degree between GO@ETS-1 and GO@ETS-2 (**Fig. 3-1** (b)). When the solution volume increases to 12 ml, the I_D/I_G value of GO@ETS-3 film becomes 2.48, which indicates a more structural disorder [63]. SEM images confirm the layer thickness difference among different samples in **Fig. 3-1** (c). The layer thickness gradually increases with increased solution volume, according to the following: GO@ETS-1 < GO@ETS-2 < GO@ETS-3. To check whether the changed structure affects the warning performance, related tests will be carried out, and the results will be further explored.

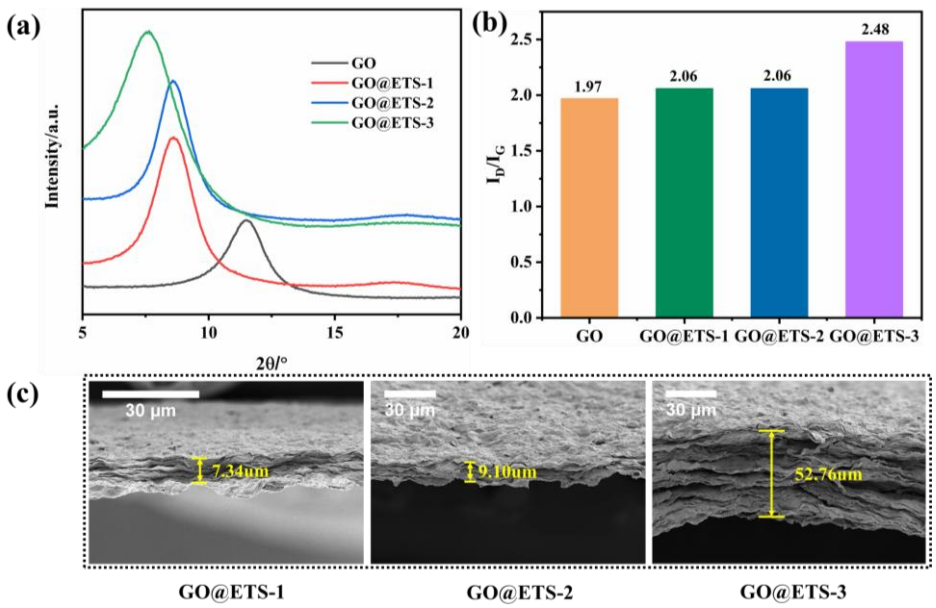

Fig. 3-1 Characterizations of tailored-thickness multi-layered structure for GO@ETS-y films: (a) XRD patterns; (b) I_D/I_G ration obtained from Raman spectra; (c) cross-section SEM images of GO@ETS-y films.

3.1.3 Electric resistance changes of tailored-thickness fire-warning films

The electrical resistance change rate is strongly relevant to the sensitive response of the fire-warning systems. To explore the warning ability at below temperatures, test temperatures of 150 ºC, 200 ºC, and 250 ºC are selected. Corresponding electrical resistance curves as a function of time are shown in **Fig. 3-2** (a), (b) and (c). The electrical resistance of films gradually decreases after a long exposure time to each test temperature. The electrical resistance of each fire-warning sample exhibits the same change tendency. However, the electric resistance change speed is different, which can be used to determine the sensitivity of the fire alarm. Because GO@ETS-y films with different thicknesses demand additional energy to vary their conductivity. In the case of GO@ETS-1, a shorter time to reach the low electric resistance value is needed than GO@ETS-2 and GO@ETS-3 at the same test temperatures.

Furthermore, higher test temperatures will provide more energy to realize the conductivity variation. Higher test temperatures can accelerate electric resistance change to reach low electrical resistance to trigger conductive pathways, resulting in a shorter response time for fire alarms. All fire-warning samples only take several seconds to achieve a lower electrical resistance value at 250 ℃, being sensitive to obtain more evacuation time.

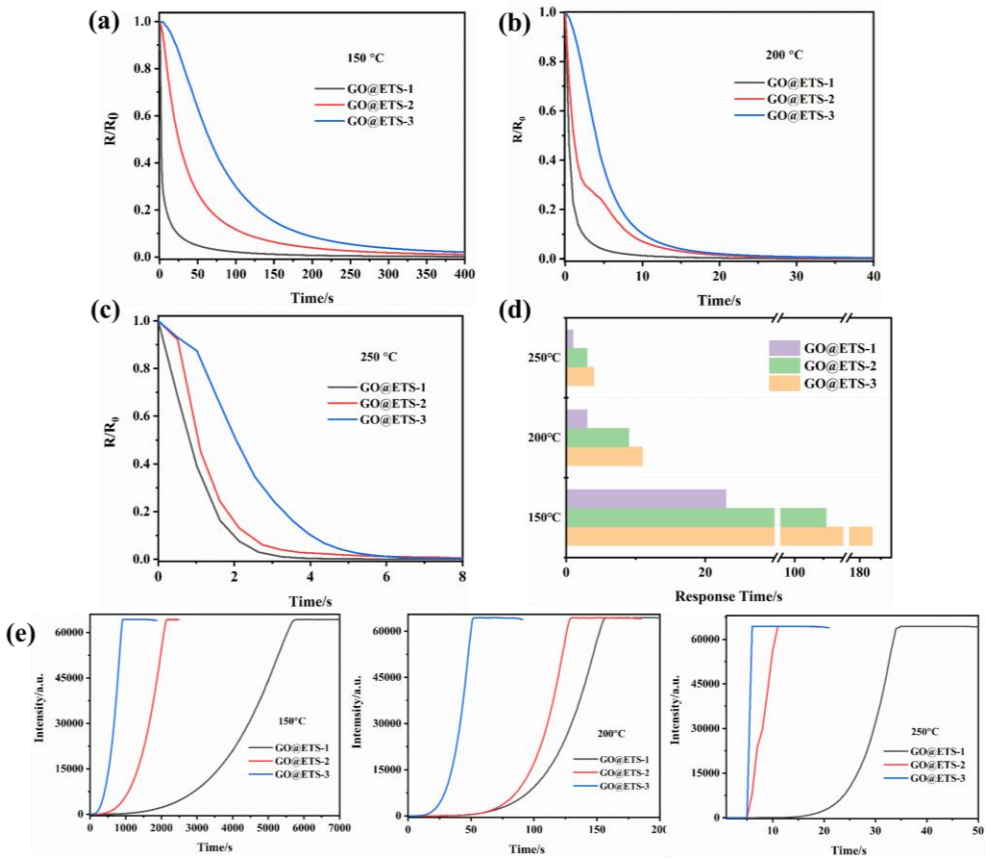

Fig. 3-2 Electrical resistance changes at different test temperatures with time: (a) 150 ºC, (b) 200 ºC and (c) 250 ºC. (d) Response time based on trigger electric resistance. (e) The light intensity change curves of all GO@ETS-y films as a function of test time.

"Trigger electric resistance" can guarantee the formation of the conductive pathway. Response time based on "trigger electric resistance" for the fire alarm can illustrate its sensitivity directly, as presented in **Fig. 3-2** (d). The response time follows this sequence: GO@ETS-1＜ GO@ETS-2 ＜ GO@ETS-3 at each temperature. At 250 ℃, all the response times are within a few seconds, showing high sensitivity.

Notably, compared with the warning temperatures and response time reported in previous works, this fire sensor presents better sensitivity at a lower temperature than at ignition temperature (**Table. 3-2**). The response time of GO@ETS-3 is only several seconds, which demonstrates the ability of a thick fire-warning nano-coating layer to provide a rapid warning. From a practical point of view, this high sensitivity can take extra time when a real fire occurs. As mentioned above, thick films need more energy to reach low electric resistance to trigger the alarm. More electric current should be provided to switch the lamp on. As a result, light intensity change curves of different

tailored-thickness GO@ETS-y films recorded by the avaspec-2048L spectrometer machine are presented in **Fig. 3-2** (e) to demonstrate this phenomenon accurately. At each test temperature, the higher light intensity is achieved using GO@ETS-3 in the electrical circuit compared with the other two samples simultaneously.

Table 3-2. Comparison of detailed information and fire response time between our fire sensor and other fire sensors.

Substrate materials	Modified materials	solvents	Flame Response Time / s	Response temperature / ºC	Ref.
Melamine-formaldehyde sponge	GO/CNFs wide-ribbon wrap	water	33	300	[104]
Polyurethane foam	APP/GO/Silane	water	11.2	300	[103]
GO	3-MPMS/LAA	water	7	300	[100]
Color changing molecular sensor	a Pcs-precursor molecular sensor containing a phthalonitrile structure	the acrylic latex paint	20	275	[123]
GO network	PEG/MMT	water	160	250	[162]
Polyurethane foam	GO/silicone resin	alcohol	415	200	[102]
GO	MPTS	water	232	200	[93]
GO	ETS	water	***1***	***250***	***this work***

[a] CNFs: carbon nanofibers; APP: ammonium polyphosphate; 3-MPMS: 3-methacryloxypropyltrimethoxysilane; LAA: L-ascorbic acid; PEG: polyethylene glycol; MMT: montmorillonite; MPTS: 3-mercaptopropyltrimethoxysilane; ETS: 2-(Diphenylphosphino) ethyltriethoxysilane

3.1.4 Response of fire sensor during the simulated fire scenario

A fire scenario simulation is performed to clearly explain the working process of the fire sensor under the actual fire conditions. The results are shown in **Fig. 3-3**. The lamp is off initially because fire-warning samples present the insulation state at room temperature. There is no current going through the electrical circuit. Once the fire-warning film is heated by flame, the lamp turns on within 1 s. This is attributed to the rapid conductivity transformation from GO to RGO. After being attacked by fire for longer, samples become more conductive to afford brighter lamplight. This mini fire-warning simulation illustrates the work process and provides a theoretical basis for applying fire sensors to a certain extent. In addition, the intensity of the lamp for different warning films is visually different at the same time. It might be because of environmental factors and visual limitations, demonstrating the limitation of using traditional lamps as a response signal. That is why an intelligent response device to send fire information is urgently needed.

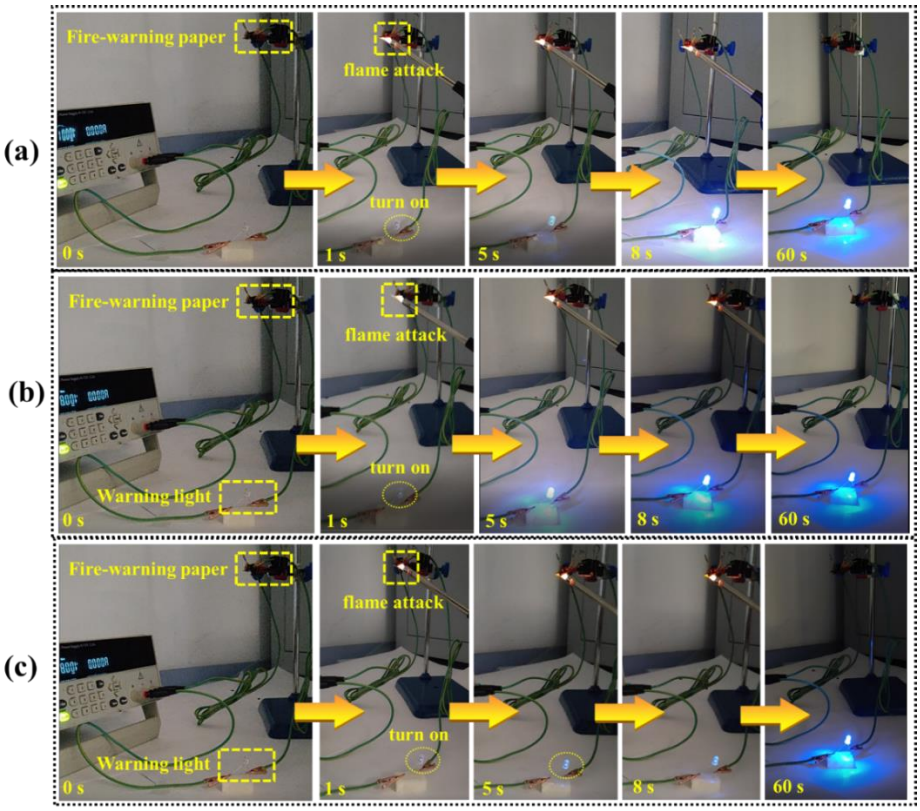

Fig. 3-3 Simulated alarm response of tailored-thickness fire sensor during combustion process: (a) GO@ETS-1, (b) GO@ETS-2 and (c) GO@ETS-3.

3.1.5 Proposed working mechanism of the multi-layered fire-warning sensor

The proposed working mechanism for GO-based fire alarms is strongly related to the conductive conversion from an insulating state at room temperature to a conducting state after being heated or burned. To verify the formation of RGO, some tests are performed. The structural characterization is presented in XRD curves (**Fig. 3-4** (a)). A new broad peak at about 21 º appears in the patterns of GO@ETS-y after being exposed at 150 °C, attributing to the (002) reflection peak of RGO [163, 164]. Moreover, a peak at around 11.5 º is assigned to the typical peak for GO, which is consistent with the previous work [60]. The coexistence of GO and RGO means that a partial oxygen-containing group is removed from the GO surface. Generally, temperature ranges needed from GO to RGO extend from 100 ºC to 250 ºC [165]. When GO@ETS-y samples are treated at 200 °C and 250 °C, more RGO will be produced, and only one characterized peak of RGO appears in XRD curves.

Furthermore, the I_D/I_G value from the Raman spectrum distinguishes between GO and RGO regions (**Fig. 3-4** (b)). The value of the I_D/I_G band intensity ratio spans from 2.27 for GO@ETS-1 (150 °C) to 2.54 for GO@ETS-3 (150 °C), in agreement with the reference [63]. Higher temperature results in the formation of more RGO, leading to more structural defects [63, 159]. Thence, I_D/I_G value rises from 2.54 for GO@ETS-3 at 150 °C to 2.61 for GO@ETS-3 at 250 °C. Additionally, the morphology of GO flakes shows a slight difference after being burned (**Fig. 3-4** (c)). The surface of burned flakes becomes relatively rougher and has more wrinkles. Especially for GO@ETS-3, the surface seems to be cracked. This might caused by the fact that the fire-warning film has experienced pyrolysis of partial oxygen-containing groups during the combustion process, and the gas release would impact surface morphology. The schematic illustration of the proposed working mechanism is in **Fig. 3-4** (d). The formation of conductive RGO can afford the construction of an electrical circuit, which can ensure fire alarm work.

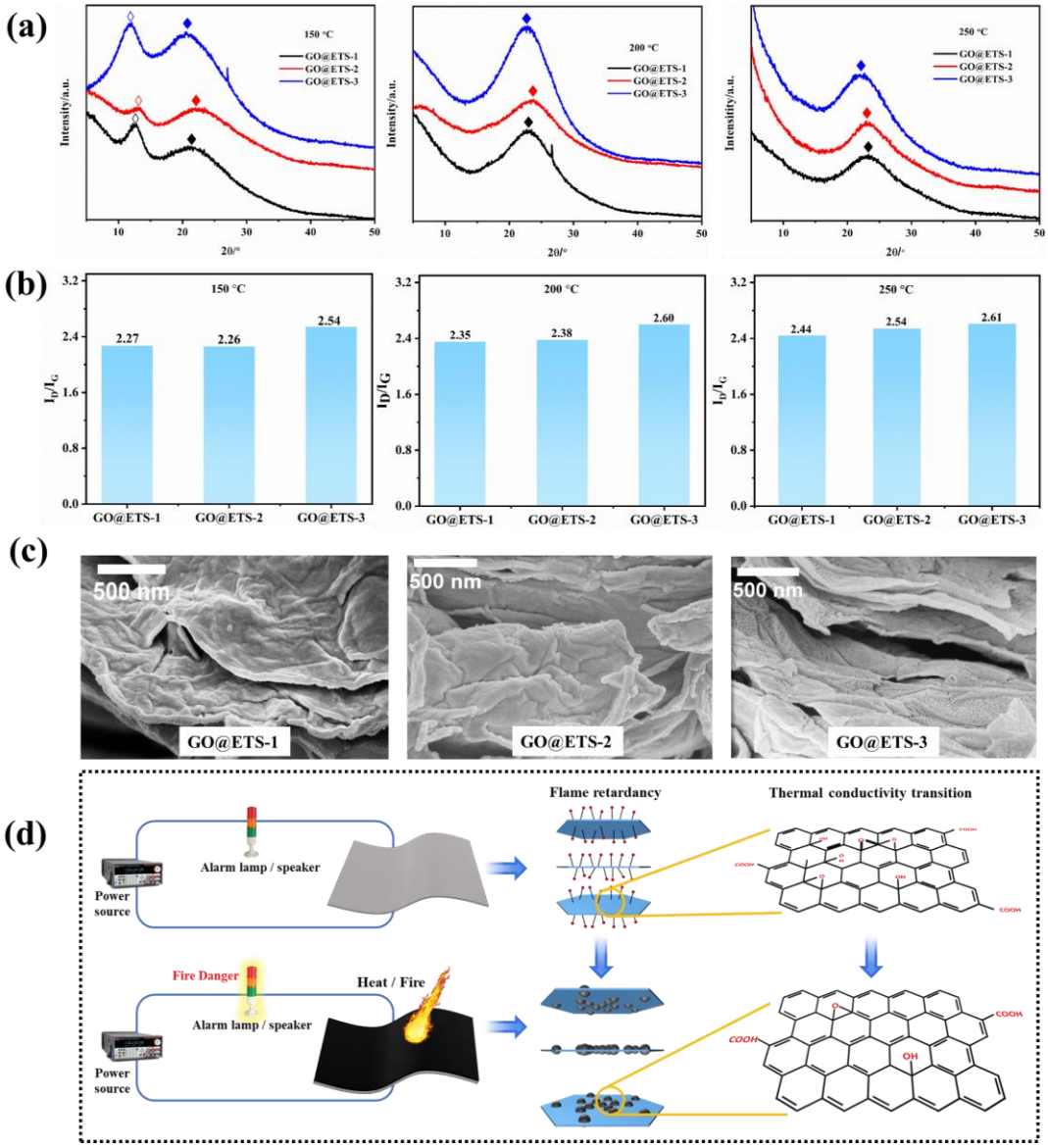

Fig. 3-4 Characterizations of multi-layered fire-warning samples after burning at different test temperatures: (a) XRD curves of burned samples; (b) I_D/I_G value of all burned samples; (c) SEM images of fire-warning samples after burning at 250 °C; (d) Schematic illustration of the proposed working mechanism of the fire-warning samples after heat treatment or fire attack.

3.1.6 Fire-warning nano-coated foam and its warning simulation

FPU foam is immersed into the above resultant mixing solution to get the fire-warning nano-coated fire sensor, shown in **Fig. 3-5** (a).

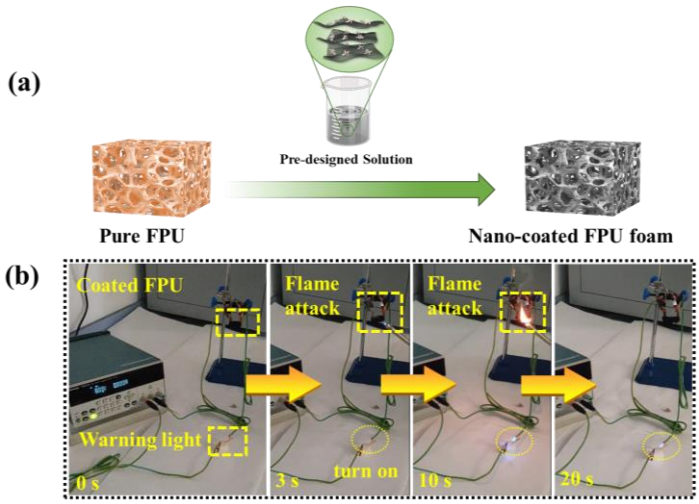

Fig. 3-5 (a) Preparation of nano-coated fire-warning FPU foam; (b) Alarm response of fire-warning FPU during the combustion process.

There is no significant difference except for the color. A simulation experiment is made to verify the feasibility of modified FPU foam as an early fire sensor. It is observed that the lamp switches on within 3 s when the foam is attacked by an ignitor, even though the lamp is not strong enough (**Fig. 3-5** (b)). This is related to the voltage used in the simulation. This proves the feasibility of a pre-designed solution to make a nano-coating layer onto a flammable substrate for fire sensors.

3.1.7 The remote wireless signal conversion of GO-based fire warning sensor

Effectively transmitting the detected fire signals into a large area is crucial for fire sensors. Fire sensors commonly use traditional sound and light devices to send alerts. They only work at a short communication distance near the target fire source unless using complex and high-cost electronic nodes and repeaters to send messages to further distances.

Considering the limitation of the transmission capability of traditional devices, a novel self-design wireless conversion system has been performed to alert fire danger to either specialized staff or the public in closed or open areas, which is shown in **Fig. 3-6**. The first one is based on a Wi-Fi communication module and consists of a similar methodology following our previous work, allowing remote advising of the dangerous fire situation with either a sound-light alarm or a warning message on display. The emitter XLPCF20 transmitter is activated as the fire begins by an ADC designed with an Arduino UNO connected to the transmitter. A receptor R080A is wired to an alarm system that can operate at V = 5 V and I=70 mA so that one output of the receptor supplies the

electrical power to the alarm. The previous alarm is a low-power device with different sound beeps. Additionally, a designed LCD with Arduino UNO Crystal libraries is connected to the second output of the R080A receptor, and the message displays change from “Normal” to “FIRE DANGER” when the XLPCF20 receives the wireless signal from the XLPCF20 emitter. Therefore, this dangerous signal can be transmitted quickly to earn more evacuation time when fires happen.

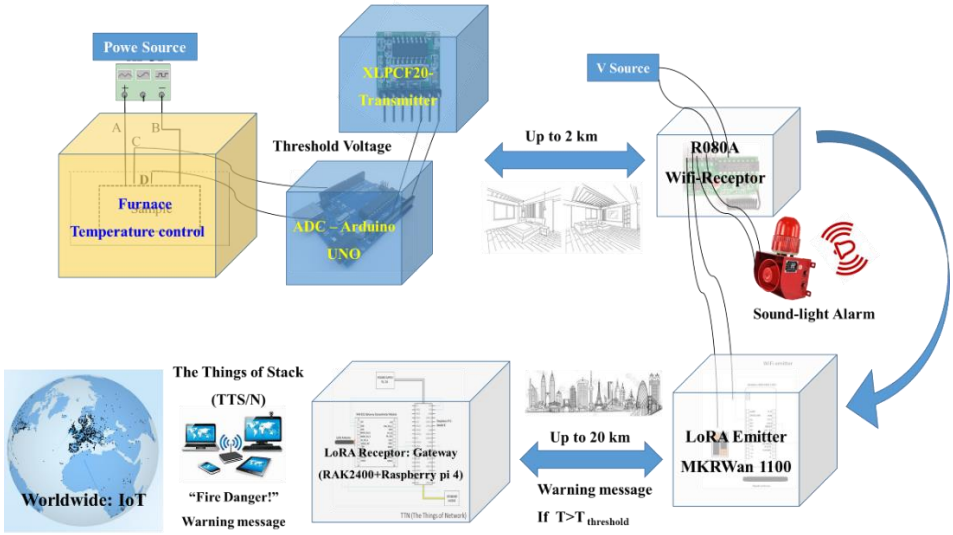

Fig. 3-6 Scheme illustrating a fire-warning sensor sending a warning signal to the public.

3.1.8 Conclusions

A kind of tailored-thickness fire sensor including temperature-sensitive GO and ETS is constructed. This fire-warning sample possessing thermal structural stability can be employed as a low-temperature sensitive detector, showing an ultrafast response of 1 s at 250 °C compared to most current thermos-sensitive fire sensors. Most importantly, a wireless signal conversion device is designed to diffuse monitored fire information to a large area for better personnel evacuation. It can make the areas up to 20 km away from the fire source to obtain a message of “FIRE DANGER” displayed on the local and remote multiple computer monitors simultaneously, which is smarter and more convenient. Additionally, the pre-designed solution can be wrapped on the FPU foam to form an FPU-based fire sensor, similarly showing a fast response to a fire. This work gives guidance for developing a new generation of intelligent and highly sensitive low-temperature fire sensors.

3.2 MXene-modified GO-based fire warning sensor

3.2.1 Introduction

Current reported fire alarms based on various materials enable fast response. However, there is still

room for improvement regarding different aspects. Usually, response sensitivity and signal conversion capability are primary parameters. Response temperature is one important criterion to prove early fire alarms' sensitivity. Generally, many detected response temperatures for early fire alarms are at either 300 °C or above, which might be at the risk of widespread fire propagation because, for most conventional materials, the ignition temperatures are between 300 °C to 500 °C [123, 150]. Therefore, a significant challenge is achieving low-temperature sensitive warnings for fire safety.

Furthermore, another evaluation of the response sensitivity is the response time, which shows timeliness. For most GO-based systems, it isn't easy to achieve rapid conductive conversion at low-temperature within a short time. Realizing fast response at low temperatures is still a considerable challenge and a current objective for effective fire alarms.

In addition, the common feedback of warning types from detected fire situations usually are warning lamps or sounds. The human visual is less sensitive to these traditional types, especially when some interferences occur from the environment. This can seriously affect the timely evacuation even though the firm alarms are working. Combining with the IoT can effectively avoid these problems, which can adapt to fast-developed times. Utilizing wireless transmission, the signal conversion of early fire alarms shows some advances in response speed and warning range. In our previous system, we proposed a wireless signal conversion system with cellulose fire-warning paper, which can send fire information to the public within 20 km, and the warning message can be displayed on a screen [121]. However, the wireless signal conversion further improves for a more precise and smarter fire warning transmission methodology, making it work efficiently in harsh environments, especially in dark backgrounds.

Regarding the preparation ways of GO-based early fire sensors, layer-by-layer self-assembly methodology with time-saving, large-scale properties, and universality is a promising technique [53, 154, 166]. The unique structural characteristic of GO allows it to form multifunctional films [50, 56], which hold a regular structure, smooth surface, and size-controllability performance [153, 155, 167, 168]. The critical attribution that makes GO a fire-warning candidate is a temperature-sensitive feature that forms conductive RGO [75, 76, 169]. However, this feature of GO has a high-temperature requirement, and the low-temperature reduction of GO is not satisfactory. Therefore,

introducing MXene is an appropriate choice to implement a low-temperature response because of its excellent conductivity and good water solubility. It serves as a bridge to enhance the possibility of forming an electrical pathway. Herein, a kind of MXene-modified GO-based fire-warning film is proposed further to achieve rapid lower-temperature response and smart wireless signal transmission.

3.2.2 Preparation and characterization of MXene powder and fire-warning films

a). Preparation and characterization of MXene powder

2 g LiF powder was added into 40 mL HCl solution (9 M) and stirred for 30 min at 35 °C. Then 2 g MAX powder was slowly introduced into the above solution for a reaction for 48 h. The mixture solution was centrifuged with deionized water until the pH value of the upper liquid was over 6. Subsequently, the final dark green suspension was collected. After a freeze-day treatment of the resultant solution, MXene was obtained (**Fig. 3-7** (a)).

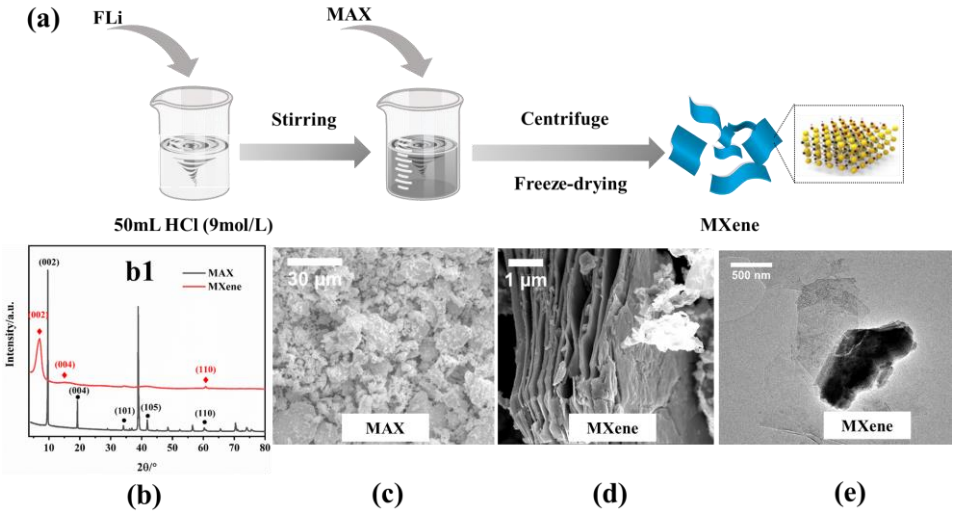

Fig. 3-7 (a) Schematic illustration for the preparation process of the MXene powder. (b) XRD curves of MAX and MXene. (c) SEM image of MAX. (d) SEM and (d) TEM image of MXene.

The structural characterization of MXene containing XRD, SEM, and TEM results are shown in **Fig. 3-7** (b), (c), (d), and (e). From the XRD results shown in **Fig. 3-7** (b), it is clearly observed nonbasal plane peaks of Ti_3AlC_2. The notable high-intensity peak is at 39 º, which represents the presence of Al. However, it disappears in the XRD spectra of MXene, showing the successful exfoliation of MAX. Additionally, the peaks of (002), (004), and (110) shift to relatively lower angles by comparison with their location in MAX. The peak intensity also displays a little lower

because exfoliation causes a loss of diffraction signal in the out-plane direction [77].

In addition, SEM and TEM tests were also used to check the characterization of MXene. As the results are shown in the picture **Fig. 3-7** (c), (d), and (e), there is no particular structure for raw materials MAX powder. After the etching of the Al element from MAX, a typical multi-layered structure appears in MXene. It is also clear to see the thin and transparent layer structure of MXene from TEM images. Both results show the successful exfoliation from MAX and the formation of multi-layer MXene.

b). Preparation and characterization of MXene modified fire-warning films

Aqueous GO suspension with a fixed concentration was prepared by sonication treatment. PTS content was diluted with DMF solution to prepare another solution. Then PTS and GO aqueous solutions were mixed to obtain the final solution. Afterward, aqueous MXene solution with different concentrations was prepared by sonication. The resulting solution was obtained by blending the MXene and the above-mixed solutions. As shown in **Scheme 3-3**, the multifunctional MXene-modified fire-warning films were prepared. Their detailed components are displayed in **Table 3-3**.

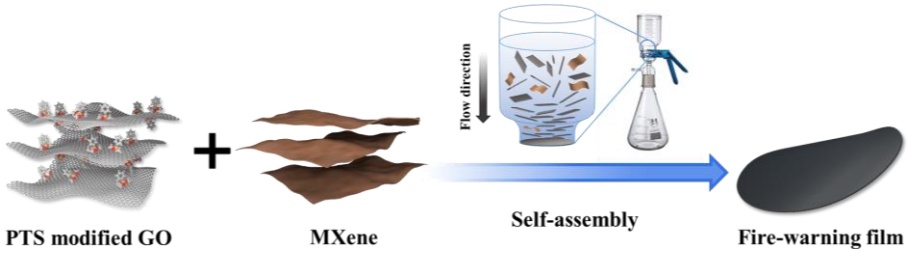

Scheme 3-2 The schematic illustration of multifunctional fire-warning film.

Table 3-3. Components of multifunctional fire-warning films.

Samples	GO Concentration (mg/mL)	PTS Concentration (mg/mL)	Concentration ratio of GO to MXene
GO-PTS10	4	10	-
M1@GO-PTS10	4	10	20:1
M2@GO-PTS10	4	10	10:1
M3@GO-PTS10	4	10	5:1

As analyzed above, the introduction of PTS can affect the structure of GO nanosheets, leading

to an increased interlayer distance of GO flakes. After further addition of MXene, XRD, Raman, SEM, and EDS tests are also carried out to verify the structural characterization of fire-warning films. Carbon, oxygen, and silicon elements appear in GO-PTS10 film. Apart from these elements, the MXene treatment introduces titanium elements in films, proving that MXene has been incorporated into films successfully, as observed in **Fig. 3-8** (a).

As observed in XRD curves presented in **Fig. 3-8** (b), GO-PTS10 film shows a sharp peak at $2\theta \approx 11$ º, assigning to the typical (001) reflection peak for GO [50, 60, 164]. For the MXene-modified films, another diffraction peak is observed at $2\theta \approx 6$ º, corresponding to the characteristic peak of MXene [77], which can prove the successful introduction of MXene into GO-based films. However, there is no significant shift in the peak position for MXene and GO characteristic peaks even though different MXene contents are used. This phenomenon occurs in Raman results similarly. As depicted in **Fig. 3-8** (c), the I_D/I_G values of different films based on the Raman spectrum do not show a notable difference, which illustrates a similar disorder level and graphitization degree for the different films. This might be due to their similar unique two-dimensional structures, which lead to the simple physical blending without intercalation reaction.

The multi-layer structure of the films can be observed from the SEM images in **Fig. 3-13** (d). From cross-section SEM images, no significant difference in film thickness is monitored, apart from a slight increase in thickness for M3@GO-PTS10 film with higher MXene content than other films. This result is consistent with the above Raman result. In addition, it seems that introducing MXene affects the surface performance of multifunctional fire-warning films. The surface of GO, M1@GO-PTS10, and M2@GO-PTS10 are smooth, as observed in **Fig. 3-13** (e). However, many wrinkles appear on the surface of the M3@GO-PTS10 film because of more MXene content. On the other hand, much more MXene might negatively influence film conductivity at room temperature. Thus, it is not appropriate to introduce excess MXene content. That is why these MXene concentrations are chosen.

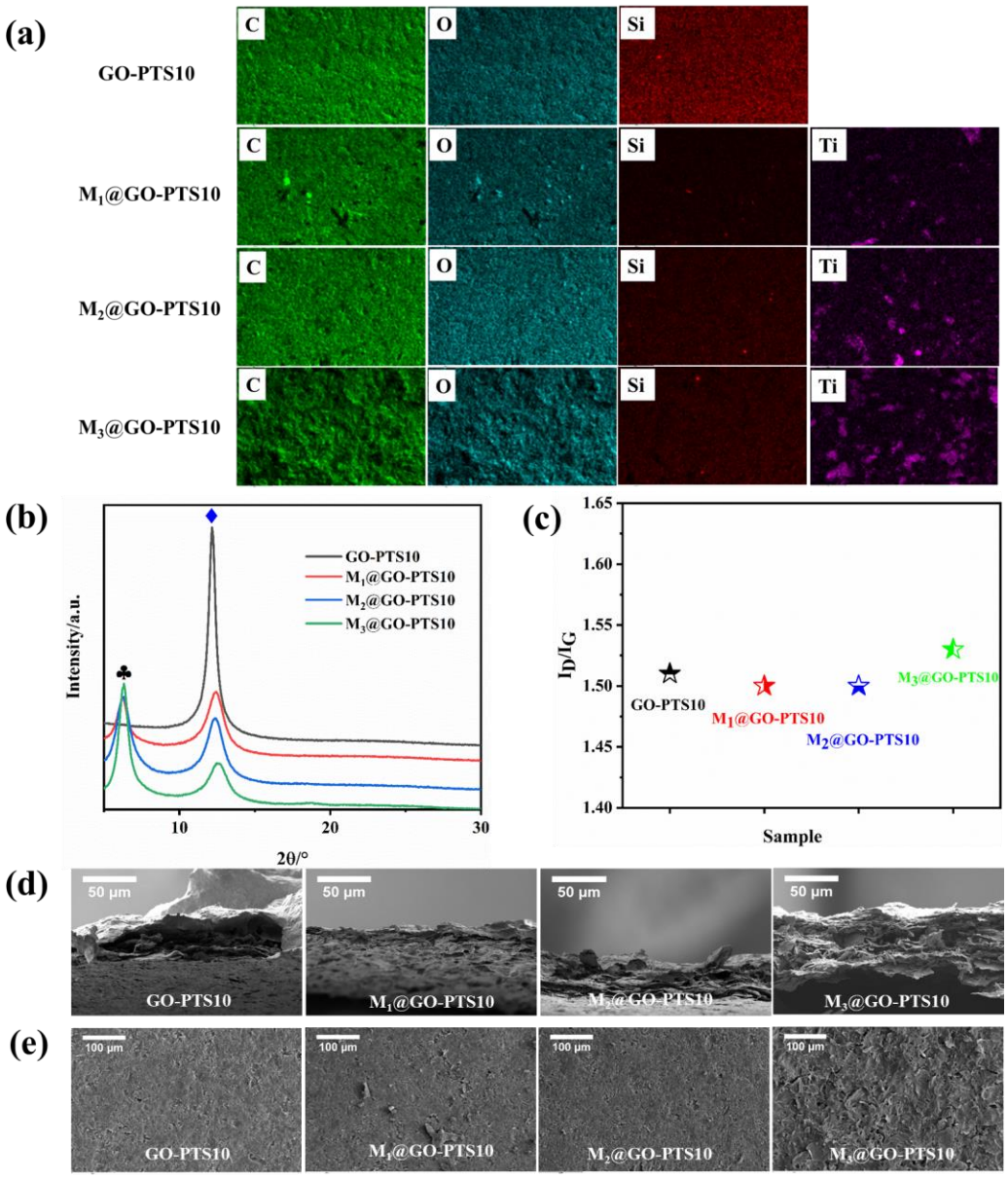

Fig. 3-8 Structural characteristics: (a) EDS mapping of the elements in MXene modified fire-warning films; (b) XRD patterns and (c) I_D/I_G value based on Raman spectra of MXene modified fire-warning films; (d) SEM observation of cross-section and (e) surface for MXene modified fire-warning films.

3.2.3 Flammability of MXene-modified GO-based films

The fire durability of materials under flame is critical for early fire sensors. Both TGA, burning test, and MCC were used to study the combustion behaviors for each film. The corresponding results are presented in **Fig. 3-9**. TGA is a valuable indicator to investigate residual char after burning films under the air atmosphere. After the introduction of MXene, the residual char of films further increases, which can be observed from the TGA curves in **Fig. 3-9** (a). More MXene content causes

increased residual char content, meaning MXene positively affects flame retardancy. Moreover, burn films with an ignitor for 60 s to check the films' situation under actual fire.

As shown in **Fig. 3-9** (b), all films maintain their morphology stable after being burned for 60 s. The films with MXene become shrinkage after being burned, and more MXene content in films causes a clearer shrinkage. However, the introduction of MXene does not show a decreased fire durability of films under real fire. This phenomenon might be caused because the solution used for each film is fixed in volume. More MXene content means relatively low PTS content in one film, which would lead to a slight difference in burning behavior.

Furthermore, the MCC test for combustion parameters is carried out. The peak heat release rate (HRR) value is essential in evaluating fire-warning films' flame retardancy. As shown in **Fig. 3-9** (c), MXene can decrease the peak value of HRR by comparison with the value of GO-PTS10 film. More MXene content further declines the peak HRR value, and M3@GO-PTS10 films have the lowest peak HRR value. In conjunction with the above TGA result, this demonstrates improved flame retardancy and better fire resistance. Fire durability can provide a strong foundation for early fire sensors.

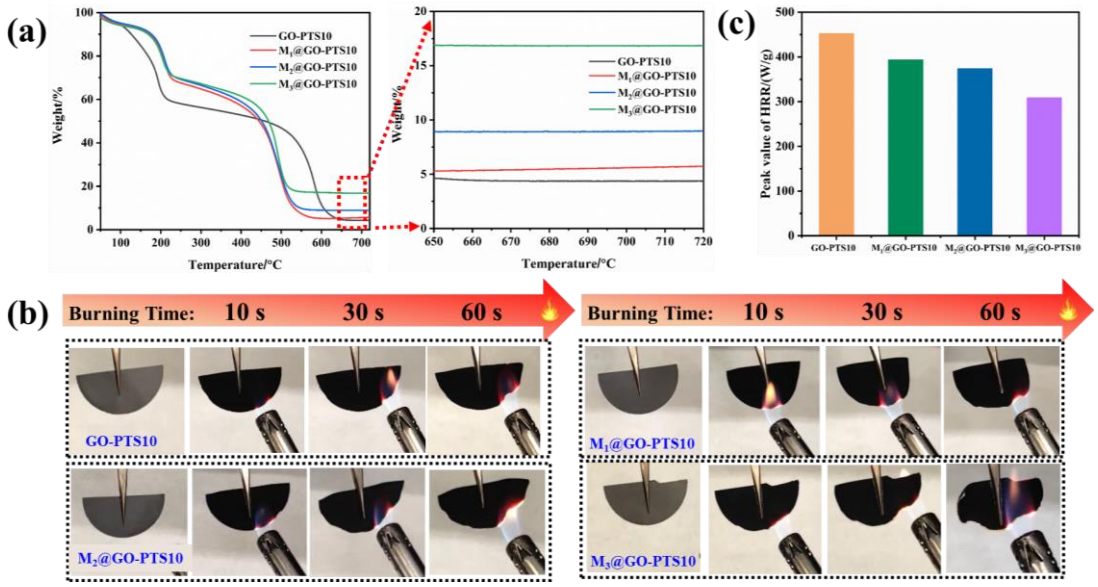

Fig. 3-9 (a) TGA curves of GO-PTS10 and other MXene-modified films; (b) combustion process of GO-PTS10 and other MXene-modified films under ignitor; (c) Peak value of HRR for GO-PTS10 and other MXene-modified films based on MCC results.

3.2.4 Fire alarm response behavior of MXene-modified GO-based films

To illustrate the warning process of the early fire alarm in this work when a fire takes place, a simple simulated fire scenario is designed, and corresponding screenshots of the experiment are predicted in **Fig. 3-10**.

The setup consists of an electrical circuit with one power supply, the fire-alarm films, and an alarm lamp. The system can send a warning signal by triggering the lamp in the pathway when the film is burned. All the films are electrically insulating at room temperature even if the conductive MXene is added because the MXene content used in this work is low. When GO-PTS10 detects a fire, the lamp turns on after 2 s. Moreover, when MXene-modified films are used, the lamp turns on after 1 s. This proves that MXene accelerates the response of fire-alarm films in the presence of a fire. Compared with the light intensity in different pathways after burning for 1 s, the light intensity in a circuit containing M3@GO-PTS10 film is stronger than others. This further suggests the rapid response caused by more MXene. With more burning time, the lamp's luminosity in all circuits becomes robust, which is attributed to the decreased electrical resistance in the circuit. Heating and flame are efficient methods to convert conductivity from GO to RGO. After flame treatment, some oxygen-containing groups will be removed from the surface of GO, leading to electrical conductivity conversion from insulation to conductivity [76, 169, 170]. More burning time results in more formation of RGO, which causes the brightened luminosity of the lamp. This is the key to a working mechanism for temperature-based early fire-warning systems. To this end, the electrical resistance change during the whole heating process is monitored for further illustration.

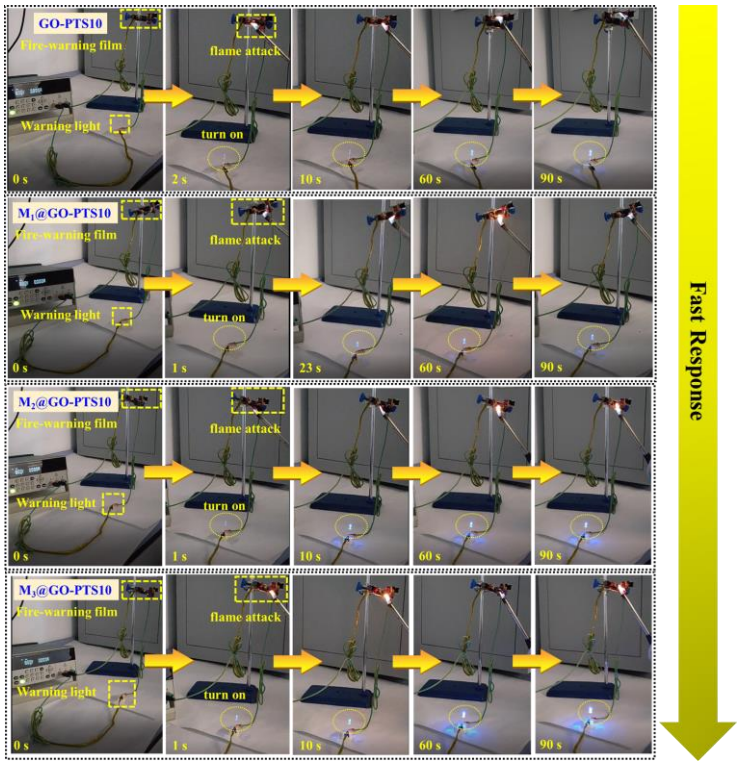

Fig. 3-10 Fire alarm simulation process of GO-PTS10 and MXene modified fire-warning films.

This present work aims to develop an ultrafast low-temperature fire alarm, which can earn more evacuation time. Therefore, different temperatures below 300 ºC, such as 180 ºC, 200 ºC, and 250 ºC are selected as heating temperatures. Electrical resistance changes upon exposure to these heating temperatures are recorded, another critical parameter to evaluate the sensitivity of fire alarms.

As presented in **Fig. 3-11**, the electrical resistance value of all fire-warning films shows a downward trend. However, the difference in film composition and heating temperatures offer different electrical resistance drop rates. At each heating temperature, the electrical resistance tendency follows as below: M3@GO-PTS10 ＞M2@GO-PTS10 ＞M1@GO-PTS10＞GO-PTS10, proving the enhanced downtrend of electrical resistance for films with more MXene. This is consistent with the fire alarm simulation result and supports the original intention of the experimental design. Moreover, different energy from various heating temperatures leads to different electrical resistance change rates. The electrical resistance of each film drops faster with the increased test temperature. At 250 ºC, the material is more conducive and prone to trigger an electrical response to form a circuit because of a more rapid decrease in electrical resistance

compared to warning films at other heating temperatures (**Fig. 3-11** (c)). During the electrical resistance decrease process, it should have an electrical resistance threshold that can trigger the electrical pathway. The time it takes for electrical resistance to drop to this value is a definite indication of the sensitivity of the fire warning system. This provides one calculation method for response time based on "trigger electrical resistance". As presented in **Fig. 3-11** (d), the response time for each film at 250 ºC is within a few seconds. The response time for M3@GO-PTS10 is only 1 s, providing further proof of the sensitivity of fire-warning film in this work.

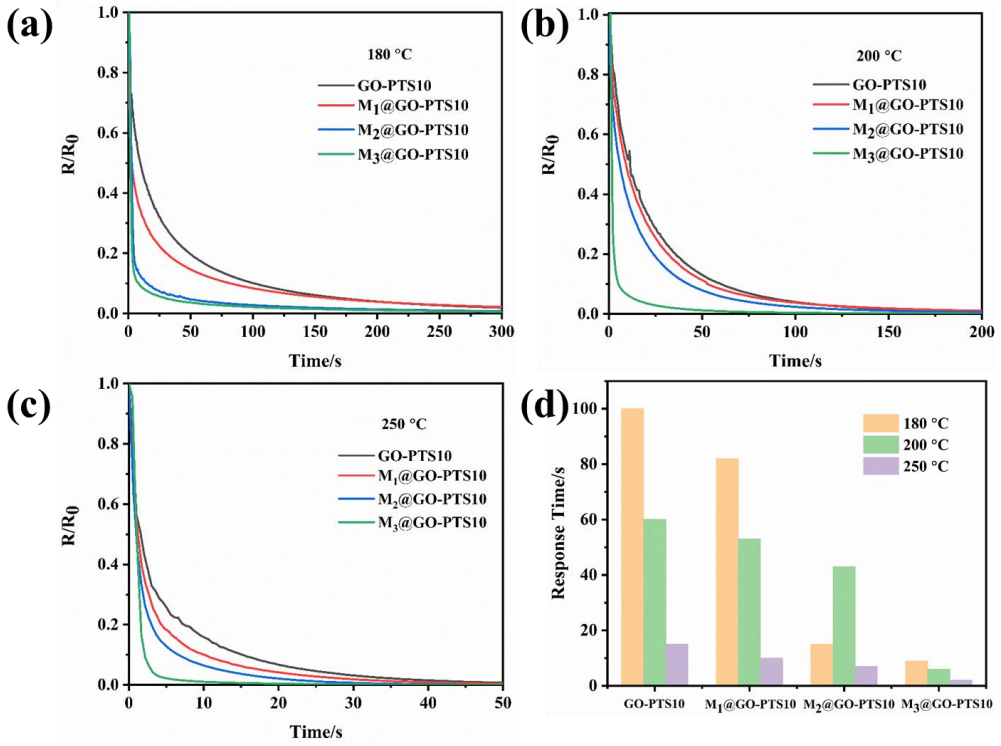

Fig. 3-11 Electrical resistance changes of MXene-modified films at (a) 180 ºC, (b) 200 ºC and (c) 250 ºC as a function of time. (d) Response time of different samples based on trigger electric resistance.

The decrease in electrical resistance reflects the conductive conversion in the circuit during the heating process. This mainly stems from the formation of RGO. Once the electrical circuit is formed, the warning signal from the fire will be triggered and displayed on a screen. This is the fire-warning system's primary working mechanism, attributed to the conductive conversion from insulated GO to RGO. This will be discussed below.

3.2.5 Proposed working mechanism of MXene-modified GO-based films

The proposed working mechanism of fire-warning films related to GO's conductive conversion is schematically presented in **Fig. 3-12**.

As XRD curves presented in **Fig. 3-12** (a), besides the characteristic peaks of GO and MXene that are at ≈ 6 º 2θ and ≈ 11 º 2θ, respectively, there is one broad shoulder peak appears at ≈ 22 º 2θ after heating treatment, which proves the reduction of GO and the presence of RGO [164, 170]. Notably, the coexistence of GO and RGO indicates the incomplete reduction of GO, which points out that the energy provided by the selected temperatures is not strong enough to afford the complete reduction of GO [76, 170]. This can further illustrate the purpose of introducing conductive MXene to realize low-temperature warnings in this work. Meanwhile, the heating treatment seems to have no significant influence on MXene in the films, further illustrating the use of low temperatures in the chosen tests. The graphitization degree of films decreases after heating treatment to form RGO [63].

Nonetheless, I_D/I_G values of MXene modified fire-warning sensors in **Fig. 3-12** (b) are almost similar, showing no noticeable difference. Some particles on the surface of burning films can be seen in the SEM figures (**Fig. 3-12** (c)), which might be the silica particles from the combustion of silicon-containing substances to inhibit the release of heat and gases, as previous reports illustrate [171, 172]. The summary of the proposed working mechanism of the fire-warning film under flame is shown in the schematic figure **Fig. 3-12** (d). As shown, the positive results observed in the samples containing MXene can be attributed precisely to a bridging effect that can accelerate the formation of the electrical pathway at low temperatures under the incomplete reduction of GO condition.

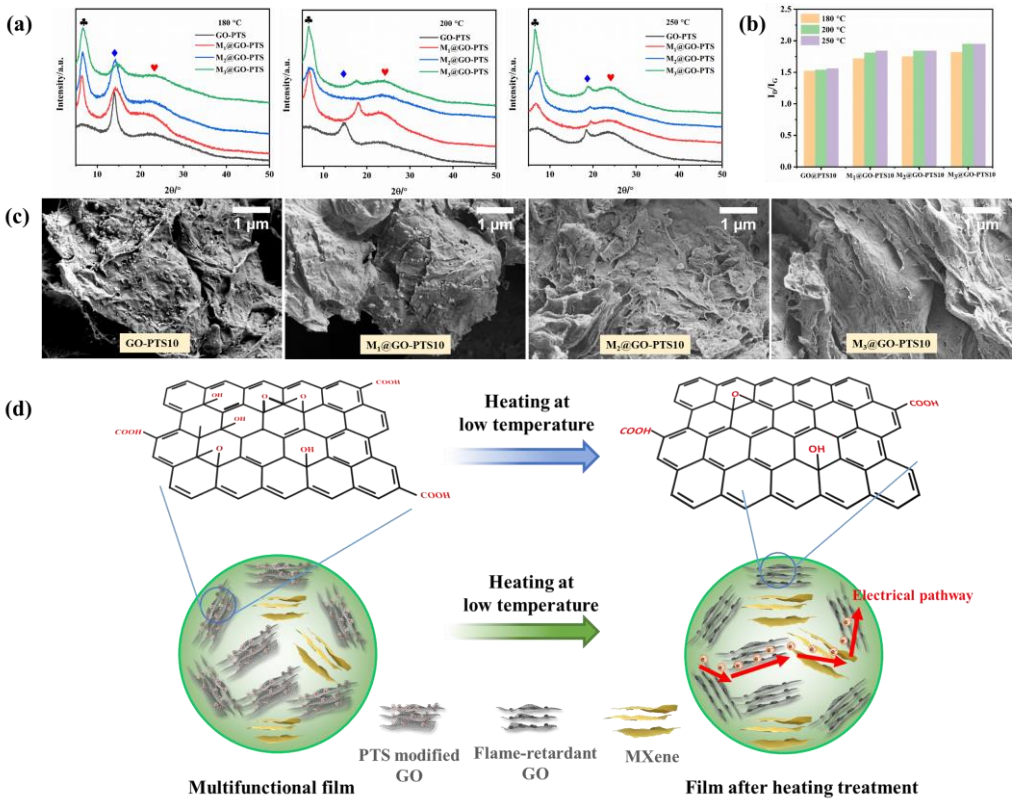

Fig. 3-12 Characterization of multi-layered fire-warning films after burning at different test temperatures: (a) XRD curves of all multi-layered fire-warning films after burning; (b) I_D/I_G value of all multi-layered fire-warning films after burning at 180 ºC, 200 ºC and 250 ºC; (c) SEM images of fire-warning films after burning at 250 ºC; (d) Schematic illustration of the proposed working mechanism of the fire-warning film after heat treatment or fire attack.

3.2.6 Remote wireless transmission and real-time luminosity monitor

A schematic illustration and a specific scenario are provided in **Fig. 3-13** to clarify the setup and working principle of this early fire alarm. According to the video, no alarm is activated when no fire occurs. Brightness is locally and remotely monitored by giving constant values. No activation of the Wi-Fi XLPCF20 emitter is performed, showing “NORMAL” on the display. The alarm is off, and no warning on the TTN is produced. Subsequently, the ignitor is switched on next to the film to change its conductivity. Then, voltage related to conductivity begins to grow. The brightness monitored in the local online processing unit increases as the fire is close to the film. Once film conductivity rises to the voltage threshold, Wi-Fi emitter XLPCF20 is activated to send the instruction to the receiver R080A so that the display interface shows the message “FIRE DANGER!!!” once a fire occurs. The TTS website associated with this set-up displays “FIRE

DANGER!!!" identically. Importantly, this information is accessible from anywhere with internet access. Meanwhile, brightness can be consulted via the internet, too.

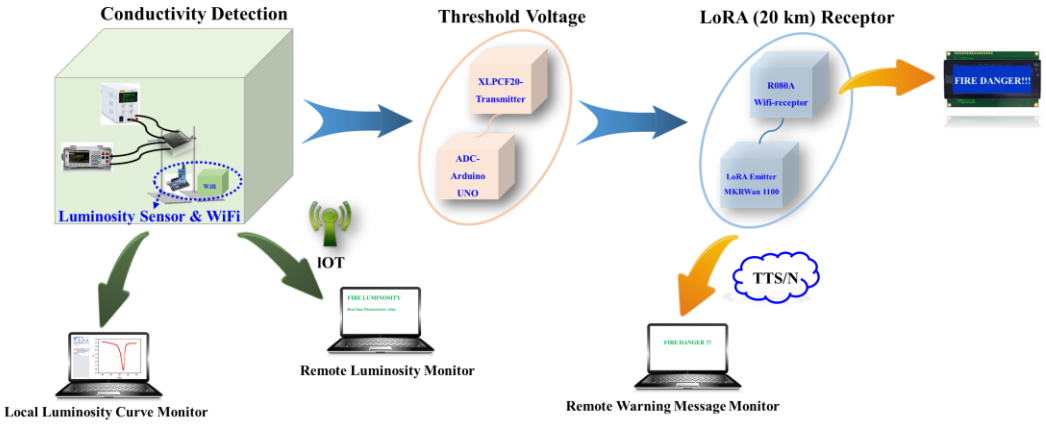

Fig. 3-13 Schematic illustration of the proposed working mechanism of the fire-warning film after heat treatment or fire attack.

To display this work from the perspective of current state-of-the-art early fire alarms, a table between this fire alarm and reported fire alarms based on several parameters has been provided in **Table 3-4** to indicate the advance of this work. The parameter comparison mainly contains response temperature, response time, and warning signal conversion type. The response temperature achieved in other research is usually 300 ºC or higher, while the response temperature in this work is down to 250 ºC, showing the advantages of a low-temperature fire alarm. However, the response time in the literature can be within seconds, being reduced to 1 s in this work. Compared with the traditional warning signal way, wireless signal transmission is proposed in our previous fire-warning work that can realize local and remote warnings. Fortunately, the luminosity sensor is introduced in this work for the first time, which can detect real-time light intensity, mainly showing advantages in fire detection during the night or in a dark environment.

Table 3-4. Comparison of early fire alarms performance among our MXene/GO warning film and other fire-warning systems in literature.

Sample systems	**Solvent used in the preparation**	**Flame retardant performance**	**Response temperature / ºC**	**Response time at temperature below 300 ºC**	**Signal conversion method**	**Ref.**
MF@GOWR	water	Yes	300	33 s	Lamp	[104]
GO/Silicone	water	Yes	300	38 s	Lamp	[102]
FGO/CNT@WPP	Water/Ethanol	Yes	300	12 s	Lamp	[99]
PVA/$AgNO_3$@ME	Water	Yes	--	12 s	Lamp	[173]
MLGO (10/40)	water	Yes	300	7 s	Lamp	[100]
PA@GO paper	water	Yes	250	2 s	Wireless	[121]
MXene/GO film	water	Yes	**250**	***1 s***	***Wireless and luminosity***	***This work***

MF: melamine formaldehyde sponges; GOWR: graphene oxide wide-ribbon; FGO: Phenoxycyclophosphazene-functionalized graphene oxide; CNT: carbon nanotubes; WPP: wood pulp paper; PVA: poly (vinyl alcohol); $AgNO_3$: silver nitrate; ME: melamine sponge; MLGO: MPMS/LAA/GO paper MPMS: 3-methacryloxypropyltrimethoxysilane; LAA: L-ascorbic acid; PA: Phytic acid.

3.2.7 Conclusions

In this work, a facile multifunctional fire-warning film was fabricated by coupling MXene and flame-retardant GO. Particularly, M3@GO-PTS10 film possesses good flame retardancy that gives a basis to detect abnormal temperatures. When burned, the M3@GO-PTS10 film can be triggered within 1 s, especially at 250 °C, and an ignitor, showing highly-sensitive warning capability at low temperatures compared with other fire-warning systems. This fire-warning film, coupled with a small wireless signal conversion device, can emit a warning message of “FIRE DANGER!!!” on the remote computer monitor. Meanwhile, an associated luminosity sensor can detect real-time luminosity value around a fire source and send it to a computer monitor. It achieves smart signal transmission for easy implementation within the Internet of Things devices. Benefiting from the facile approach, low cost, and ultrafast fire-warning ability, it is expected to be applied in firefighting and smart fire alarms. This fire alarm, integrated with low-temperature fast warning capability and intelligent wireless transmission, is crucial in guiding a new generation of smart fire sensors.

CHAPTER 4

Biomass cellulose paper-based fire-warning sensors

"Genius only means hard-working all one's life."

-Mendeleyev

4.1 Eco-friendly cellulose paper (CP)-based fire warning sensor

4.1.1 Introduction

While the majority of the current research works employ GO, due to its temperature-dependent electrical resistance transition effect [65, 174], the works above are limited by response temperatures above 300 °C, and all the detected electric signals are converted into traditional warnings, such as light or a sound alarm signal to show fire danger. Therefore, as combustible materials usually get ignited while exhibiting violent burning and rapid flame spread behavior [93, 150, 162] at temperatures rise above 300 °C, and to the best of our knowledge, there are only a few works on fire alarms focused on rapid response to fire at lower temperatures (＜300 °C) with wireless signal transmission. Considering the convenience of wireless signal transmission and the urgency of detecting fire hazards at lower temperatures, it is necessary to design fire alarms with capabilities to rapidly detect fire at low temperatures and transmit the electrical via a wireless communication system.

Moreover, the previous chapter describes the GO-based early fire-warning sensors, presenting a restriction in practical application. Comprehensive consideration of detection scenarios and sustainable development, biomass CP is chosen to fabricate early fire alarms against indoor fire hazards in this study. Herein, we developed a novel flame-retardant fire sensor decorated with GO and 2D material MXene with low-temperature detection and wireless communication capabilities by employing bio-based CP as a substrate for the fire-warning system and PA as a flame retardant to keep the structure intact in case of abnormally high temperature or fire.

4.1.2 Preparation and characterization of modified CP-based fire-warning sensor

As presented in **Scheme 4-1**, CP was immersed in PA solution several times and dried at room temperature. CP after PA modification was named PAx, where x was PA concentration. Next, the

homogeneous MGO suspensions with different concentration ratios of GO to MXene were prepared for subsequent usage. Using a simple dip-coating way to put PAx samples into MGO suspension (GO suspension), final PA@MGOy (PA@GO) papers were obtained, where y meant the concentration ratio of GO to MXene. In **Table 4-1**, the component of each specimen is provided.

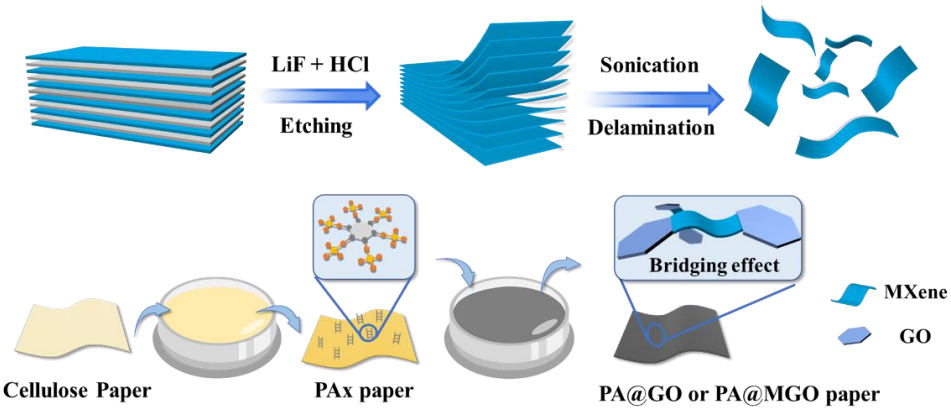

Scheme 4-1 Schematic fabrication process of PA@MGOy alarm samples.

Table 4-1. Components of PA@GO and PA@MGOy papers.

Samples	PA concentration/*wt%*	GO concentration/*(mg/mL)*	Concentration ration of GO to MXene
PA@GO	20	2.5	-
PA@MGO20	20	2.5	20:1
PA@MGO15	20	2.5	15:1
PA@MGO10	20	2.5	10:1
PA@MGO5	20	2.5	5:1

The successful and homogeneous coating is critical for the samples' performance. For evaluating the coating, FTIR, SEM, and EDS analyses were conducted, and the corresponding results are shown in **Fig. 4-1**.

From the FTIR spectra in **Fig. 4-1** (a), it is observed that all the samples exhibit relatively sharp peaks at 3330 cm^{-1} and 1025 cm^{-1}, corresponding to O-H stretching vibrations and C-O stretching vibrations, showing typical characteristic peaks in cellulose [175]. However, in contrast to pure CP, PA@GO, and PA@MGOy samples exhibit weak characteristic peaks at 1630 cm^{-1} and 1720 cm^{-1} assigned to C=C from unoxidized sp^2 bonds and C=O stretching vibration of GO. This indicates the

successful coating of GO on the surface of CP due to hydrogen bonds [176]. It can also be seen from SEM figures that intact coating forms on the surface of CP successfully (**Fig. 4-1** (b)). EDS test is also employed to verify coating composition further. Only C and O elements are detected in the PA@GO sample. At the same time, a homogeneous Ti element also appears in the PA@MGO5 sample besides C and O elements, compared to the PA@GO sample (**Fig. 4-1** (c) and **Fig. 4-1** (d)). This shows that MXene also has been successfully coated on the surface of CP. These results imply the successful coating on the CP surface, which might be attributed to the hydrogen bonding [176].

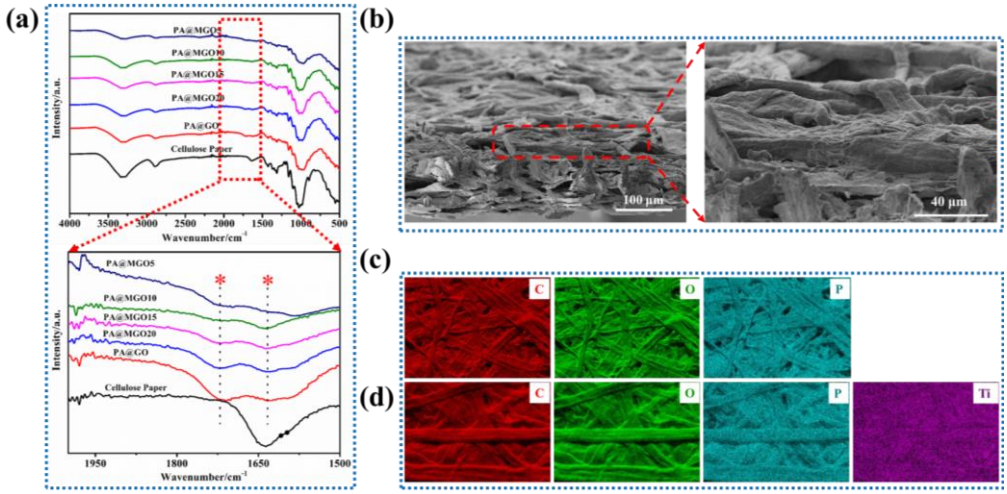

Fig. 4-1 Structure characterization and analysis: (a) FTIR spectra of PA@GO and all PA@MGOy samples. (b) SEM observation of PA@MGO5. (c) EDS mapping of the element in PA@GO. (d) EDS mapping of element in PA@MGO5.

4.1.3 Flammability of modified CP-based fire-warning sensor

Excellent thermal stability is crucial to maintain the sample's structural integrity, which is the basis for a fire-warning sample. To evaluate the thermal stability of modified CP, TGA measurements were performed, and the corresponding results are shown in **Fig. 4-2** (a). While all the samples exhibit one-stage decomposition, the residual weight of the different samples display apparent differences, especially at high temperature. Accordingly, the residual weight of PA@MGOy increases with more load of MXene. PA@MGO5 sample shows a relatively higher residual weight at 700 ºC, which indicates the improvement of flame retardancy for PA@MGOy as MXene content increases. Therefore, MXene addition can play a positive role in improving flame retardancy. It is likely due to the synergistic effect between MXene and PA, in which MXene can assist PA synergistically to inhibit heat release and isolate oxygen [177].

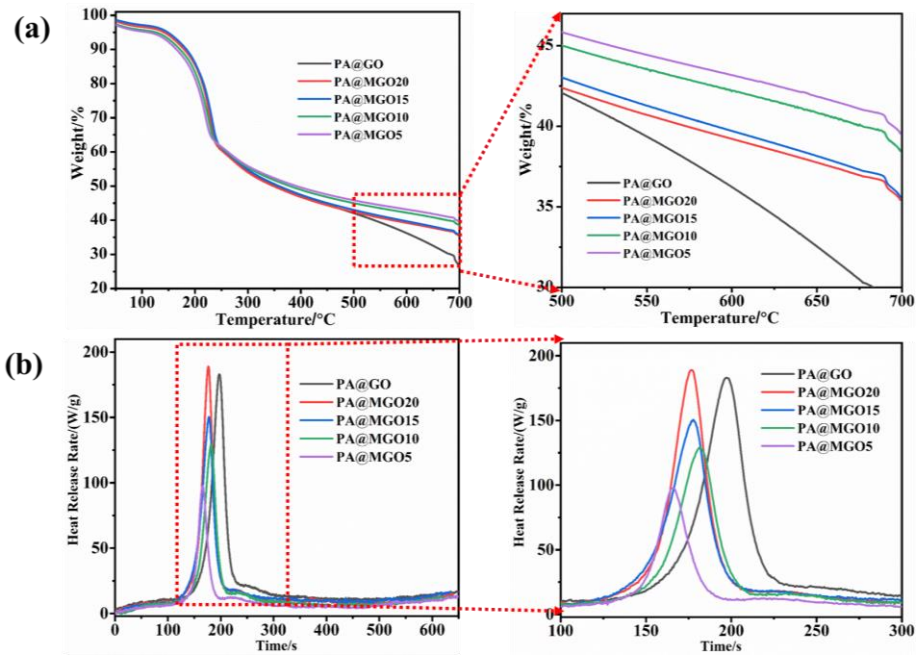

Fig. 4-2 (a) TGA curves of PA@GO and PA@MGOy samples. (b) MCC curves of PA@GO and PA@MGOy samples.

MCC test was also used to investigate the combustion behavior of the samples (**Fig. 4-2** (b)). The heat release profiles of all the samples show only one sharp peak, which implies a good homogenous coating. Moreover, the peak heat release rate (pHRR) gradually decreases after loading with MXene. In comparison to pure CP with a pHRR value of 183 W/g, all PA@MGOy samples exhibit a lower pHRR value. Notably. the pHRR value of PA@MGO5 drops by 46.7 % to 97.5 W/g. These results demonstrate that MXene plays an essential role in improving flame retardancy. In this work, the combination of PA and MXene results in better flame-retardant performance, further proving the synergistic effect of MXene in promoting flame retardancy [177].

4.1.4 Electric resistance change vs time of modified CP-based fire-warning sensor

The fire response of the fire-warning system mainly replies upon the transformation of GO from an insulator to a conductor during the heating process, which leads to samples' electrical resistance changes. So electric resistance changes as a function of time were measured at different temperatures (150 ºC, 200 ºC, and 250 ºC), and the corresponding curves are provided in **Fig. 4-3** (a) i-iii. As expected, all samples' electric resistance sharply decreases when exposed to heat. At the defined temperatures, the electrical resistance of the PA@GO sample takes a relatively longer time to decline to a lower value, which can support the transfer of electrons. Notably, after the addition of MXene,

electrical resistance changes of PA@MGO samples exhibit a shorter time compared to that of PA@GO samples. In addition, the time for electrical resistance decreases exhibits further decrease with more loading of MXene content. At the same test temperature, the time for samples' electric resistance change to the value required to form an electrical circuit exhibit the following trend: PA@GO＞PA@MGO20＞PA@MGO15＞PA@MGO10＞PA@MGO5.

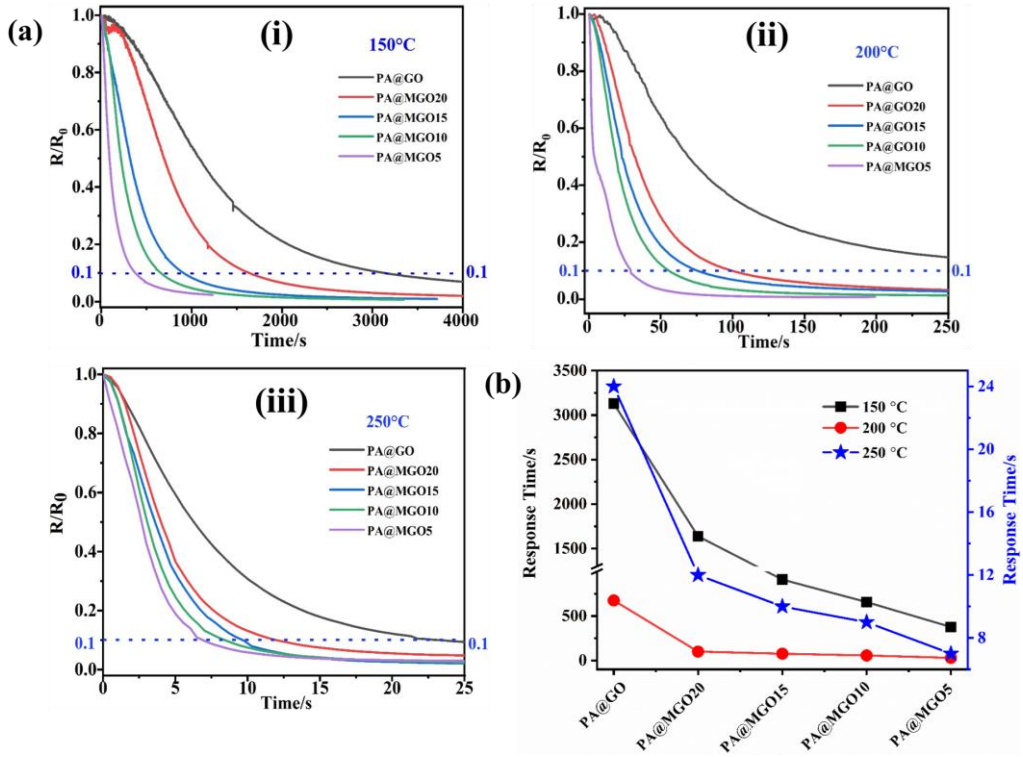

Fig. 4-3 (a) Electrical resistance changes at different test temperatures: (i) 150 ºC, (ii) 200 ºC and (iii) 250 ºC. (b) Response time calculated by "trigger electric resistance".

Interestingly, it is worth noting that electrical resistance change is strongly related to test temperature. Higher test temperature can lead to faster electrical resistance change due to the increased amount of heat energy at high test temperature, Thereby leading to a shorter time for electrical resistance transition to support the fire-warning system. With the test temperature increasing from 150 ºC to 250 ºC, all the sample's electrical resistance change time further shortens, which indicates increased sensitivity for the fire-warning system. Therefore, all the samples at the test temperature of 250 ºC show the shortest time for electrical resistance change, hence displaying early fire detection.

4.1.5 Response time of modified CP-based fire-warning sensor

a). Response time based on "Trigger Electrical Resistance"

Normally, response time is set as one way to appraise the sensitivity of the fire-warning system. One approach is to calculate the response time of the fire-warning system based on "trigger electrical resistance". Usually, when the electrical resistance decreases by over 90 %, the value is small enough to support the electrical circuit formation, which means a fire alarm can be triggered immediately [119]. Hence, the time required to reach controlled trigger electrical resistance is selected to evaluate the sensitivity of the fire warning system. When electrical resistance reduces to trigger electrical resistance, the ratio of R/R0 becomes 0.1. Therefore, the exact response time from the original electrical resistance to trigger electrical resistance for the fire alarm system is counted by this method, and the corresponding response time of each sample is displayed in **Fig. 4-3** (b).

The PA@GO sample shows the relatively longest response time at each test temperature. After the MXene introduction, the response time of PA@MGOy samples gradually decreases. With MXene content increases, the response time of PA@MGO further decreases. Moreover, the response time decreases at high test temperatures due to the increased heat energy. Compared to the response time at other test temperatures, the response time at 250 ºC is relatively short. The response time at 250 ºC follows the sequence: 24 s (PA@GO), 12 s (PA@MGO20), 10 s (PA@MGO15), 9 s (PA@MGO10) and 7 s (PA@MGO5), respectively. Comparatively, PA@MGO5 displays the shortest response time of 7 s based on the "trigger electrical resistance" calculation method. Generally speaking, the trigger electrical resistance in this work is the lowest electrical resistance, which can guarantee the electrical circuit formation. Therefore, it is possible for the electrical circuit to be formed when electrical resistance is slightly higher than the value of trigger electrical resistance selected in this work. To verify whether the above situation exists, another method is proposed in this work based on light intensity to calculate response time. The details of the way are shown in the section below.

b). Response time based on "Light Intensity Change"

Theoretically, once the transformation from insulation to conductive mode is realized, the electrical circuit will be formed, and the lamp in the circuit will be on. Therefore, the fire-warning system has

begun to work when the light intensity is detected. This period until light intensity change is detected and set as response time, which shows the sensitivity of the fire-warning system. Regarding this calculation method, **Scheme 4-2** presents the detailed test method to precisely obtain the quantified response time. Fire-warning samples are put in an oven for heating. Once the coated GO on the sample's surface is reduced to conductive RGO, the conductive circuit will turn the lamp on. The avaspec-2048L spectrometer machine will record the light intensity change when the lamp is on. As expected, the collected light intensity increases with the test time increase. When light intensity remains stable, it reaches its maximum value. In this work, a sharp peak that appears at the wavelength of 529 nm when the lamp is on signifies the response time. Therefore, the light intensity will change with test time. The corresponding curves of light intensity change at 529 nm as a function of time are shown below in **Fig. 4-4** (a). The response time calculated by "light intensity change" is also demonstrated in **Fig. 4-4** (b).

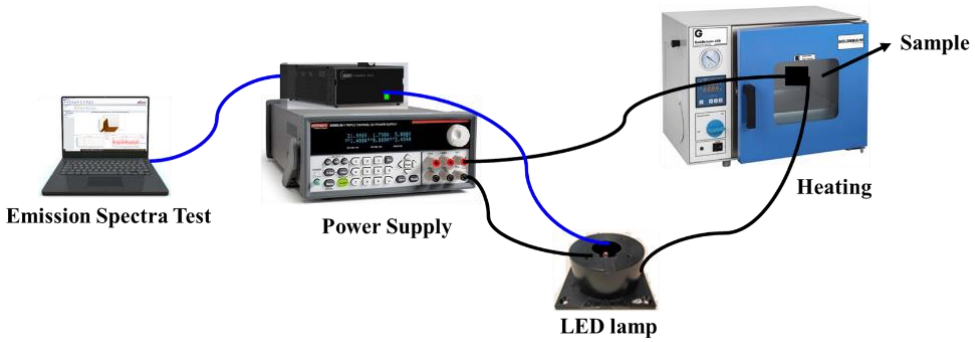

Scheme 4-2 Schematic test process for fire alarm samples.

As seen in **Fig. 4-4** (a), the light intensity change of each sample exhibits a similar trend when the electrical circuit is formed. The light intensity gradually increases to a constant value over test time. Comparatively, the highest light intensity is exhibited by PA@MGO samples, which is attributed to the excellent conductivity property of MXene. Therefore, the light intensity is further enhanced with the MXene content increase. It is a well-known fact that high temperature can accelerate the reduction of GO coated on the surface of the samples, which explains why the light intensity change of every sample becomes faster as the test temperature increases (**Fig. 4-4** (a) (i, ii and iii)). When the test temperature reaches 250 ºC, all the samples take less time to form a conductive pathway.

In accordance with the response time calculation method of "light intensity change" the time

at which the light intensity is the critical point for the fire-warning system. Therefore, this point at which light intensity changes is defined by making a tangent, and the corresponding time is set as the response time for the fire alarm. As shown in **Fig. 4-4** (b), the change tendency of response time obtained by this method is consistent with the changing trend of response time calculated by "trigger electric resistance". Similarly, the PA@GO sample exhibits a relatively longer response time by comparison with PA@MGOy samples. Once MXene is introduced on the surface of CP, the response becomes more rapid, showing a shorter response time. As the test temperature increases from 150 ºC to 250 ºC, all the samples' response time gradually decreases. At the test temperature of 250 ºC, the response time of PA@MGOy samples is relatively short compared to the lower test temperatures. The PA@MGO5 sample exhibits the fastest response time of 2 s at this test temperature. This shows that the coated CP is endowed with rapid electrical conductivity-responsive behavior at a relatively lower test temperature.

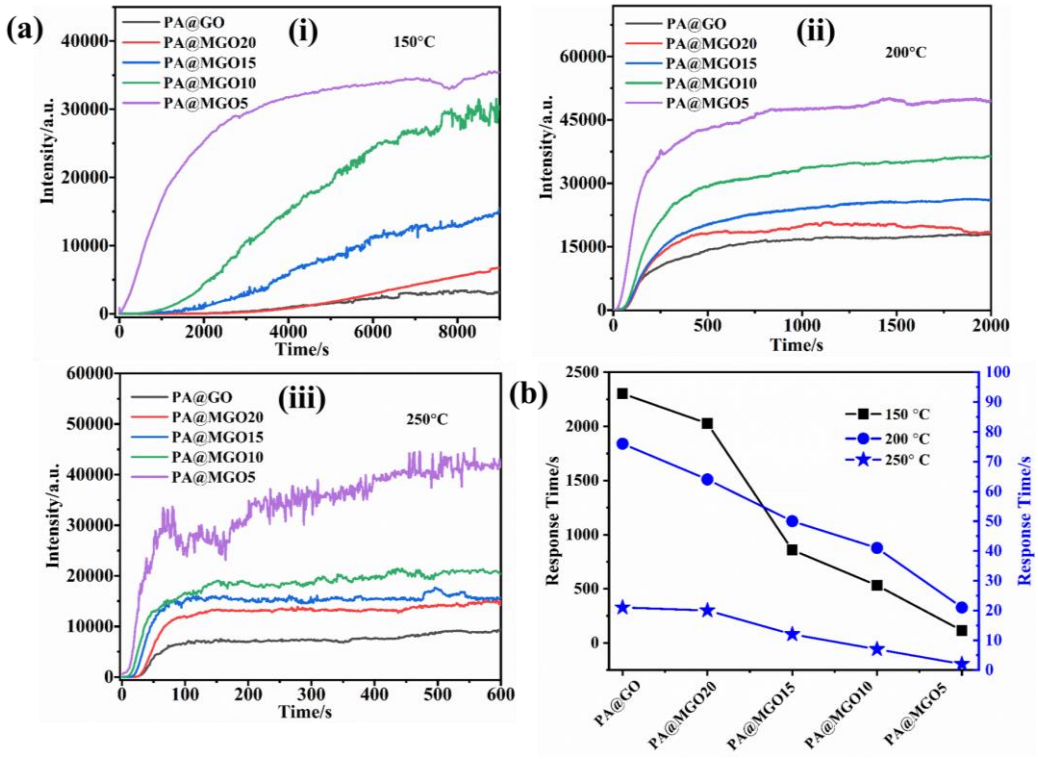

Fig. 4-4 (a) Curves of light intensity change versus different test time: (i) 150 ºC, (ii) 200 ºC and (iii) 250 ºC. (b) Response time calculated by "light intensity change".

As mentioned above, two methods are employed to calculate response time for fire-warning systems. To better understand the distinction, a comparison of response time calculated by each

method at different test temperatures is exhibited in **Fig. 4-5** (a) - **Fig. 4-5** (c). At each test temperature, the response time of different samples shows a slight difference but the same tendency. The response time obtained by "trigger electrical resistance" is relatively longer than by "lamp intensity change." The possible reason is that the value of the selected "trigger electrical resistance" is relatively lower than the one that can form a circuit pathway. As previously explained, when the electrical resistance decreases to "trigger electrical resistance" about 90 % of electrical resistance drops. Therefore, it is quite possible that at an electrical resistance of less than 90 %, a certain amount of RGO could be formed to facilitate electron transfer through the electrical circuit, which means the light intensity method can trigger the fire-warning system earlier. Comparatively, the obtained response time calculated by the light intensity change is more quantifiable and realistic. The response time of PA@MGO5 calculated by "light intensity change" is only 2 s at a test temperature of 250 ºC, which shows advantages in low-temperature rapid detection of the fire-warning system.

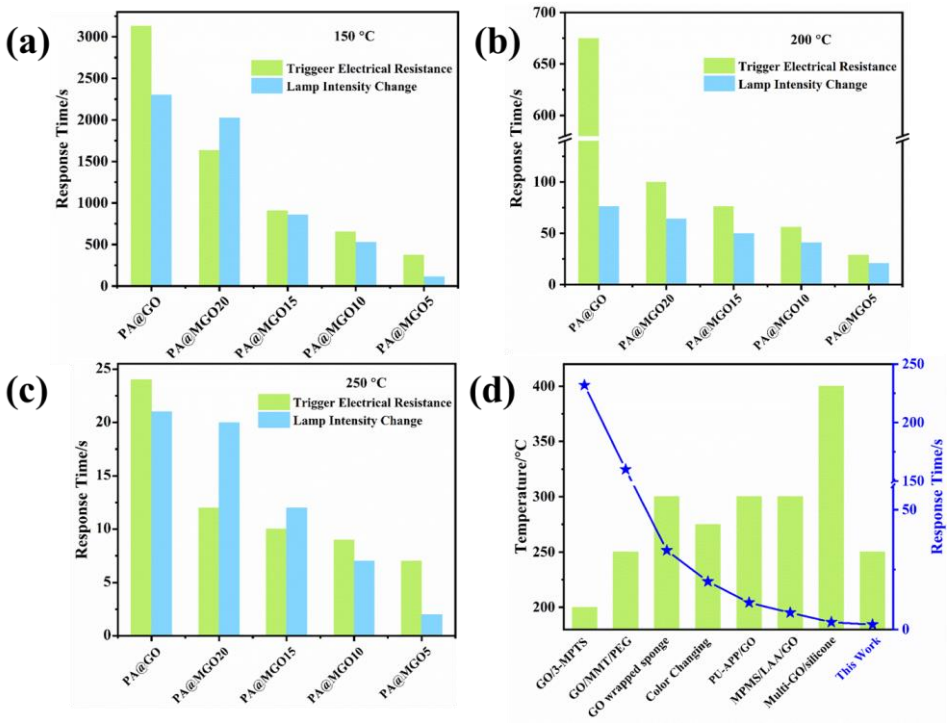

Fig. 4-5 (a) Comparison of response time calculated by two methods at 150 ºC. (b) Comparison of response time calculated by two methods at 200 ºC. (c) Comparison of response time calculated by two methods at 250 ºC. (d) Comparison of alarm response time for other state-of-art fire-warning systems (Abbreviation: 3-mercaptopropyltrimethoxysilane (3-MPTS); montmorillonite (MMT); polyethylene glycol (PEG); ammonium polyphosphate (APP); polyurethane (PU); L-ascorbic acid (LAA); 3-

methacryloxypropyltrimethoxysilane (MPMS); Multilayered graphene oxide (Multi-GO)).

The response time obtained in this work is compared to the values reported in other fire alarm research and summarized in **Fig. 4-5** (d) for better comparison. From the comparison, GO becomes the preferred material for fire-warning systems because of its electrical resistance-switching effect. Moreover, the fast response time mentioned in some research occurs when the test temperature exceeds 300 °C. A few studies involve quick response at low temperatures, but the response time is extended. Therefore, this work can quickly respond to fire signals at relatively low temperatures, gaining more time for fire control.

4.1.6 Proposed temperature-responsive resistance transition mechanism

The critical factor for fire-warning systems is the successful transition from electrical insulation at room temperature to electrical conductivity at high temperatures. In this work, GO undertakes conductivity transformation. To verify the successful reduction of GO to RGO, proving the proposed working mechanism for fire-warning system. XRD and Raman tests are carried out, and results are shown in **Fig. 4-6**. From the XRD curve of GO in **Fig. 4-6** (a), it is easy to see a sharp peak at $2\theta \approx 11$ º, belonging to (001) reflection peak [164]. After GO reduction by the heating process, (001) reflection peak disappears. There is a broad peak at $2\theta \approx 26$ º, corresponding to the typical characteristic (002) graphene crystal plane of RGO [164].

In addition, the Raman test is also used to detect structural change caused by the heating reduction process (**Fig. 4-6** (b) and **Fig. 4-6** (c)). Both of the Raman spectrums include two strong characteristic peaks at ≈ 1348 cm^{-1} (D band of carbon) and ≈ 1595 cm^{-1} (G band of carbon) [178]. The relative intensity ratio I_D/I_G values are different, indicating the change in graphitization degree. After heating treatment, I_D/I_G value of the PA@MGO sample increases from 0.59 to 0.78 due to an increase in surface defects content or edge area for RGO [63, 159, 164, 179]. It also indicates that most of the oxygen-containing functional groups on the GO surface are removed due to the heating reduction process. Additionally, D and G peaks in the PA@MGO sample after heating become slightly sharp, showing a decreased average size of the SP^2 domain [179]. Based on the above results, RGO has been successfully formed in the sensor samples after the heating process, which provides conductivity for the circuit.

Because of the analysis mentioned above, the proposed working mechanism for a fire-warning

system is revealed in **Fig. 4-6** (d). The fire-warning alarm response is due to GO nanosheets' fast thermal reduction process. Once fire or high-temperature rise occurs, most oxygen-containing groups, like carboxyl groups, epoxy groups, and hydroxyl groups on GO nanosheets' surface, experience thermal cracking and are removed from the GO surface [98, 180]. This leads to the formation of RGO, which will form a conductive pathway on the GO surface. It is consistent with the above Raman and XRD results.

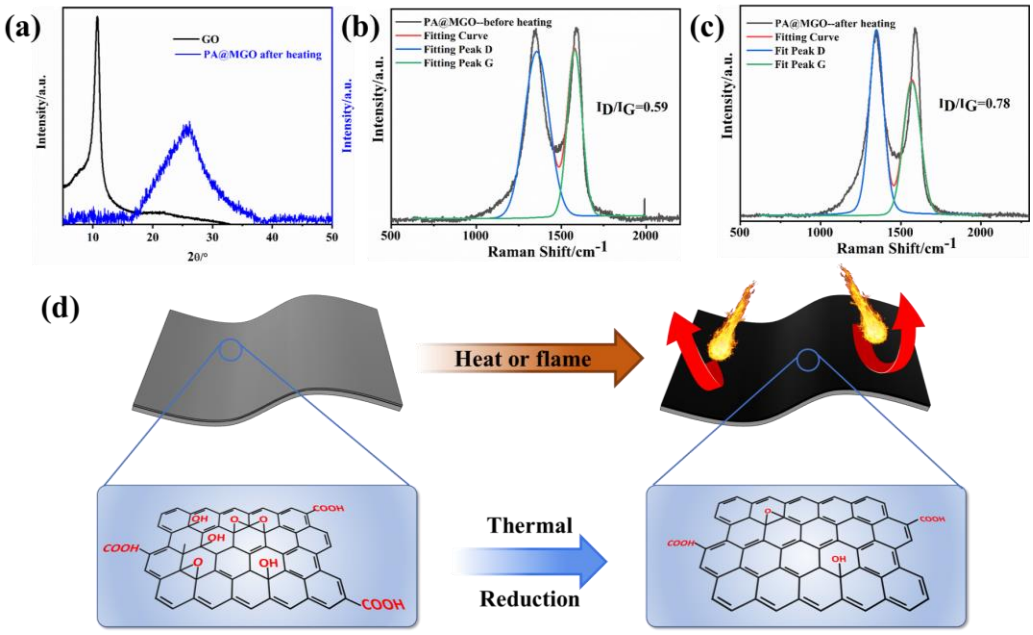

Fig. 4-6 Proposed temperature-responsive resistance transition mechanism: (a) XRD curves of PA@MGO after heating. (b) Raman spectra of PA@MGO sample before heating. (c) Raman spectra of PA@MGO after heating. (d) Proposed working mechanism for fire-warning system.

4.1.7 Fire-alarm response process based on wireless conversion device

The scheme of fire warning system-to-wireless signal conversion and communication process for remote monitoring of the fire process is presented in **Fig. 4-7**. Correspondingly, a video to show its function is also present in supporting information. Once the material is calibrated with the proper thresholds, the system is placed at different locations in closed or open areas where continuous monitoring of environmental parameters is needed, such as the temperature supported by the fire warning system presented in this work. As soon as the electrical circuit is formed after the electrical resistance transformation of GO, due to a temperature increase or fire, a fire warning message will be sent to an operator who will be controlling the state of such parameters in another remote location.

Moreover, another LCD display could be directly connected to the Wi-Fi emitter in the case a warning message is required at the location where a fire or high-temperature increase occurs. Besides, the remote fire warning radius can be extended using a LoRa internet of things (IoT) system, and automated actuators such as fire extinguishers could be activated once the system warns of the danger.

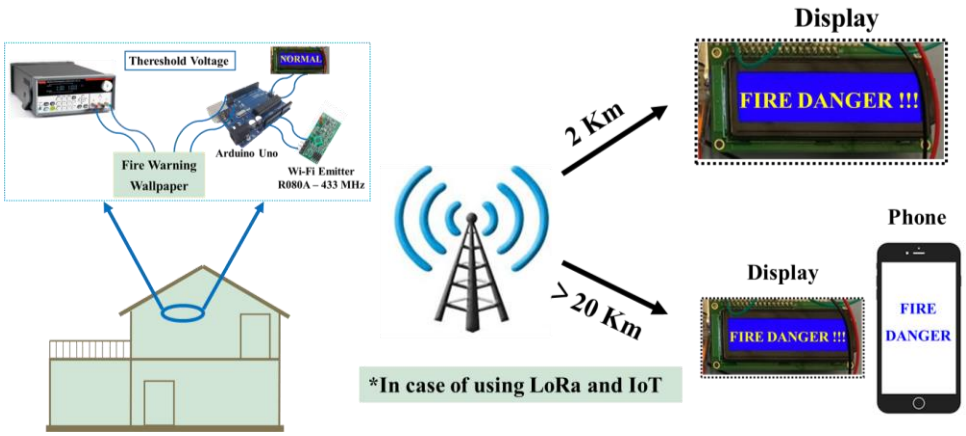

Fig. 4-7 Schematic of wireless conversion from fire information to Wi-Fi signal for remote monitoring fire alarm process.

4.1.8 Conclusions

A highly sensitive fire-warning system based on PA@MGOy CP was successfully prepared via a simple dip-coating method. After modification with two-dimensional GO and MXene, the flame-retardant PA@MGO5 paper exhibited a highly sensitive response to abnormal temperature during the pre-combustion process, showing a rapid response time of 2 s at a relatively low temperature of 250 °C, which will earn more time to ensure safe rescue and evacuation of people before fire development. A novel method to detect fire warning signals based on light intensity has been demonstrated to evaluate response time for the fire-warning system, which is more quantifiable and precise. It is noteworthy that a designed wireless signal conversion and communication device has been integrated into the fire-warning system for the first time, which successfully converts the received signal of the fire-warning system into wireless signals and displays a fire warning message on an LCD screen during high temperature or fire scenarios, within a radius of 2 km from the incident location.

4.2 Flexible functional cellulose paper (CP) as a fire alarming

4.2.1 Introduction

Wallpaper-based fire-warning sensors are one operating and efficient approach for indoor fire detection, which provide a potential advantage in daily household items, such as wires, wallpaper, smart fabrics, or decoration. Specifically, using eco-friendly CP sourced from cotton, wood, or bamboo as the wallpaper endows sustainability, strong stability, and biocompatibility with the system [181-183]. Thus, wallpaper-based systems are emerging as new fire alert strategies. There are yet some challenges that these systems need to face before becoming a well-established fire-warning technique, such as compatibility, flexibility, etc.

In addition, our previous work, including CP-based and GO film-based fire-warning systems, has shown a significant decrease in the response temperature down to 250 °C - lower than the minimum combustion temperature of substrate materials [146, 147, 184]. However, we find that adding organic flame retardants plays a negative role in the mechanical properties of GO-based systems. Excellent flexibility is a critical feature of fire-warning systems, especially for the CP-based fire-warning sensor. So, how to balance flame retardancy and flexibility has yet to be realized. Moreover, current systems rarely focus on the multifunction of these materials and other applications, such as wireless connectivity, strongly linked to comprehensive performance, smart modernization, and practical application.

This work focuses on achieving a balance by optimizing flame retardancy and flexible performance. Introducing a flexible molecular segment is one approach to improving the flexibility of materials. For example, PEO has excellent structural flexibility, amphiphilicity, and biocompatibility [185-187]. In addition, PEO can be dissolved into water, which is advantageous to mix with GO aqueous solution. Moreover, PEO can form film, which is helpful for the formation of GO [185]. In terms of signal conversion, developing temperature sensors has aroused considerable attention, which can improve the accuracy and expand the application of fire-warning systems. Herein, a CP-based fire-warning system with a low-temperature warning, ultrafast response, flexibility, remote wireless luminosity signal transmission, and novel temperature-aid wireless signal conversion ability is studied.

4.2.2 Preparation and characterization for flexible functional CP

As shown in **Scheme 4-3** (a), homogenous GO, MTM, PEO, and CNT solutions were prepared for subsequent use. First, GO and MTM solutions were mixed and stirred for 0.5 h to improve the dispersion. Subsequently, the PEO solution was added to the above-mentioned solution, which was then magnetically stirred for 2 h for the final homogenous composition. Finally, P_xM_y@GO films were obtained by the blade coating method. Considering the negative influence of flame-retardant particles on flexibility, tune the concentration of MTM and PEO to balance mechanical property and flame retardancy. Comprehensively, P15M15@GO with a PEO concentration of 15 mg/ml and MTM concentration of 15mg/ml is selected for the following experiments.

Moreover, the homogenous solution was applied to the CP to obtain modified cellulose paper (GCP) via the dip-coating method (**Scheme 4-3** (b)). Next, the CNT solution was sprayed onto the GCP surface to gain the final fire-warning sample (N@GCP).

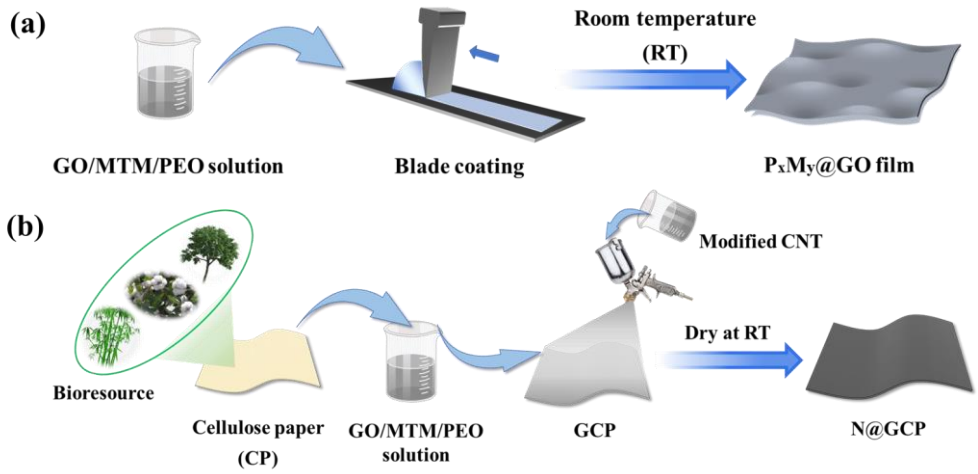

Scheme 4-3 Schematic illustration of the fabrication procedures: (a) P_xM_y@GO film; (b) the modified cellulose paper.

FTIR, XRD, SEM, and EDS were performed to check the structural features of CP, GCP, and N@GCP. From the FTIR curves in **Fig. 4-8** (a), each paper has its representative peaks with peaks at about 3320 cm^{-1}, 2894 cm^{-1}, 1630 cm^{-1}, and 1428 cm^{-1}, attributing to the stretching vibration of the hydroxyl group, -CH stretching vibration of hydrocarbon constituent, the vibration of absorbed water, and bending vibrations of $-CH_2$ of cellulose, respectively [175]. Compared to the pure CP sample, the new peaks at around 1280 cm^{-1}, 947 cm^{-1}, and 843 cm^{-1} appear in GCP and N@GCP samples, corresponding to the characteristic peaks of PEO [188-190]. This result verifies the coating

of the functional layer. In addition, the peak at 1590 cm^{-1} corresponding to the -NH group only appears in N@GCP, showing the successful coating of functional CNT [191]. XRD test is also used further to study the structure change (**Fig. 4-8** (b)). CP has two characteristic peaks corresponding to the characteristic (110) and (200) reflection peaks for CP [192, 193]. Rather, GCP and N@GCP have another peak at about $2\theta \approx 8.0$ °, corresponding to the (002) diffraction peak of GO. This peak shifts to a slightly lower peak in comparison to the peak for pure GO, which reveals the expended layer distance [194].

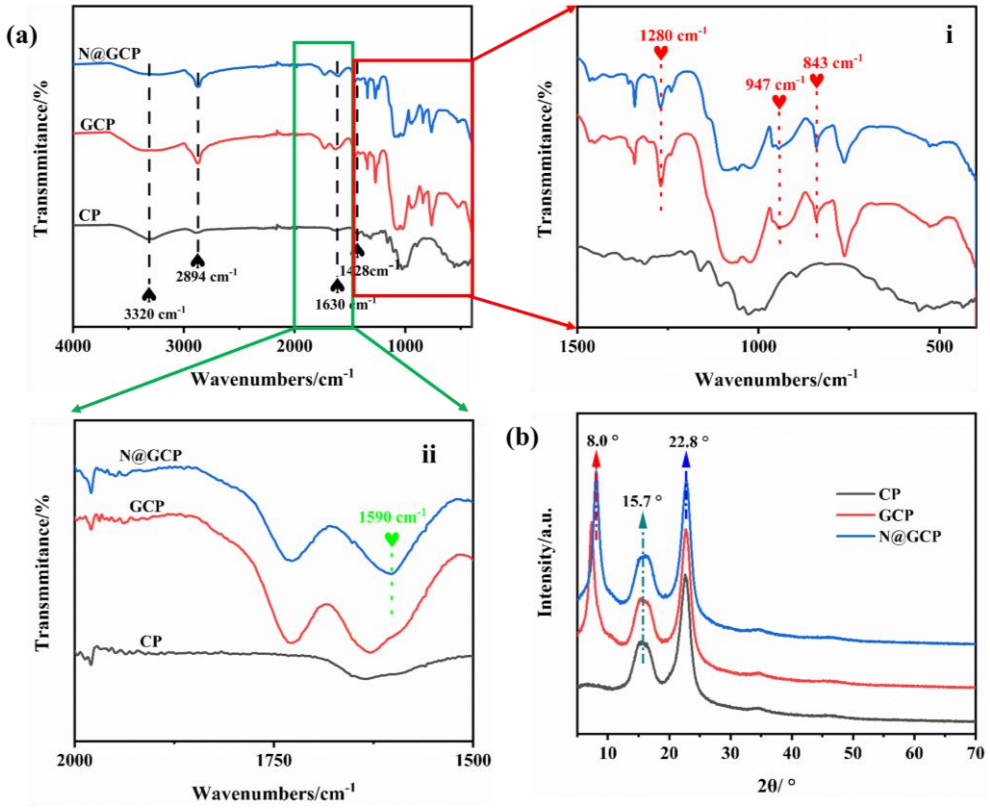

Fig. 4-8 (a) FTIR spectrums, (b) XRD diffract grams, (c) SEM images, and (d) EDS element mappings of the cross-section for pure CP and CP-based fire-warning system.

Moreover, SEM, a powerful tool, is applied for surface morphology analysis, and the results are displayed in **Fig. 4-9** (a). The pure CP shows a porous structure on the surface. However, the modified CP reveals a continuous surface topography. After introducing functional CNT, the surface of N@GCP becomes rough, and some small particles are on the surface, showing successful coating. The EDS images in **Fig. 4-9** (b) exhibit the elements in each paper, proving the successful coating of functional CNT as well.

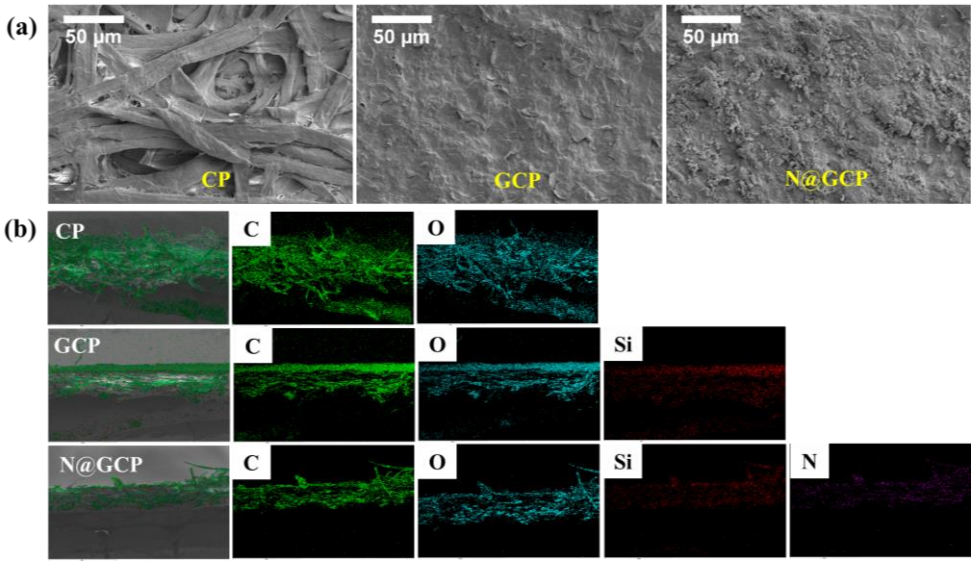

Fig. 4-9 (a) SEM images, and (b) EDS element mappings of the cross-section for pure CP and CP-based fire-warning system.

4.2.3 Mechanical property and flame retardancy of flexible functional CP

The stress-strain curves of different CP-based fire-warning systems are presented in **Fig. 4-10** (a). The stress of each paper increases with the long strain. However, the surface modification for each paper is different, leading to the distinct strength and elongation at a break between them. The stress strength of N@GCP can increase up to 15 MPa. This might be caused by the introduction of CNT, which can also reflect the good adhesion of GO-MTM composite on the cellulose surface [195].

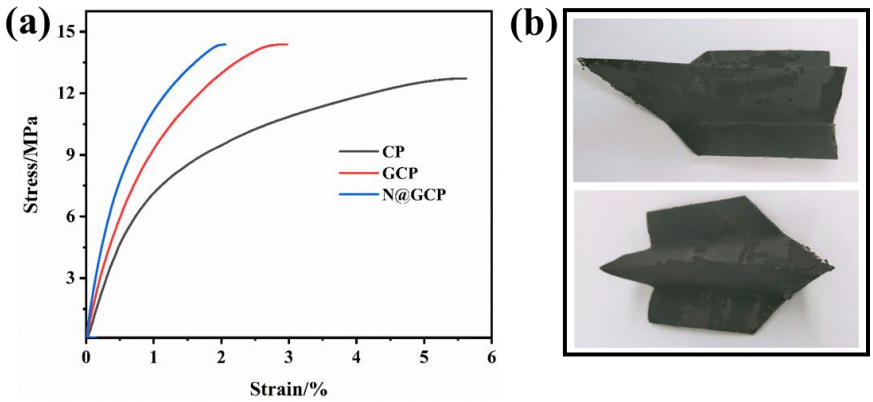

Fig. 4-10 (a) Time profile of the tensile strength curves of pure CP and CP-based fire-warning system; (b) images of folded coated CP.

Additionally, the coated CP is folded into an airplane shape to illustrate further its flexibility (**Fig. 4-10** (b)). There is no visible breakage signal, even at the folded edges. Both results show the flexibility of modified paper, which provides different possibilities for the potential shape designs

of the wallpaper-based fire-warning system.

Excellent fire resistance is essential for a fire-warning system. Therefore, the flame retardancy of coated paper is verified via the results of TGA, MCC, and combustion behavior, as presented in **Fig. 4-11**. All the TGA curves in **Fig. 4-11** (a) show a descending tendency but different remaining weight at high temperatures, with the following sequence: N@GCP＞GCP＞CP, indicating the improved flame retardancy after modification. Additionally, an MCC test was performed to record combustion parameters, including the peak heat release rate (HRR) and oxygen content. The peak HRR value is closely related to oxygen consumption [145]. As shown in **Fig. 4-11** (b), GCP has less oxygen consumption than pure CP, leading to a lower peak HRR value. When GCP is further modified by NH_4-CNT, the peak HRR value of N@GCP becomes slightly lower again, which displays the further reinforcement of fire resistance. Furthermore, the combustion behavior of samples under ignition treatment is carried out to observe the morphological change intuitively. From the optical images in **Fig. 4-11** (c), neat CP burns out into ashes within 10 s. However, GCP and N@GCP still maintain their shape for burning for 90 s, resulting in a higher flame resistance, which can provide a solid foundation for manufacturing a fire-warning system.

The schematic illustration of the flame-retardant mechanism is shown in **Fig. 4-11** (d). Under flame exposure, a functional layer on the surface of CP can form a protective layer composed of the accumulating silicon dioxide, primarily attributed to the burned MTM. Importantly, this physical layer can be used as thermal insulation to protect the substrate and as a barrier against oxygen release and heat transfer [46, 172].

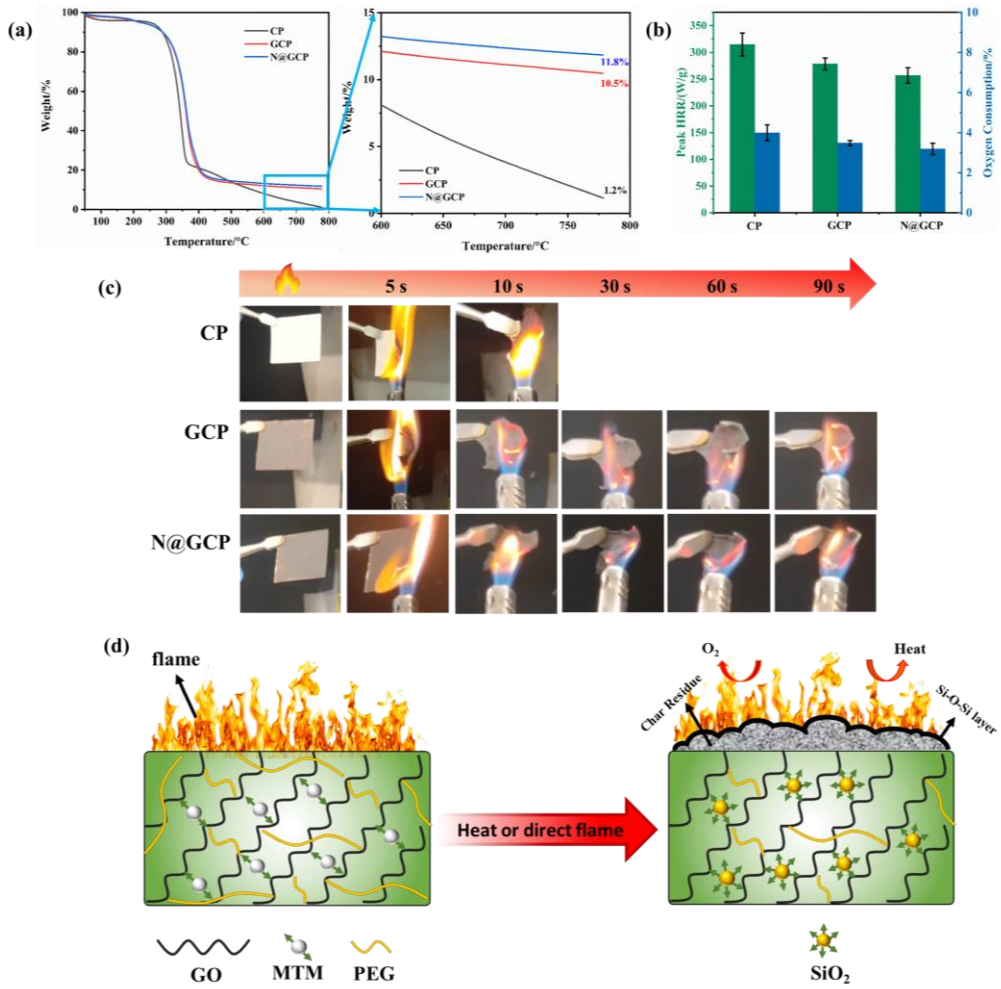

Fig. 4-11 (a) TGA curves, (b) peak HRR and oxygen consumption change, and (c) screencaps of combustion process of pure CP and CP-based fire-warning system. (d) scheme illustration of the flame-retardant working mechanism.

4.2.4 Fire warning process of flexible CP-based fire-warning sensor

The change of conductive state is the response to temperature for GO-based fire-warning systems. Therefore, studying samples' electrical conductivity as a temperature function is crucial. This work records the electrical resistance change to reflect the change in an electric conductive state. To verify the response-ability at low temperatures, the oven at 250 °C is used as a heating source, and the electric resistance of fire-warning samples is collected vis time. As seen in **Fig. 4-12** (a), the electric resistance of GCP and N@GCP gradually decreases with the increasing heating time, showing the same downward trend. However, the rate of decline for each sample is different. N@GCP has a faster descent, indicating a lower electric resistance after heating for the same time by comparison with GCP.

Furthermore, an ignitor is applied to burn the sample because this flame type is similar to a real flame. Identically, the electrical resistance of GCP and N@GCP are monitored during the combustion process, as shown in **Fig. 4-12** (b). The electric resistance of GCP and N@GCP display the same decreasing trend under continued burning treatment. N@GCP also holds a faster descent rate than GCP. However, it is worth noting that a turning point appears in the curve of electric resistance. This might result from the unstable state of the paper during the burning process. By contrast, an ignitor can provide more powerful thermo-energy, leading to a slight shape change during burning. This is consistent with the above shape change results during the continued burning process.

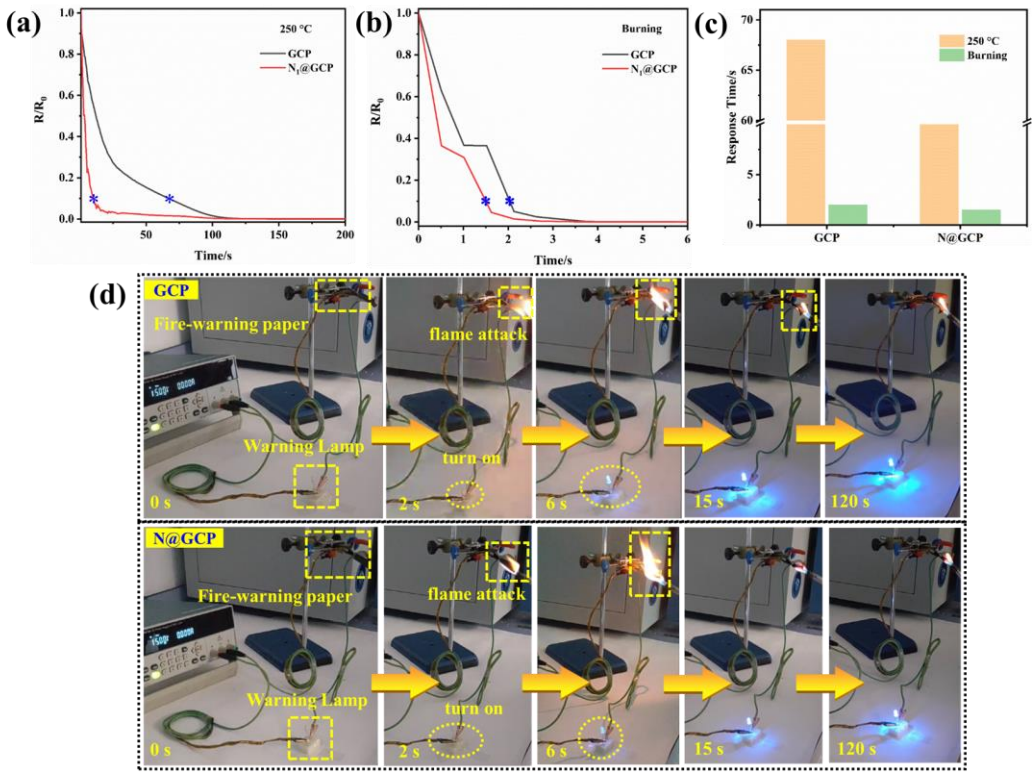

Fig. 4-12 The electrical resistance changes of CP-based fire-warning system under (a) 250 ºC and (b) burning situation. (c) response time of fire-warning systems after heating and burning situation. (d) fire-warning simulation process of GCP and N@GCP fire-warning systems under fire attack.

It has been proposed that one way to calculate response time is based on “trigger electric resistance” [14]. For this method, there is an electrical resistance threshold. The electrical resistance threshold here is 90% of the initial electric resistance. In this way, the response time of each sample is obtained, and results are shown in **Fig. 4-12** (c). In contrast, N@GCP has a slightly shorter response time than GCP, even if the provided thermos-energy is different. Under the other heating

treatment conditions, the ignitor can give more assertive energy to achieve a fast reduction of GO to form an electrical pathway, which reflects a short response time. Fortunately, the response time of N@GCP is only 2 s, demonstrating the warning occurs within 2 s. This result strongly proves the highly sensitive warning ability of the fire-warning system in this work.

To explain how the fire-warning system works, simple fire-simulation scenarios are prepared. The change of lamp state (on or off) is employed to send a warning signal. Images in **Fig. 4-12** (d) change the lamp state during the fire-warning simulation. At the beginning of the simulation, the lamp is off. After burning, the fire-warning sample turns into a conductive condition to afford the lamp to be on. As the burning time increases, the lamp becomes brighter due to more formation of RGO. Notably, the warning signal can continue for at least 120 s under burning conditions.

4.2.5 Working mechanism of the fire-warning process

GO-based fire-warning systems primarily rely on the change of conductive states for GO to respond to abnormal temperatures during combustion. The successful change of conductive state means the formation of RGO, which can lead to the corresponding structural change. To verify the successful reduction of GO, XRD, Raman, and SEM tests are carried out, and the related results are presented in **Fig. 4-13**.

For the XRD curves of heating treated paper (**Fig. 4-13** (a)), two sharp peaks appear at about 15.8 ° and 21.7 °, assigning to (110) diffraction peak of CP and (200) diffraction peak or characteristic peak for RGO. It isn't easy to distinguish the assignment of a peak of 21.7 ° due to the overlap of the peak from CP and RGO. In contrast, the burned paper has two small shoulder peaks at around 15.8° and 22.0 °, respectively. This might result from the increased thickness of the char layer covering the surface of the paper. The instrument could select relatively less information on cellulose. However, the comparison reveals the structural changes of burned paper are more significant than the ones of heated paper. This might be attributed to the different content of the char layer, which is caused by different thermo-energy.

Moreover, structure change is further revealed by the I_D/I_G value from Raman spectroscopy (**Fig. 4-13** (b)). The I_D/I_G value of heated paper slightly increases, and the further advanced I_D/I_G ratio of burned paper is observed. The ratio assesses the average size of the sp^2 cluster of materials [196]. This result implies more formation of smaller fragments and edge carbon atoms after

combustion treatment, leading to decreased graphitization degree [159].

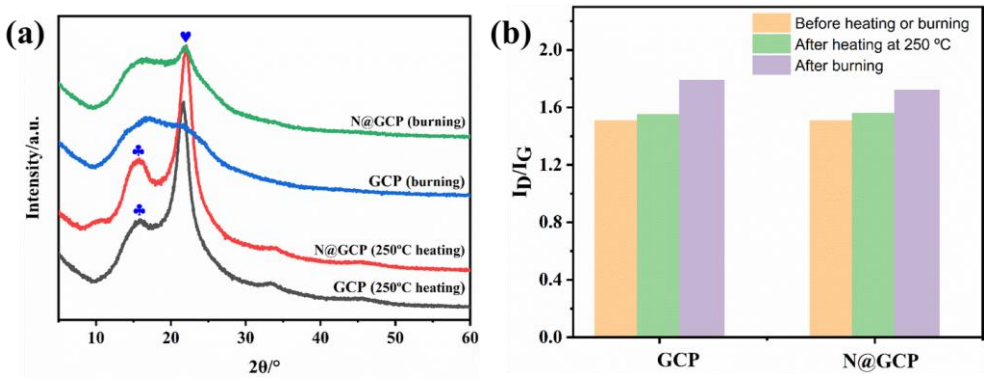

Fig. 4-13 (a) XRD diffract grams, (b) I_D/I_G value of GCP and N@GCP after heating treatment at 250 ºC and burning treatment.

The surface offers further insights into GO's structural changes. The morphologies of the heated and burned paper are depicted in **Fig. 4-14** (a) and **Fig. 4-14** (b). After thermal treatment, the carbon layer can be formed on the surface, leading to a continuous structure compared to pure CP's pore structure. At the same time, some particles appear on the surface, which might be from the heating treatment of CNT. The same phenomenon is also observed in the burned paper. The SiO_2 network is seen in the image with high magnification, which plays a positive role in improving flame retardancy [172]. This is consistent with the above results.

All the above results strongly prove the successful reduction of GO. The proposed reduction process is schematically shows in **Fig. 4-14** (c). It is significant to note that structural damage could happen to basal carbon planes after thermal treatment. The defects could form in the carbon layer, leading to an influence on conductivity [169].

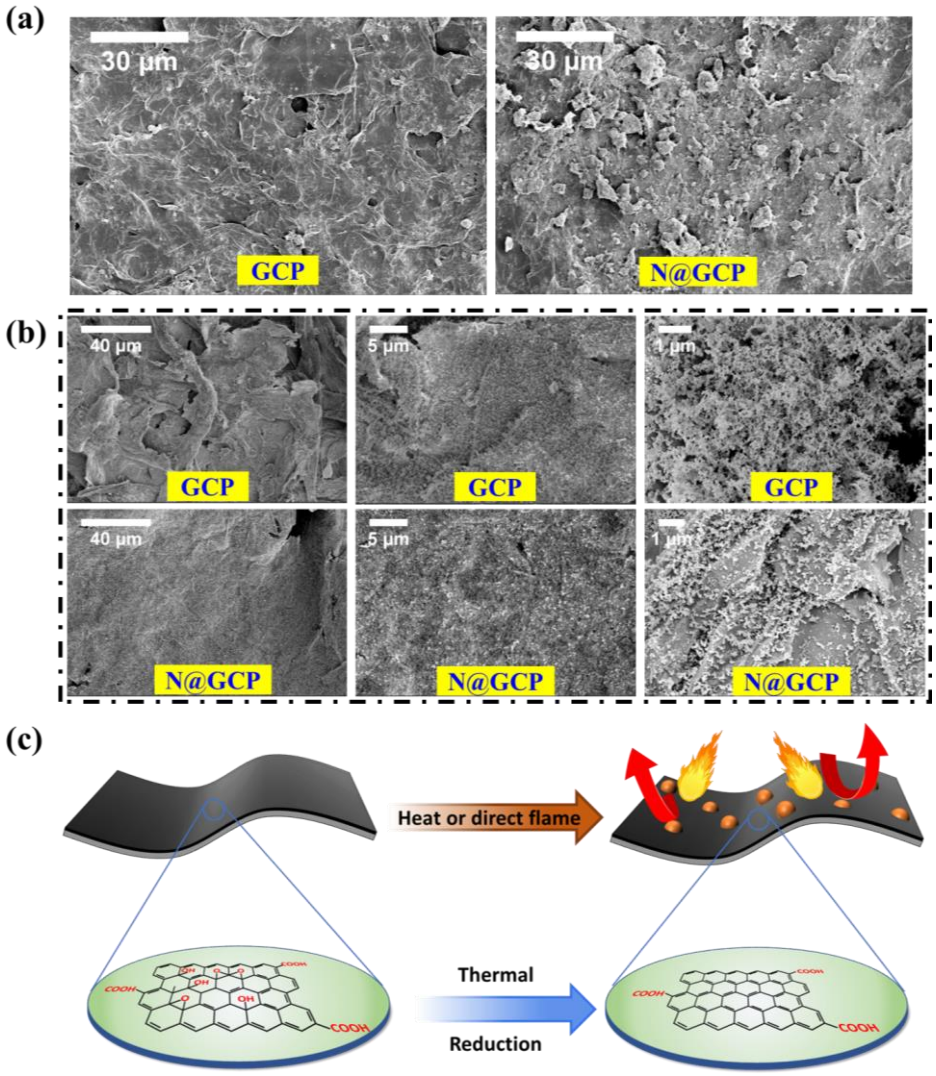

Fig. 4-14 (a) SEM images of heated GCP and heated N@GCP, and (b) burned GCP and N@GCP. (c) schematic illustration of the proposed working mechanism after a fire warning.

Apart from the conversion of conductive property, NH_4-CNT also plays a significant role in facilitating the formation of electric pathways. As depicted in **Scheme 4-4,** NH_4-CNT is expected as a bridge to connect the separate GO layers, providing the possibility of the formation of a conductive pathway, especially when the sample is exposed to a low temperature. To prove the proposed "bridging effect" of conductive NH_4-CNT, some tests are conducted, and analysis is shown in the next section.

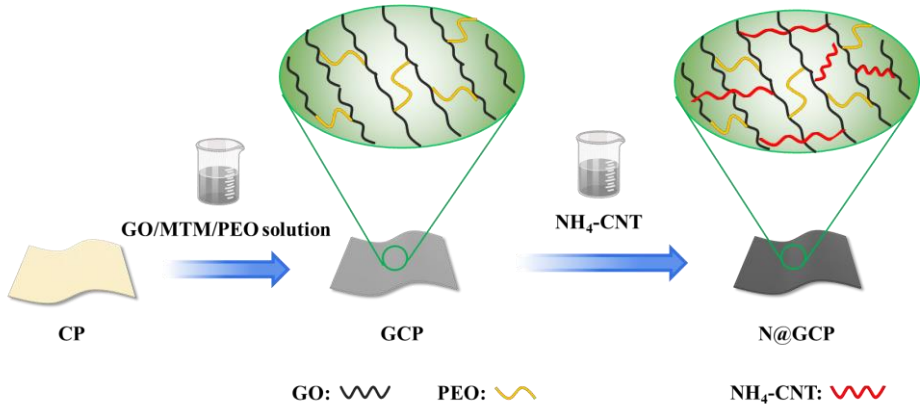

Scheme 4-4 Scheme illustration for the structure of modified CP.

4.2.6 Remote wireless conversion of monitored warning signal

Temperature and luminosity are highly correlated with fire development. Thus, a new temperature and luminosity sensors were employed to monitor these changes under a fire attack. As illustrated in **Fig. 4-15**, temperature and luminosity values are visualized once the sample is ignited. As a comprehensive overview, changes in luminosity are sent to a WiFi (wireless fidelity) network using a Wi-Fi module connected to a photoresistor sensor. Thus, any device connected to this network can access the data, including computers or cell phones. In addition, the real-time temperature is measured with a thermocouple and transmitted remotely via LoRA (long-range radio), which is also connected to the WiFi network.

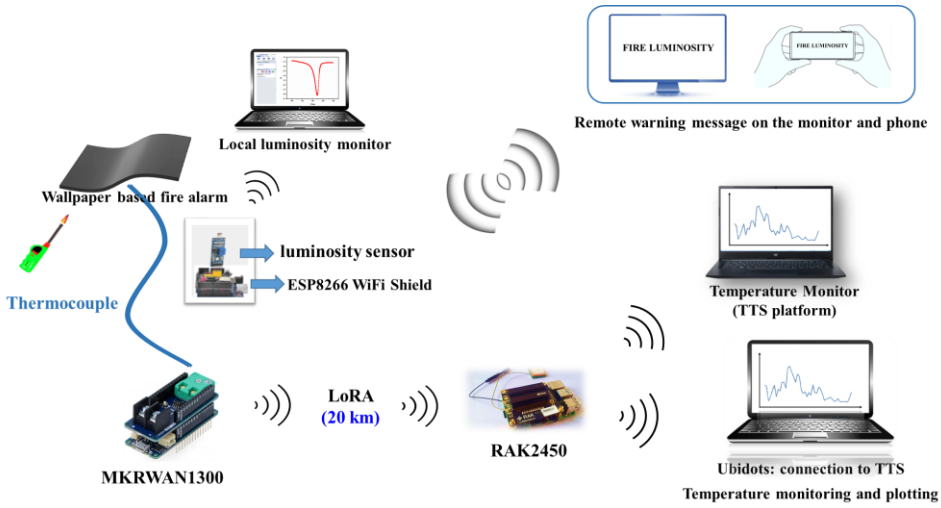

Fig. 4-15 Experimental set-up of the temperature and luminosity communication remote system.

The response and signal conversion properties are essential for estimating one fire-warning system. A summary of previously reported fire-warning systems and this work is provided in **Table 4-2**. In comparison, this work offers a lower response temperature (250 ºC) and accurate real-time temperature detection, leading to a lower fire risk and an improvement of the feasibility of practical applications.

Table 4-2. Comparison analysis between partial fire-warning systems.

Systems	Methods	solvents	Response Time / s	Response temperature	Signal conversion	Multifunction	Ref.
Graphene/SF/FA/Ca^{2+}	electro-blown spinning	FA/Ca^{2+}	2	-	Yes	Self-adhesive, humidity	[197]
GO/BP-MoS_2	vacuum filtration	-	1	-	-	-	[198]
SF/CaHIs battery	-	-	5	-	Yes	Self-healing	[199]
PA/GO/MXene	Dip-coating	water	2	250 ºC	Yes	-	[184]
MV or ME paper	Evaporation	water	1.8	-	-	hydrophobicity	[121]
SPI/MSF/GN/CA	-	-	2	-	-	Tensile strength	[101]
N@GCP	***Dip-coating/Spary***	***water***	***2***	***250 ºC***	***Yes***	***flexibility***	***this work***

[a] SF:silk fibroin; FA:formic acid; BP: black phosphorene; MoS_2: molybdenum disulfide; CaHIs:Ca^{2+} hydro-iontronics; PA:phatic acid; MXene:titanium carbide; MV:titanium carbide/polyvinyl pyrrolidone; ME:titanium carbide/polyethylene glycol; SPI:soy protein isolate; MSG:sisal cellulose microcrystals; GN:graphene nanosheets; CA:citric acid.

4.2.7 Conclusions

In summary, a functional coating layer over modified CP is used as a fire warning system. It presents excellent flexibility and flame retardancy, which can keep shape under continued burning treatment, leading to a solid function for a fire-warning system. After the temperature rises to 250 ºC or burning treatment, the warning signal can be monitored within 2 s, indicating the high sensitivity at low temperatures. In addition, it is possible to transmit local and remote messages with the hazard information simultaneously with a luminosity sensor and temperature sensor. The real-time temperature and luminosity changes are recorded and transferred to the computer or phone monitors within 20 km. This work aims to provide new insight into the next-generation smart fireproofing materials.

4.3 The mechanism of low-temperature fire warning behavior

As mentioned in the work, the introduction of conductive MXene and NH_4-CNT accelerates the formation of conductive pathway at low temperature of 250 ºC. The appropriate amount of conductive materials can not only maintain the materials' insolating situation at room temperature, but also be helpful to form electric conductive passages. The added conductive materials are assumed as a bridge to connect separated GO nanosheets to increase electron flow channels. To prove the proposed bridge effect of conductive material in the GO-based fire alarm, NH_4-CNT is chosen as an example to prepare GO/NH_4-CNT films for further illustration.

AFM, X-ray tomography, and TEM tests are employed for analysis. The surface morphology of GO and GO/NH_4-CNT films is analyzed by AFM. As the in-phase image of GO film depicted in **Fig. 4-16** (a), the surface of GO film after the assembly technique is a crumpled and rough structure consistent with the previous work [200]. The average roughness value (Ra) of GO film is 0.3464, showing its roughness to a certain degree (**Fig. 4-16** (b)). Comparatively, the surface of GO/NH_4-CNT film does not present obvious wrinkle feature. In addition, there are some white spots appearing, which might be attributed to the NH_4-CNT. The Ra value of GO/ NH_4-CNT films is 0.2884, indicating the decreased roughness comparatively. This result might be caused by the ultrasonic treatment of CO/NH_4-CNT mixed solution, leading to unbundles of NH_4-CNT and removing partial troublesome protrusions [201, 202]. Based on this result, the surface structure of

films slightly changes after the addition of NH_4-CNT in macroscopic.

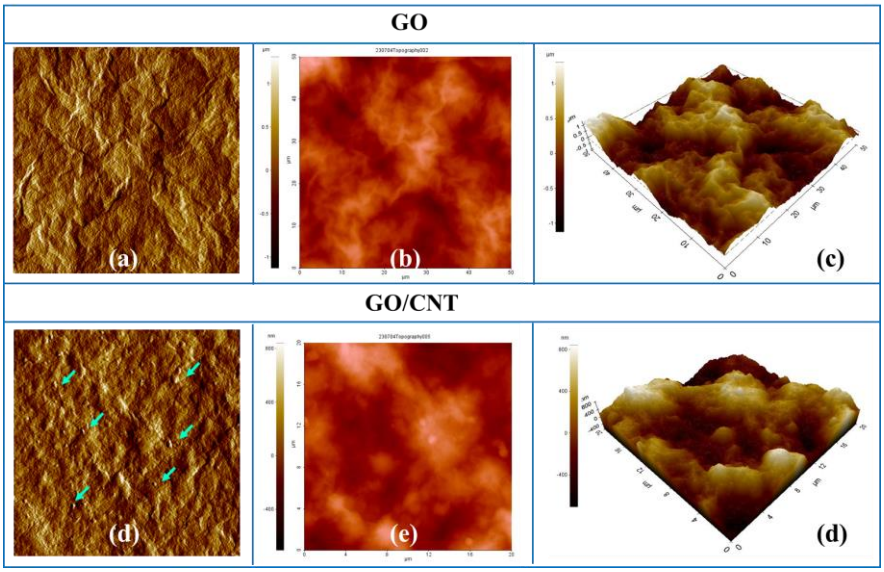

Fig. 4-16 AFM results of GO and GO/NH_4-CNT films: (a) in-phase image of GO; (b) phase image of GO; (c) 3-D topography of GO; (d) in-phase image of GO/NH_4-CNT film; (e) phase image of GO/NH_4-CNT film; (d) 3-D topography of GO/NH_4-CNT film.

X-ray tomography results are shown in **Fig. 4-17**. The film exhibits layered structure clearly. From the cross-section of films, the connections between different layers are not tight enough. There is air inside, which is a normal phenomenon for GO-based films. In addition to air, there seems to be nanoparticles in the NH_4-CNT film. In the plan view, the particles are seen clear, which might be resulted from the addition of NH_4-CNT. However, the resolution of images is not highly enough due to the limited resolution of the test. To further explain the dispersion of NH_4-CNT in the hybrid film, a TEM test is carried out and corresponding results are discussed below.

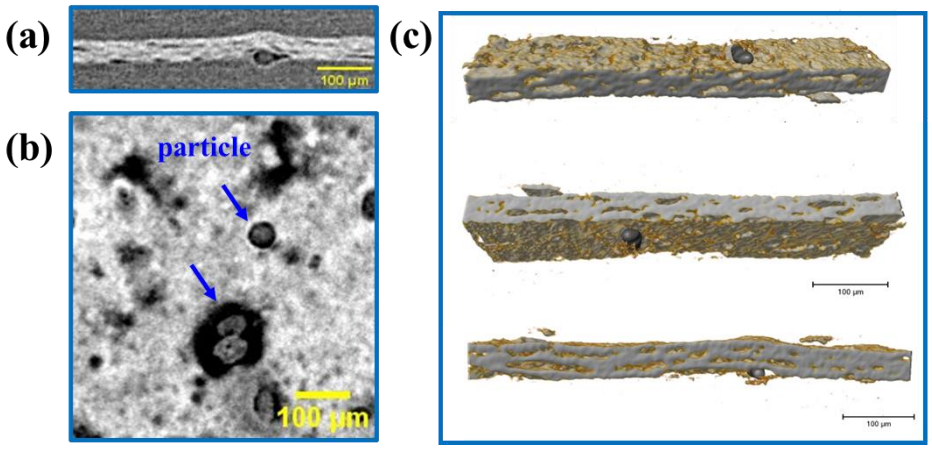

Fig. 4-17 Tomography results of GO/NH_4-CNT hybrid film.

In **Fig. 4-18** (a), GO and NH_4-CNT show layered structure and tubular structure respectively, which are consistent with the previous work [203]. The ends of NH_4-CNT tube connect two separate GO nanosheets, showing like a bridge connecting two isolated regions. After a quick heating treatment, the oxygen-containing group on the surface of GO flakes is removed and transformed to become RGO, presenting the same layer structure. As depicted in **Fig. 4-18** (b), some RGO nanosheets are still unconnected in heated GO/NH_4-CNT film. NH_4-CNT tube remains overlapped on two separate GO nanosheets in a tubular structure. This connection provides another conductive pathway except for the conductive pathway made only by RGO nanosheets. This phenomenon implies a increasing probability of triggering fire warning. For better understanding, the schematic illustration of the bridging effect is depicted in **Fig. 4-18** (c). Once heated at ~ 250 ºC, GO/NH_4-CNT film presents a higher possibility to form the conductive pathway, making compensation for the limitation for partial reduction of GO in developing conductive paths. Therefore, fire warning is fast realized at low temperature of 250 ºC.

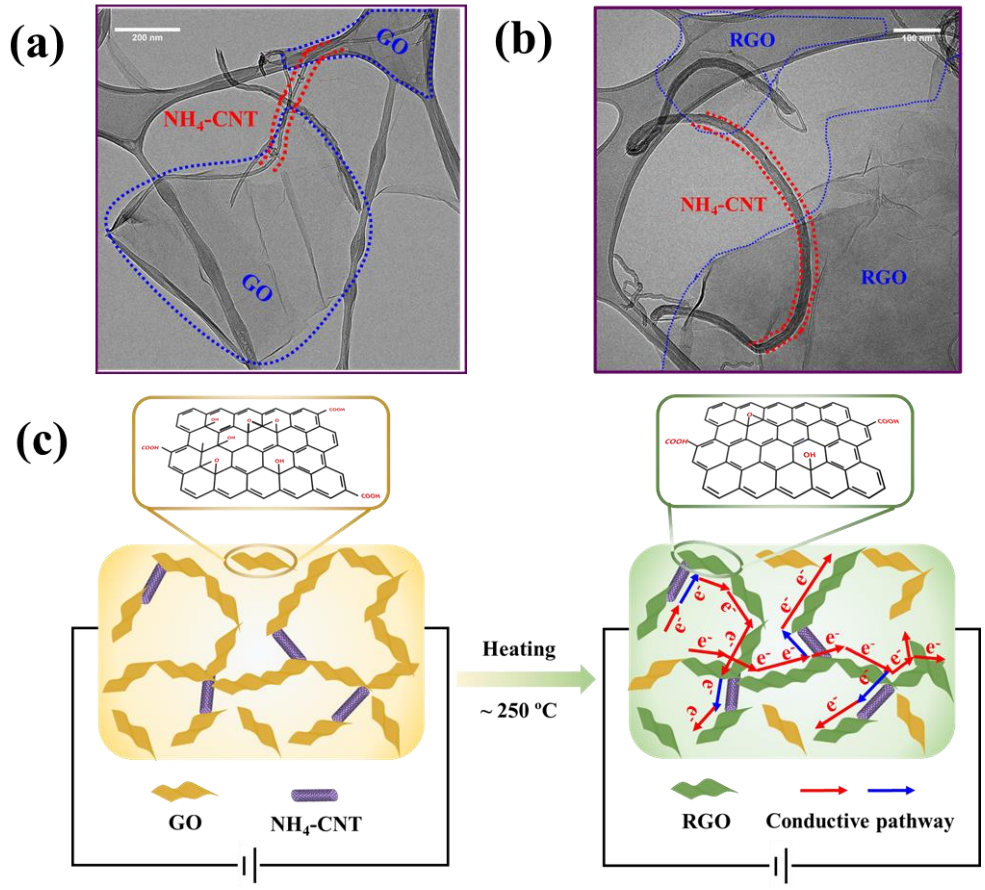

Fig. 4-18 TEM images of GO/NH_4-CNT film to show the proposed bridge effect: (a) original film, (b)

film after treatment at 250 ºC for a few minutes, (c) schematic illustration of the bridging effect for low-temperature fire-warning behavior.

CHAPTER 5

A reused biomass fire-warning sensor in varied humidity conditions

"I am a slow walker, but I never walk backwards."

-Abraham Lincoln

5.1 Introduction

As mentioned in the previous chapters, the primary working mechanism of early fire-warning sensors is the conductive conversion of GO. However, there still exist some limitations in their development path. In terms of GO material, its thermal sensitivity is irreversible and unidirectional. After GO is reduced to a conductive state, it cannot return to its original insulated condition, leading to one-time usage of GO-based fire alarms [106]. The narrow response temperature range and the need for an external power supply make GO-based fire sensors more complex [107]. In addition, the harsh environmental conditions negatively influence the accuracy of fire-warning ability.

Furthermore, traditional warning transmission methods like lamps or buzzers are no longer competitive in the digital era. In other words, developing smart low-temperature fire sensors is still a challenge. Herein, eco-friendly CS is selected as the foremost fire-warning material to fabricate a smart fire sensor.

CS is converted from chitin, a natural polymer mainly derived from shrimp, oysters, crabs, or cuticles of insects [204, 205]. CS has a similar structure to cellulose but abundant amino groups, which is one kind of alkaline polysaccharide [206]. CS is a non-toxic material with excellent physicochemical properties, exceptional biocompatibility, antibacterial effect, and polycationic properties, widely utilized in tissue engineering, the food industry, or drug delivery [82, 205, 207]. Moreover, on account of the existence of functional groups, CS material is sensitive to environmental factors such as temperature [208], humidity [209, 210], ionic condition [211], pH value [149, 212], ultraviolet lamps [213], and magnetic fields [214, 215]. Thus, CS is considered a potential "intelligent material, " attracting more attention to broadening its application fields like sensor development, energy storage, batteries, etc. Some progress has been made in the use of CS

for fire sensors. For instance, Yang et al. prepared CS and GO nano-coated melamine foam as a fire alarm, showing a response time of 3 s [216]. Chen et al. fabricated CS/montmorillonite/carbon nanotube composite aerogel to achieve fire warning [119]. However, most fire-warning systems use CS as the flame-retardant additive. CS is rarely reported as the primary fire-warning material despite the potential advantages of its working mechanism. Furthermore, considering the ability of CS in humidity detection, it is also expected to be thoroughly combined with a fire-warning sensor to improve its sensitivity and accuracy.

In this work, CS-based sensors are exploited by taking advantage of the thermo-sensitive and humidity-sensitive properties of CS. Three different salts, including sodium chloride (NaCl), ammonium chloride (NH_4Cl), and calcium chloride ($CaCl_2$), were added to CS to study their effect on the generated electric current. Under the co-driven of temperature and RH, the electric current of salts-modified CS films results in the following order: CS-NaCl, CS-$CaCl_2$, CS-NH_4Cl, CS. Moreover, RH detection can improve the accuracy of fire warnings for fire sensors, especially on rainy and foggy days. Furthermore, the advantage of integrating a wireless transmission system to provide a novel functional smart sensor is highlighted. This kind of sensor presents an advantage in household electrical appliances.

5.2 Preparation and characterization of chitosan (CS)-based sensors

The illustration of sample preparation is shown in **Scheme 5-1**. First, a homogenous CS solution was obtained for subsequent use by dissolving CS powder into an acetic acid solution with a concentration of 5 wt%. Next, the different salts were put into the above solution and stirred at room temperature until a uniform solution was obtained. Ultrasonic treatment of the solution mentioned above was made to remove the bubbles. Then, the resultant solution was poured into the dish and put in the oven at 40 ºC for 24 h to obtain the final CS-based films. Detailed component information is presented in **Table 5-1**.

Scheme 5-1 Scheme of fabrication procedures for CS-based films.

Table 5-1. The formulation for CS-based films.

Samples	CS Concentration *(wt%)*	Ration of salts to chitosan *(wt%)*	Solution Volume *(mL)*
CS	2	5	30
CS-NaCl	2	5	30
CS-NH_4Cl	2	5	30
CS-$CaCl_2$	2	5	30

The morphology of different CS-based films is studied. In **Fig. 5** (a), both CS, CS-NaCl, CS-NH_4Cl, and CS-$CaCl_2$ films are intact due to the good film-forming ability caused by the intramolecular and intermolecular hydrogen bonds between hydroxyl, amino, and N-acetylamino groups [44, 45]. All the films present good optical transparency, indicating that no significant change happens in the transparency of the films at the macroscopic scale, even if a small amount of salt content is added. The transmittance of all the films is about 92 % at 550 - 750 nm in the UV spectra (**Fig. 5** (b)), indicating good transparency similarly. However, these films display some differences at a microscopic scale, for example, in the surface performance of the films.

In the SEM images (**Fig. 5** (c)), the surface of pure CS film is relatively smooth. The surfaces of CS-NaCl, CS-NH_4Cl, and CS-$CaCl_2$ become slightly rough, possibly caused by the weak entanglement phenomenon reported from films after adding salts [84]. FTIR spectra are recorded to illustrate further the structural change of salt-modified CS-based films (**Fig. 5-1** (d)). All the films display the typical peaks of CS. Specifically, a prominent broad peak appears at 3312 cm^{-1}, assigned to the stretching vibrations of the N-H and O-H groups [217-219]. Two peaks at 2876 cm^{-1} and 2926 cm^{-1} correspond to the symmetric and asymmetrical -CH_2 and -CH_3 stretching bending. These peaks' intensity decreases due to the weakening of hydrogen bonds after adding the salts [220]. Besides, the peaks at 1637 cm^{-1} and 1536 cm^{-1} are attributed to C=O stretching bending (amide I) and N-H bending (amide II), shifting to a slightly lower wavelength. These results confirm the weakening of the intramolecular and intermolecular bonds of CS chains due to the introduction of salts, consistent with the previous works [206, 221]. Moreover, peaks at 1376-1403 cm^{-1} belong to -CH_2- bending

of CS [217]. These results are consistent with the above SEM analysis.

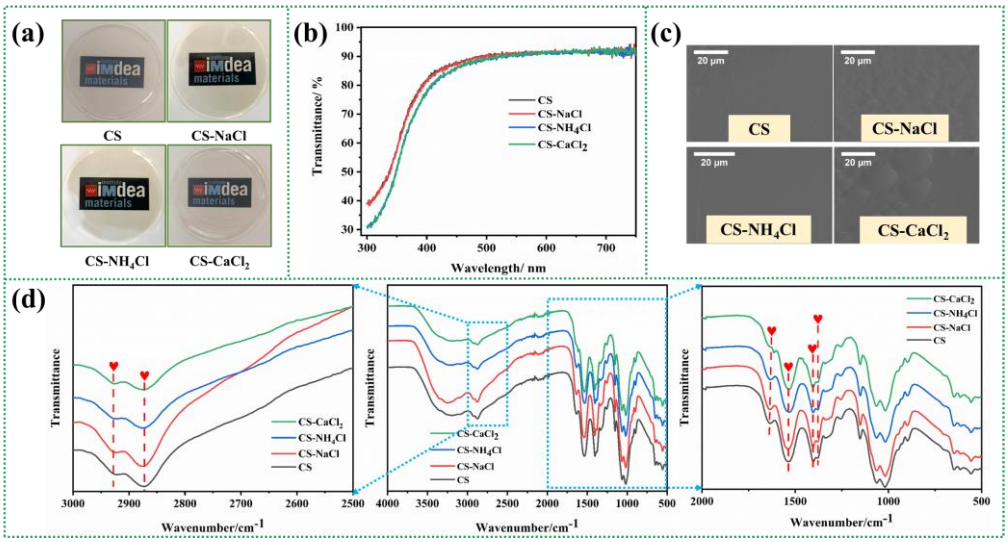

Fig. 5-1 Structural characteristics of distinct CS-based films: (a) optical images; (b) SEM images; (c) FTIR spectrum.

XRD and DSC analysis demonstrate the films' structural alteration after adding each salt, especially the change in the crystalline structure. According to the XRD results in **Fig. 5-2** (a), all XRD curves have a broad peak at 2 θ ≈8 º and a distinguishable intense diffraction at 2 θ ≈22 º, belonging to the (020) plane and (040) plane, respectively [206, 222]. These peaks are ascribed to the average intermolecular distance of the crystalline domain in CS-based films [223]. By contrast, the peak at 2 θ ≈22 º becomes broad, and the intensity decreases significantly. These results indicate a weakened crystallization, which can also imply a growth of the amorphous regions when salts are introduced into the CS film.

Moreover, DSC curves can also reveal the change in the crystallization behavior of the salt-modified CS films (**Fig. 5-2** (b)). During heating, there are three endothermic peaks at around 100 °C, 150 - 155 °C, and 180 - 220 °C. The first endothermic peak corresponds to the dehydration behavior of films [224, 225]. Furthermore, a change at 150 °C -160 °C is assumed to the glass transition temperature (T_g), indicating the molecular movement caused by the dissociation of hydrogen bonds and the scissions of CS chains [148]. After adding salt to CS, the T_g of the salt-modified CS films shifts to a lower temperature. This might be attributed to the complexation between metal ions and CS chains, leading to the increased irregular structure and decreased crystallization behavior [226, 227]. Likewise, this result can provide more amorphous regions to enhance ionic mobility [226]. In

addition, a strong endotherm peak occurs near 180 °C - 210 °C, showing the melting of the crystalline part in CS-based films [222]. The addition of salts hinders the crystallization of CS, decreasing the melting temperature of the films.

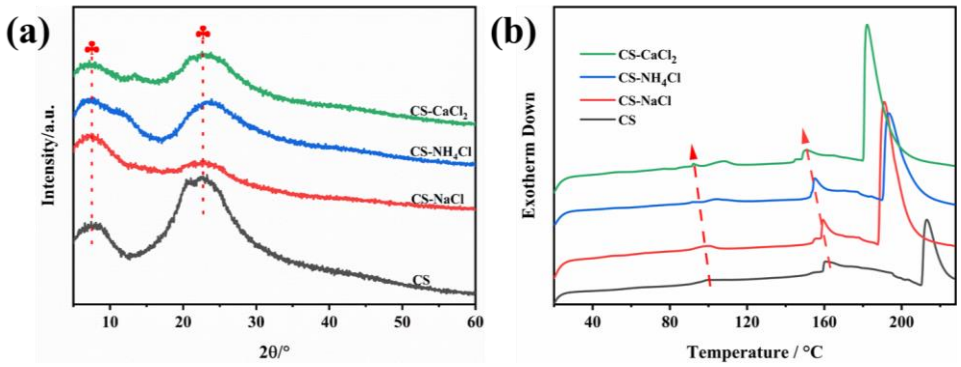

Fig. 5-2 Structural characteristics of distinct CS-based films: (a) XRD; (b) DSC curves at second heating.

Based on the mentioned results, adding salts gives rise to a declined crystalline region and increased amorphous correspondingly. For CS, ion conduction mainly happens in the amorphous phase [206, 227, 228]. Thus, the increase of the amorphous phase caused by adding salts favors ion conduction, providing the foundation for the potential warning capability.

5.3 Flammability of CS-based films

The change in weight of each film as a function of temperature is presented in **Fig. 5-3** (a). As temperature rises, less and less remaining weight of each film is left. Likewise, every sample shows a similar tendency for weight loss. Identically, they exhibit three significant steps for mass loss during heating, shown in **Fig. 5-3** (b). The first step at about 95 °C - 110 °C corresponds to the evaporation of volatile compounds that contain physical-absorbed water, hydrogen-bond water, and residual acid dissolvent [229]. The water evaporation in CS-CaCl2 film arises at the lowest temperature, showing slightly more water content in this film, which dovetails with the hygroscopicity ability of $CaCl_2$ [230]. The second step of mass loss happens in the temperature range of 150 °C - 180 °C because of the CS chain degradation caused by the decay of the amine group [218].

Further, the last step of mass loss is associated with the decomposition of the backbone CS chain at high temperatures. The minor differences in degradation temperature might be relevant to the complexation degree of the films [227]. The remaining weights of each film after heating

treatment are different. As presented in **Fig. 5-3** (c), the salt-modified CS films retain an increased remaining weight compared to pure CS film because the formed metal oxides differ at 700 °C, showing a better fire resistance property of salt-modified CS films. Comparatively, CS-$CaCl_2$ exhibits the highest remaining weight.

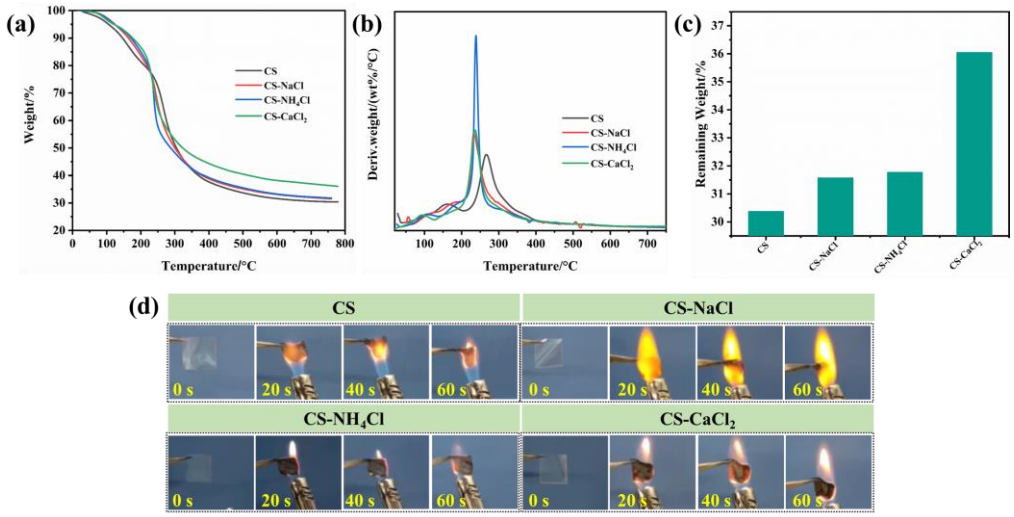

Fig. 5-3 (a) TGA curves and (b) DTG curves of each film under a nitrogen atmosphere from 50 ºC - 750 ºC; (c) remaining weight of each film at 700 ºC; (d) screen images of continued burning different films for 60 s.

Additionally, the films are continuously ignited to study the burning behavior of films. The shape changes for each film are displayed in **Fig. 5-3** (d). All the films wrinkle when they are under direct fire attack. With the increase in burning time, some residue is formed. A little residue is created for pure CS film, and no dripping phenomenon occurs after burning for 60 s. The combustion behavior of CS-NaCl film does not display a significant enhancement against a flame. However, CS-NH_4Cl film shows considerable improvement in fire resistance due to the increase of nitrogen elements that can positively improve flame retardancy. In addition, CS-$CaCl_2$ film can also keep its shape. This result illustrates the good combustion performance of CS-NH_4Cl and CS-$CaCl_2$ films, which supports implementing a fire-warning system.

5.4 Variation of electric current with temperature of CS-based films

The thermal sensitivity of CS-based films is the key to achieving early fire warnings. Variations of electric current for CS-based films with temperatures are measured to explore the influence of temperature on CS conductivity. As presented in **Fig. 5-4**, the electric current of each film increases

continuously, demonstrating the positive effect of temperature on the formation of electric current. The increased temperature might accelerate the salt dissociation, resulting in faster ion transport for the ionic conductivity [206]. However, the electric current of each film is distinct at a specific temperature, and the corresponding sequence is as follows: CS-NaCl ＞CS-NH_4Cl ＞CS-$CaCl_2$. This can be attributed to the size of salts (Na^+ ＜ NH_4^+ ＜ Ca^{2+}), resulting in higher electric currents due to the migration of smaller ionic sizes in CS systems. Furthermore, each film reaches a different maximum electric current at about 170 °C, showing a low response temperature. This difference might be related to the internal ability of ion movement caused by the different salt structures [211]. In contrast, the electric current of CS-NaCl film changes fastest, suggesting a better potential for sensitive fire-warning ability. Therefore, CS-NaCl film is chosen for the following reused fire-warning process.

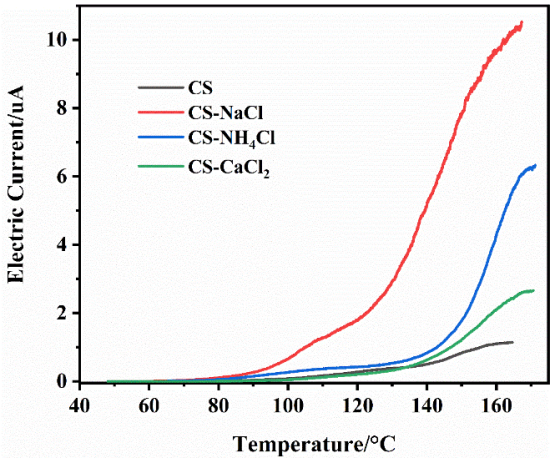

Fig. 5-4 The changes of each film's electric current with temperatures.

Response time is applied to evaluate the warning capability. One calculation method for response time is based on "trigger electric current" [14]. Specifically, the trigger electric current corresponding to the occurrence of a fire warning (LED turns on) needs to be made sure. In this work, the changes in light intensity and electric current with time are detected simultaneously using different devices (**Fig. 5-5** (a)). The electric current and light intensity curves are shown in **Fig. 5-5** (b) and **Fig. 5-5** (c), respectively. After recording for about 50 s, the light intensity of the LED gradually increases, demonstrating the happening of fire warning. Moreover, this implies the corresponding "trigger electric current" is lower than 5 μA. More precisely, the value of 5 μA is set as the threshold electric current to calculate response time in the follow-up tests.

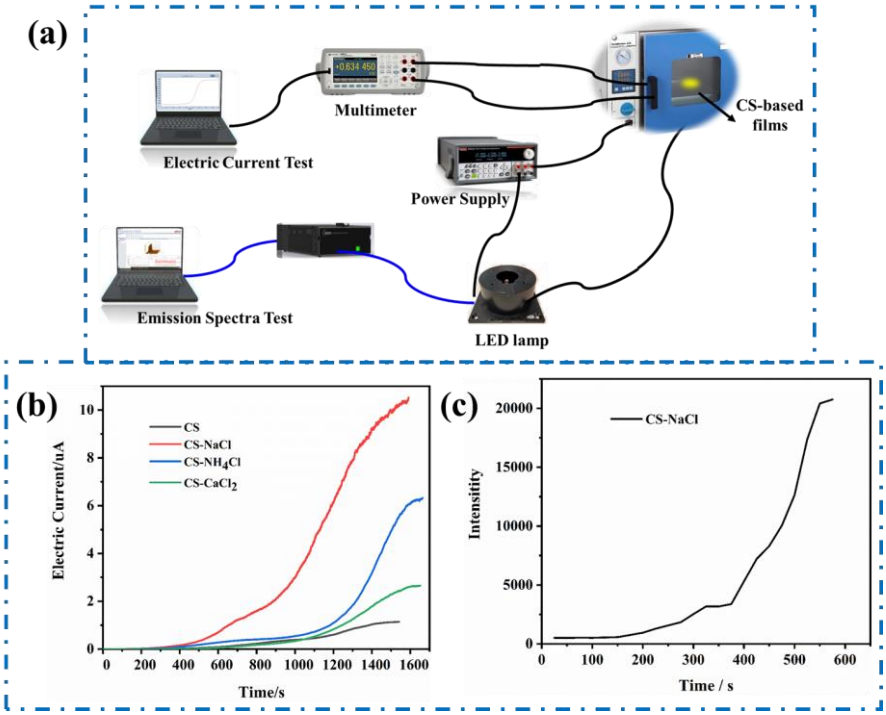

Fig. 5-5 (a) the connection between equipment to simultaneously test electric current and light intensity. (b) The light intensity changes for each CS-based film with test time. (c). The light intensity changes of CS-NaCl film with test time.

5.5 Reused fire-warning performance of CS-based films

A simulated scenario is adopted to demonstrate the early fire-warning process. The warning behavior of CS-NaCl after continuous burning is displayed in **Fig. 5-6** (a). Once CS-NaCl film is attacked by an ignition gun, a LED lamp connected to the film turns on within 2 s. The light of the LED becomes brighter when ignition time increases. After sustained treatment for 20 s, the light turned off, leading to the end of the fire warning. As the continuous burning makes the film form a carbon layer, the phenomenon of creating an electric circuit within the CS-based films completely disappears. So, the early fire-warning ability of film fades away.

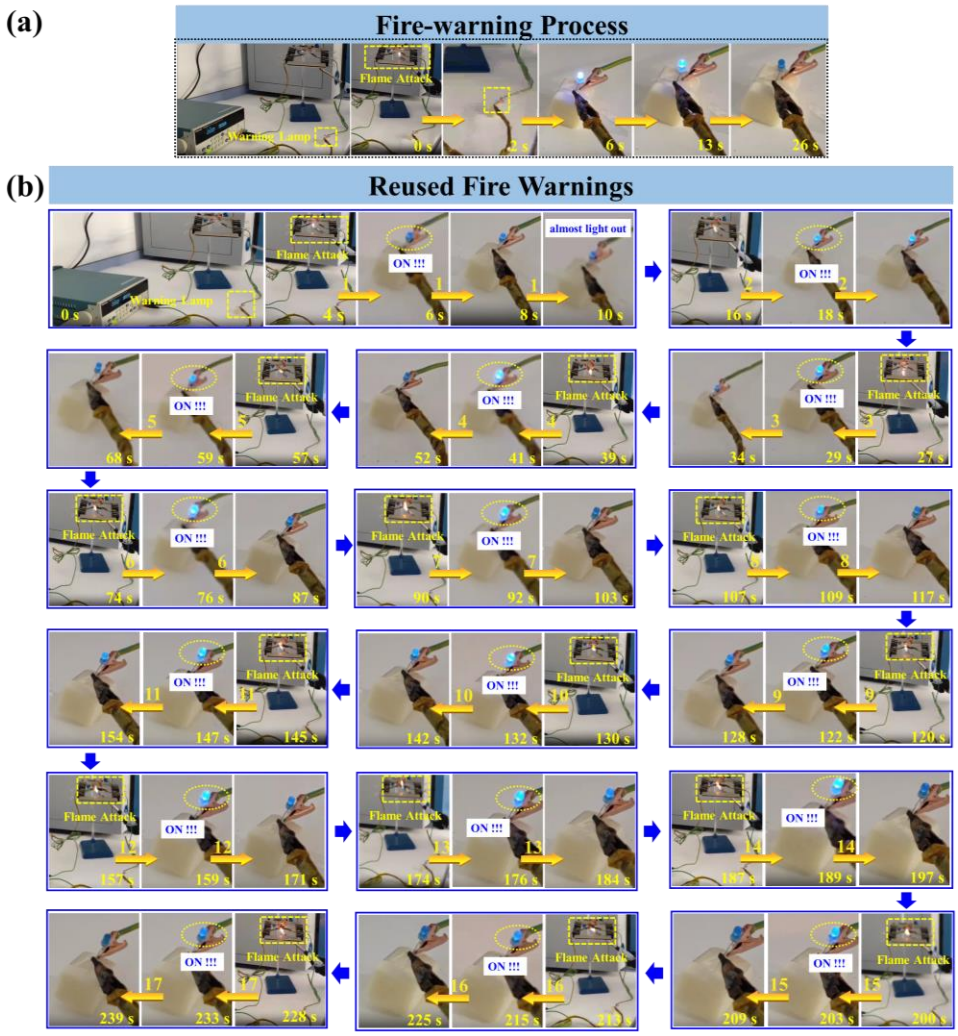

Fig. 5-6 The photographs of burning CS-NaCl film under a flame attack: (a) continue burning and (b) multiple burning by an ignitor.

In addition, the CS-NaCl film is ignited many times to observe the reusability of early fire-warning capability; the results are shown in **Fig. 5-6** (b). After igniting the film, the LED in the electric circuit turns on within 2 s. The LED can stay on for several seconds, even after removing the ignition gun. Since the temperature of the film cannot decrease expeditiously, charges will move to form an electric current under the driven temperature. Once the LED turns off, the film is ignited to trigger the LED again. Similarly, the LED can stay on for a while before turning off after removing the ignition gun. This process is then reused several times to check multiple light-dark state swaps. After a five-time burning treatment, the light intensity of the LED slightly increases. However, the reusing warning ability was lost after about 17 burnings. This might be caused by the almost

complete carbonation of CS-NaCl film after multiple burnings.

The reusability of CS response to a flame is strongly related to the formation of electric current. A short-time fire attack results in increased temperature but scant carbonization. Driven by high temperature and external voltage, the internal ions can overcome energy limitations to move directionally, leading to electric current [51]. This result reveals that the formation of the electric current of CS is a thermally driven process, implying the importance of temperatures [206]. Therefore, the LED turns on for a warning. However, multiple burning treatments gradually increase the degree of carbonization until CS-based films are entirely carbonized. Then, the early fire-warning ability is destroyed.

5.6 Humidity detection of CS-based films

Due to the presence of polar groups, CS has a strong hygroscopicity, showing potential as a humidity sensor. Therefore, when exposed to a humid environment for a while, the moisture uptake of CS material occurs. In general, the moisture absorption capability depends on the deacetylation degree of CS and humidity parameters [148, 149]. Thereby, CS-based films were exposed to 90 % humidity at room temperature for 36 h for subsequent use. In addition, the changes in electric current were measured to clarify the effect of high humidity conditions.

As shown in **Fig. 5-7** (a), the maximum electric current of each film at different temperatures is distinct because of the limited water-holding capacity. The maximum electric current for a specific CS-based film increases as the temperature rises. At each fixed test temperature, salt-modified CS films have a higher maximum electric current than pure CS film, in this order: CS-NaCl ＞CS-$CaCl_2$＞CS-NH_4Cl＞CS. It is important to note that the maximum electric current of each film is higher than the value without humidity treatment in **Fig. 5-5**. This might be attributed to the combined effect of salts and humidity because the humidity uptake can introduce water into CS films, forming more hydrated ions between water molecules with metal ions or protons to provide more hopping points for ion movement [231]. Moreover, the tendency of electric current mainly caused by the ions' size of salts displays a slight difference compared to the above result. One possibility is the strong water absorbency of $CaCl_2$, leading to more formation of hydrated ions as the hopping points, which helps increase electric current.

Furthermore, the duration time of CS-based films was calculated based on the above-mentioned "trigger electric current" (**Fig. 5-7** (b)). Comparatively, CS-NaCl film has the longest working time. The longer working time is more beneficial from the practical consideration.

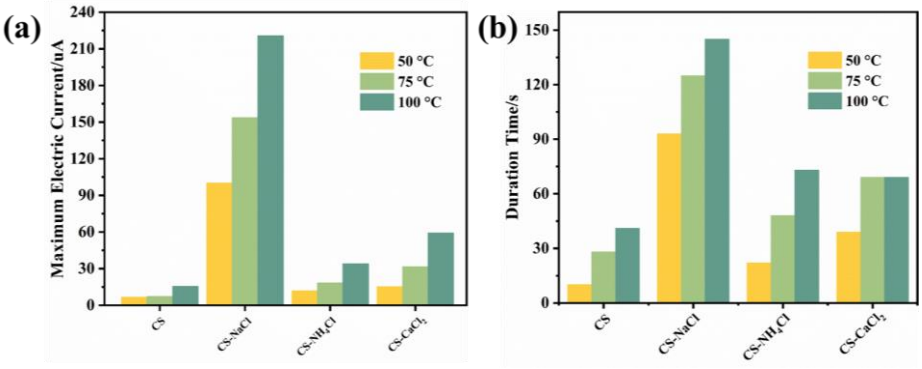

Fig. 5-7 (a) Maximum electric current changes with time of CS-based films after 90 % humidity treatment for 3 days. (b) Each CS-based film's duration time for fire warning corresponds to "trigger electric current".

To better expound the influence of humidity, the electric current changes for each film as a function of humidity changes at the set temperature were recorded. As plotted in **Fig. 5-8** (a), the electric current of each CS-based film steadily increases with increasing humidity. Compared to pure CS film, CS-NaCl, CS-$CaCl_2$, and CS-NH_4Cl exhibit a faster change rate of electric current. The electric current of CS-NaCl film exhibits a most sensitive response to the rising RH value. No clear difference between CS-$CaCl_2$ and CS-NH_4Cl is seen during the humidity-changing process. When RH reaches 100 %, the electric current of each CS-based film is continuously recorded, presented in **Fig. 5-8 (b).** The electric current of CS-$CaCl_2$ is slightly higher than that for CS-NH_4Cl in the continued test at the RH of 100%, which might be attributed to the water absorption capacity of $CaCl_2$. Moreover, curves of electric current vs. humidity for each film in **Fig. 5-8 (c)** become steeper at 75 °C, indicating a faster change of the electric current. The electric current of CS-$CaCl_2$ exhibits significantly higher than that of CS-NH_4Cl film only when RH is over 60 %, showing that a high temperature is favorable to form an electric current in CS-$CaCl_2$ with water absorption. This phenomenon implies the positive influence of increased test temperature on the electric current.

Similarly, the maximum electric current during rising humidity at 50 ºC and 75 ºC is present in **Fig. 5-8** (d). The trend presented is as follows: CS-NaCl ＞ CS-$CaCl_2$ ＞ CS-NH_4Cl ＞CS. But electric current values here are slightly higher than those shown in **Fig. 5-7** (b). This result is

possibly attributed to the absorbed water content. This humidity treatment is a short-time process, and water molecules penetrate the pores of CS-based films [232]. Here, films are continuously exposed to the humidity environment, even when the humidity reaches 100%. Therefore, a water layer might be formed on the surface of CS films after water molecules fill the pores [232, 233]. This difference between the obtained maximum electric current values possibly implies the importance of water molecules.

Based on the previous analysis, the electric current of all CS-based films changes faster under humid conditions, improving fire-warning accuracy in harsh environments, such as rainy and foggy days.

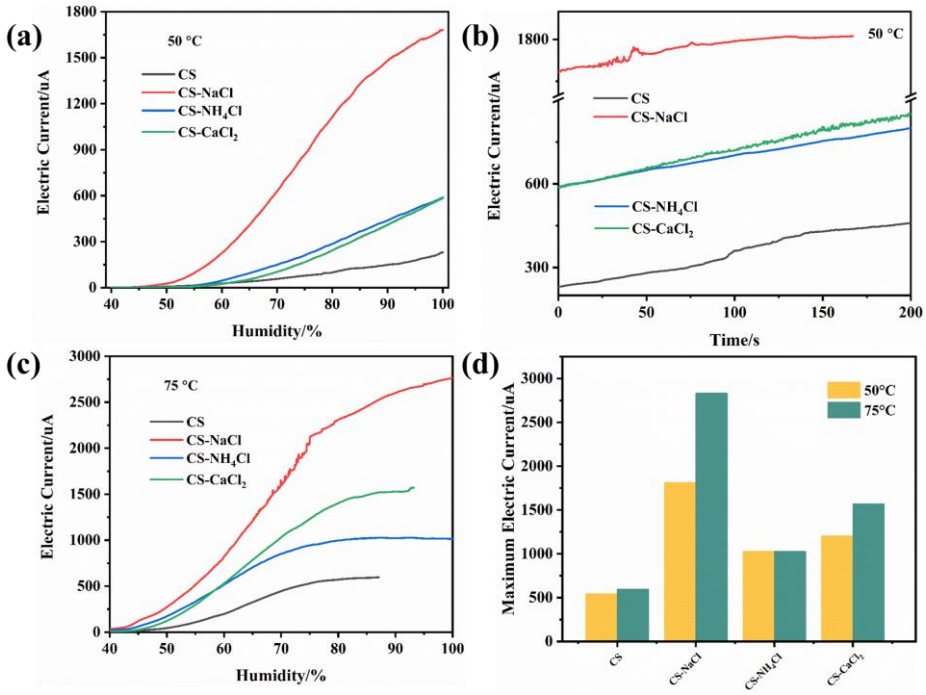

Fig. 5-8 (a) Electric current change curves in increasing humidity at 50 ºC. (b) Curves of electric current change vs time under humidity of 100 % and temperature of 50 ºC. (c) Curves of electric current change in increasing humidity at 75 ºC. (d) The maximum electric current value of each CS-based film in the process of growing humidity at different temperatures.

5.7 Mechanism of the formation of electric current of CS-based films

The fire-warning mechanism to form the electric current of CS-based films is proposed in **Scheme 5-2**. In the CS solution, protonated amino groups (NH_3^+), hydrated molecules (H_3O^+), and acetate ions (CH_3COO^-) exist. CS can be a host of polymers solvated by salts because of its polycationic

properties caused by abundant NH_2 amino groups [234]. Therefore, when a salt is added to CS, positive ions (Na^+, NH_4^+, or Ca^{2+}) and chloride ions (Cl^-) are introduced. Pure CS film is an insulator at room temperature. However, an electric current can be formed for CS-based films when they are subjected to a combination of voltage and high temperatures, which might be caused by the directional movement of ions after overcoming the energy barrier [235].

Specifically, the directional movement of ions in CS-based films is mainly attributed to the hopping transfer of active protons between different hopping points [236]. For pure CS film, protonated amino groups (NH_3^+), hydrated molecules (H_3O^+), and acetate ions (CH_3COO^-) exist. They can provide hopping points to assist proton movement. Driven by the set voltage and temperature, the activated protons can jump to form a proton conduction channel to form an electric current [237].

The introduction of positive ions (Na^+, NH_4^+, or Ca^{2+}) and chloride ions (Cl^-) from salts increases the number of charge carriers, which improves the electric current [235]. Moreover, the ion size of positive ions affects the electric current by the hopping transfer of charge, where the smaller size of ions facilitates the jumping and the diffusion rate of ions [211]. Adding salts also increases the amorphous region by inhibiting the crystallinity of CS, leaving more space for ion migration. Furthermore, the proper complexation between salts and CS molecular chains is beneficial to provide active proton jumping sites. However, if the salt concentration is too high, more salts would result in spatial entanglement and ion pairs might be formed to inhibit complexation, negatively affecting the electric current [149, 226].

The ions hopping to form an electric current need to be thermally driven [206]. As the temperature increases, the CS chains gradually become flexible, which is helpful for the ions migration to increase the electric current of CS-based films progressively. The salt dissociation can also be improved at high temperatures, encouraging ion transport and raising ionic conductivity [206]. However, if the temperature increases to a specific value or continues at a high temperature for a certain period, the films become dryer and gradually enter the thermal degradation process. Then, the structure of CS could be destroyed. They are losing the ability to form an electric current.

Moreover, water is also essential for the hopping transfer of active protons [233, 238]. The

water on the physically-absorbed water molecular layer can react with H^+ to form H_3O^+, providing extra proton hopping [239]. In addition, the positive ions (Na^+, NH_4^+, or Ca^{2+}) from salts could react with water to form hydrated ions, making slightly more water retention in CS-based films [240]. For these reasons, these salt-modified films have a better ability for ion hopping than CS under the influence of temperature and humidity, leading to a faster change of the electric current. This result demonstrates an improved fire-warning capability of salt-modified CS-based films.

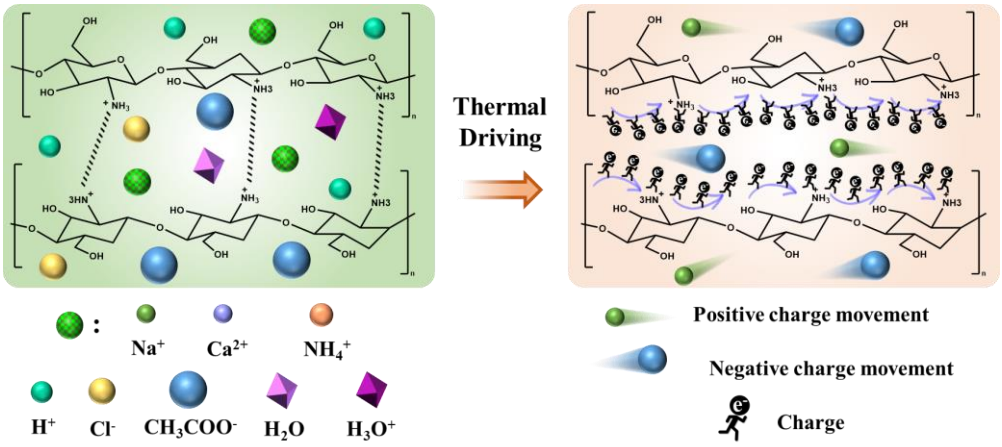

Scheme 5-2 Schematic illustration of the working mechanism of CS-based films as fire-warning sensors.

5.8 Remote wireless transmission of monitored information

A signal wireless transmission technique is employed to quickly warn the public about the detected flame danger. As presented in **Fig. 5-9**, temperature sensors and humidity sensors are combined to achieve real-time monitoring. Once a fire-warning sample is under a high temperature and an increasing humidity attack, the electric current of the sample changes. Because of the cooperation with the wireless transmission technique, temperature and humidity changes in real-time are recorded and shown on local and remote computers.

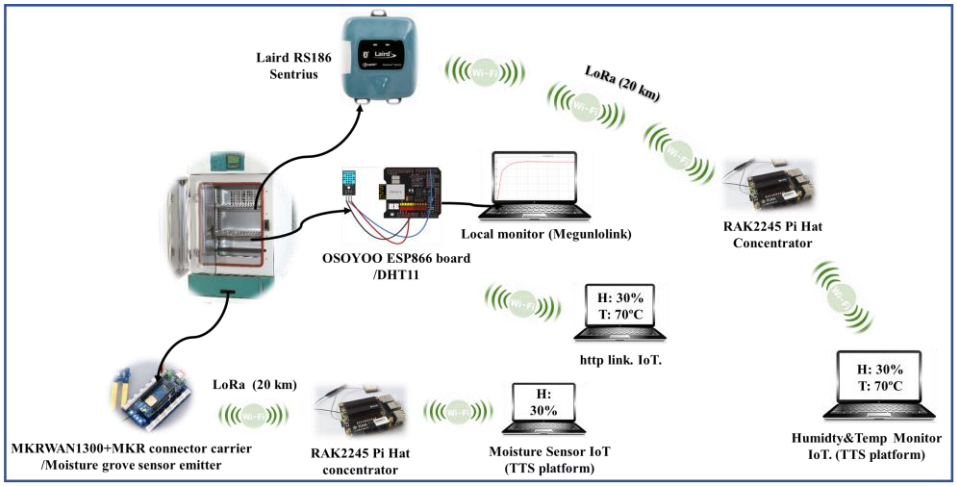

Fig. 5-9 Experimental set-up of the humidity and temperature LoRa and Wi-Fi sensors.

5.9 Conclusions

In summary, three salts are added to the CS solution to fabricate functional CS-based films, respectively. These CS-based films are transparent and have thermo-sensitive and humidity-sensitive properties. Specifically, the response temperature of CS-NaCl film starts at 50 ºC, showing improved sensitivity of fire-warning ability, especially in comparison with GO-based fire-warning sensors. Moreover, the response time is only 2 s when CS-NaCl film is under a fire attack. And CS-NaCl film can still send warnings when it is ignited multiple times. In addition, CS-NaCl and CS-$CaCl_2$ films are highly sensitive to high-humidity conditions, leading to a rapid increase in the electric current for a fast warning. Furthermore, a comparison between distinct CS-based films demonstrates the effect of humidity, temperature, and ion size of salts on CS material to form an electric current. Notably, a wireless transmission device is incorporated to collect real-time humidity and temperature information. Therefore, a prospective strategy to generate functional sensors is put forward, contributing significantly to expanding the practical applications of CS material.

CHAPTER 6

Conclusions and future work

"However difficult life may seem, there is always something you can do and succeed at."

-Stephen Hawking

6.1 Conclusions

In this thesis, three kinds of early smart fire alarms have been successfully fabricated: *i)*. functional GO-based films with the cooperation of self-designed wireless signal conversion parts as smart low-temperature fire alarms; *ii)*. modified biomass CP-based paper with the combination of luminosity sensor and temperature sensor as smart low-temperature fire-warning sensors; *iii)*. bifunctional monitoring detector through the modified CS-based films, especially showing the reusability and accurate warning under harsh environments. The subsequent sections elaborate comprehensively on the evolution of these advanced early fire-warning systems.

The novelty of the P/Si-modified GO-based fire-warning sensor includes a highly sensitive response, smart remote wireless conversion, and demonstrative application scenarios. The smart film is prepared by the simple layer-by-layer assembly, which also allows the fire-warning nanocoating to be wrapped on the surface of FPU foam. Fortunately, this intelligent fire alarm can quickly respond to a fire within 1 s at 250 ºC, showing a sensitivity of fire warning in low temperatures. Notably, a self-designed device sends received signatures to the public up to 20 km from the target fire source, fully considering the practical application. Additionally, the fire-warning nano-coating wrapped FPU foam develops another polymer-based fire alarm with a similar quick response similarly. To further advance the sensitivity of early fire-warning sensors, two-dimensional MXene is selected to prepare MXene-modified GO-based samples, which have a highly sensitive response to a fire and remote wireless transmission capability. More advances in this work compared with the current fire alarm system are as follows: *i)*. A simulated scenario is prepared to show the warning process vividly, indicating that the fire-warning film can achieve an ultrafast response

within 1 s by using an ignitor as an energy source. It is close to the real warning scene. *ii).* The fire-warning film has a better early warning ability at 250 ºC, below the conventional ignition temperature, compared with response temperatures shown in other GO-based systems. *iii).* a small self-designed wireless signal conversion device can convert detected abnormal behavior into a "FIRE DANGER!!!" message on the computer monitor. Interestingly, this message is accessible to show anywhere via internet access. The real-time luminosity value can also be exhibited on a computer monitor by coupling with the luminosity sensor.

Considering the potential applied scenario for indoor fireproofing, a CP-based fire-warning sensor loaded with a layer of GO and MXene is fabricated via the dip-coating method. During a fire incident, the partial reduction of the oxygen-containing groups on GO will transform GO into RGO, which forms a conductive circuit within the device. Additionally, introducing MXene can enhance fire detection speed and accelerate response time to only 2 s at 250 °C. Moreover, a novel and quantitative method for calculating response time is employed for the first time based on light intensity change. More importantly, the designed fire alarm sensor is coupled to a wireless communication interface to conveniently transmit fire warning signals and messages remotely to a liquid crystal display screen. This work provides an instantaneous and convenient method of fire hazard warning. An eco-friendly fire alarm is proposed to improve the performance of wallpaper-based fire alarms for smart abnormal temperature detection to avoid indoor fire hazards. In detail, the novelty of this work is as follows. Firstly, CP from bio-based sources is selected as a substrate to fabricate wallpaper-based fire alarms. The low-temperature, highly efficient response capability is emphasized, which optimizes the current response temperature of more than 300 ºC. In addition, the balance between flexibility and flame retardancy is achieved, which can offset the negative influence of introducing flame retardant. Furthermore, the new temperature sensor is applied to create a smart real-time temperature monitor, then sends information to the remote area.

The lower response temperature can facilitate monitoring electric household products to control electric appliance fires. For this purpose, eco-friendly functional sensors based on salt-modified chitosan are proposed for monitoring abnormal working temperatures and humid environments of household appliances, especially electric equipment, to avoid fire hazards caused by short circuits. Compared to the reported fire-warning sensors, the novelty of this work is mainly

relevant to fast low-temperature response, reused fire-warning ability, fast high-humidity response, smart wireless conversion, and illustration of the working mechanism. In detail, the advances are as follows: (1) Bio-based chitosan-based films are fabricated by simply volatile in this work, which is rarely used for fire-warning sensors. (2) the functional film can respond to 50 ºC quickly, leading to a low-temperature warning. (3) the functional film can be ignited multiple times to realize fire warnings, showing reusability. (4) the functional film can respond quickly to a highly humid environment, showing the potential for humidity sensors. (5) a wireless transmission device is applied to achieve smart transmission locally and remotely of the detected temperature and humidity information, improving intellectual development. (6) the mechanism to form the electric current is indicated for better understanding.

6.2 Future work

6.2.1 To enhance the stability of fire sensors in harsh environment

As mentioned in this thesis, how to develop smart low-temperature fire alarms is mainly concerned. It has been confirmed that rapid-fire warning and intelligent transmission of detected signals can allow the public to implement fire management timely. However, most of the related performance tests of reported early fire-warning sensors are under an ideal environment, without considering the influence of environmental factors, especially the detection of fire hazards under harsh environments. Therefore, how to achieve efficient and accurate fire monitoring needs to be paid attention to when the detection environment is a rainy day, a solid windy day, a heavy foggy day, *etc*.

Take a rainy day as an example. GO-based functional early fire-warning systems with strong hydrophobicity could be an opportunity to improve the accuracy of fire warning. The introduction of NH_4-CNT and a silane coupling agent are supposed to modify the early fire-warning system in further work. First, the feasibility of improving the sensitivity of fire alarms through reasonable modification of GO-based systems has been proved in previous studies. Secondly, the silane coupling agent with silica element has a positive influence on improving flame retardancy, and the structure and molecular model are presented in **Fig. 6-1**. Moreover, the NH_4-CNT chemical is beneficial in improving the early warning performance to a certain extent. Therefore, a kind of GO-based fire alarm with the co-modification of NH_4-CNT and silicon-containing chemicals can be

desirable. To evaluate the sensitivity of fire warnings, tests about flame retardancy and electric resistance change will be characterized (*e.g.*, MCC, TGA, XRD). The hydrophobic ability of fire-warning samples will be systematically elucidated. Furthermore, the simulated early fire-warning process under rainy weather will be illustrated. Significantly, the silicon-containing chemical-modified CNT possibly is as nano-coating wrapped on the surface of polyurethane foam for an early fire-warning system.

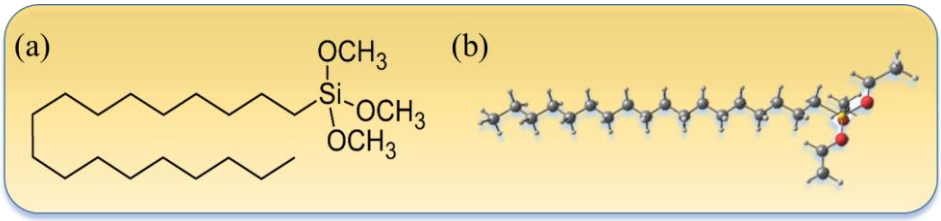

Fig. 6-1 (a) the structure and (b) molecular model of hydrophobic chemical.

6.2.2 To develop a multifunctional early fire warning sensor

Concerning the extensive application of early fire-warning systems in different scenarios, the multifunctional development deserves attention. Some new technologies are being implemented with early fire-warning systems to develop comprehensive performances, besides fire-warning properties. This can actively accelerate cooperation with other research, such as thermoelectric, nano-triboelectric generators, wind-induced electricity, etc. Moreover, the design and analysis of advanced materials for early fire sensors should be vigorously promoted to accomplish their multi-function. This multifunctionality consists of self-healing, reusability, humidity detection, water resistance, gas selection performances, etc., an inevitable development trend to broaden the practical application scenarios of early fire-warning systems. In addition, integrating fire sensors with e-textiles offers an exceptionally promising designability of early fire-warning systems, which can open the idea of protecting firefighters and localization. Nonetheless, other fabrics, such as cotton and flax, have been mixed with thermosensitive materials with clear potential for smart clothing and e-textiles. Similarly, self-sustaining fire alarms could remotely control inhabited areas and factories in the outer suburbs.

Therefore, the multifunctional early fire-warning systems will be a development direction in further work. 2D conductive MXene might be one suitable candidate. Apart from its own MXene features, other functions could be introduced into systems by the various modifications of MXene.

Their structure should be characterized to understand the structural change (e.g., SEM, XPS, TEM, SRD) and to establish the relationship between structure and performance.

CHAPTER 7

List of publications and conferences

"Living without an aim is like sailing without a compass."

-Alexandre Dumas

1) The listed papers have been published during the PhD study.

[1] **Xiaolu Li**, José Sánchez del Río Sáez, Shuanglan Du, Raquel Sánchez Díaz, Xiang Ao, De-Yi Wang*. Bio-based chitosan-based film as a bifunctional fire-warning and humidity sensor. *Int J Biol Macromol. 2023.*

[2] **Xiaolu Li**, José Sánchez del Río Saez, Antonio Vázquez-López, Xiang Ao, Raquel Sánchez Díaz, De-Yi Wang*. Eco-friendly functional cellulose paper as a fire alarming via wireless warning transmission for indoor fireproofing. *Ind Crops Prod.* 200, 116805, 2023.

[3] **Xiaolu Li**, Antonio Vázquez-López, José Sánchez del Río Saez, De-Yi Wang*. Recent advances on early-stage fire-warning systems: mechanism, performance, and perspective. *Nanomicro Lett* 14 (1), 197, 2022.

[4] **Xiaolu Li**, José Sánchez del Río Saez, Xiang Ao, Abdulmalik Yusuf, De-Yi Wang*. Highly-sensitive fire alarm system based on cellulose paper with low-temperature response and wireless signal conversion. *Chem. Eng. J.* 431, 134108, 2022.

[5] **Xiaolu Li**, José Sánchez del Río Saez, Xiang Ao, Baoyun Xu, De-Yi Wang*. Tailored P/Si-decorated graphene oxide-based fire sensor for sensitive detection at low-temperature via local and remote wireless transmission. *Constr Build Mater.* 128600, 2022.

[6] **Xiaolu Li**, José Sánchez del Río Saez, Xiang Ao, Antonio Vázquez-López, Xiaoli Xu, Baoyun Xu, De-Yi Wang*. Smart low-temperature responsive fire alarm based on mxene/graphene oxide film with wireless transmission: Remote real-time luminosity detection. *Colloids Surf. A Physicochem. Eng. Asp.* 651, 129641, 2022.

[7] **Xiaolu Li**, Jing Zhang, Lu Zhang, Alaitz Ruiz de Luzuriaga, Alaitz Rekondo, De-Yi Wang*.

Recyclable flame-retardant epoxy composites based on disulfide bonds: Flammability and recyclability. *Compos. Commun.* 25, 100754, 2021.

[8] Jing Zhang, Juan Pedro Fernández-Blázquez, **XiaoLu Li**, Rui Wang, Xiuqin Zhang, De-Yi Wang*. A facile technique to investigate the char strength and fire retardant performance towards intumescent epoxy nanocomposites containing different synergists. *Polym. Degrad. Stab.* 202, 11000, 2022.

[9] Zhu-Bao Shao, Jing Cui, **XiaoLu Li**, José Luis Díaz Palencia, De-Yi Wang*. Chemically inorganic modified ammonium polyphosphate as eco-friendly flame retardant and its high fire safety for epoxy resin. *Compos. Commun.* 28, 100959, 2021.

[10] Zhu-Bao Shao, Jing Zhang, Rong-Kun Jian, Chang-Chun Sun, **XiaoLu Li**, De-Yi Wang*. A strategy to construct multifunctional ammonium polyphosphate for epoxy resin with simultaneously high fire safety and mechanical properties. *Compos. Part A Appl. Sci. Manuf.* 149, 106529, 2021.

2) Presentation and poster in international conferences

[1] **Xiaolu Li**, José Sánchez del Río Saez, Xiang Ao, Abdulmalik Yusuf, De-Yi Wang*. Highly-sensitive fire alarm system based on cellulose paper with low-temperature response and wireless signal conversion. **Poster presentation** in European Meeting on Fire Retardant Polymeric Materials, 26 - 29 June 2023, Zurich, Switzerland.

Reference

[1] D.M. Bowman, J.K. Balch, P. Artaxo, W.J. Bond, J.M. Carlson, M.A. Cochrane, C.M. D'Antonio, R.S. Defries, J.C. Doyle, S.P. Harrison, F.H. Johnston, J.E. Keeley, M.A. Krawchuk, C.A. Kull, J.B. Marston, M.A. Moritz, I.C. Prentice, C.I. Roos, A.C. Scott, T.W. Swetnam, G.R. van der Werf, S.J. Pyne, Fire in the Earth System, Science 324 (5926) (2009) 481-484.

[2] J.T. Randerson, H. Liu, M.G. Flanner, S.D. Chambers, Y. Jin, P.G. Hess, G. Pfister, M.C. Mack, K.K. Treseder, L.R. Welp, F.S. Chapin, J.W. Harden, M.L. Goulden, E. Lyons, J.C. Neff, E.A. Schuur, C.S. Zender, The Impact of Boreal Forest Fire on Climate Warming, Science 314 (5802) (2006) 1130-1132.

[3] M.P. North, S.L. Stephens, B.M. Collins, J.K. Agee, G. Aplet, J.F. Franklin, P.Z. Fulé, Reform Forest Fire Management, Science 349 (6254) (2015) 1280-1281.

[4] Y. Kim, Park, D., Rie, D., Evaluation of the Flame-Retardant Performance and Fire Risk of Cellulose Building Finishing Material Due to the Particle Size of Expandable Graphite, Sustainability 15 (6) (2023) 5426.

[5] R. Rossi, Fire Fighting and Its Influence on the Body, Ergonomics 46 (10) (2003) 1017-1033.

[6] D. Liu, Z. Xu, C. Fan, Predictive Analysis of Fire Frequency Based on Daily Temperatures, Nat. Hazards 97 (3) (2019) 1175-1189.

[7] H. Knicker, How Does Fire Affect the Nature and Stability of Soil Organic Nitrogen and Carbon? A Review, Biogeochemistry 85 (1) (2007) 91-118.

[8] L.-Y. Lv, C.-F. Cao, Y.-X. Qu, G.-D. Zhang, L. Zhao, K. Cao, P. Song, L.-C. Tang, Smart Fire-Warning Materials and Sensors: Design Principle, Performances, and Applications, Mater. Sci. Eng. R Rep. 150 (2022) 100690.

[9] A. Ramgobin, G. Fontaine, S. Bourbigot, Thermal Degradation and Fire Behavior of High Performance Polymers, Polym. Rev. 59 (1) (2019) 55-123.

[10] P. Joseph, S. Tretsiakova-McNally, R. Zhang, Techniques for Assessing the Combustion Behaviour of Polymeric Materials: Some Current Perspectives and Future Directions, Macromol. Symp. 362 (1) (2016) 105-118.

[11] M. Elomaa, L. Sarvaranta, E. Mikkola, R. Kallonen, A. Zitting, C.A.P. Zevenhoven, M. Hupa, Combustion of Polymeric Materials, Crit. Rev. Biotechnol. 27 (3) (1997) 137-197.

[12] L. Wu, L. Chen, X. Hao, Multi-Sensor Data Fusion Algorithm for Indoor Fire Early Warning Based on Bp Neural Network, Information 12 (59) (2021) 1-12.

[13] L. Liu, J. Feng, Y. Xue, V. Chevali, Y. Zhang, Y. Shi, L.C. Tang, P. Song, 2D Mxenes for Fire Retardancy and Fire‐Warning Applications: Promises and Prospects, Adv. Funct. Mater. 33 (9) (2022) 2212124.

[14] X. Li, A. Vazquez-Lopez, J. Sanchez Del Rio Saez, D.Y. Wang, Recent Advances on Early-Stage Fire-Warning Systems: Mechanism, Performance, and Perspective, Nano-micro. Lett. 14 (1) (2022) 197.

[15] X. He, Y. Feng, F. Xu, F.-F. Chen, Y. Yu, Smart Fire Alarm Systems for Rapid Early Fire Warning: Advances and Challenges, Chem. Eng. J. 450 (2022) 137927.

[16] L. Zhang, Z. Li, Y.-T. Pan, A.P. Yáñez, S. Hu, X.-Q. Zhang, R. Wang, D.-Y. Wang, Polydopamine Induced Natural Fiber Surface Functionalization: A Way Towards Flame Retardancy of Flax/Poly(Lactic Acid) Biocomposites, Compos. B. Eng. 154 (2018) 56-63.

[17] X. Li, J. Zhang, L. Zhang, A. Ruiz de Luzuriaga, A. Rekondo, D.-Y. Wang, Recyclable Flame-Retardant Epoxy Composites Based on Disulfide Bonds: Flammability and Recyclability, Compos. Commun. 25 (2021) 100754.

[18] W.-J. Hu, Y.-M. Li, Y.-R. Li, D.-Y. Wang, Highly Efficient Intumescent Flame Retardant of Dopamine-Modified Ammonium Polyphosphate for the Thermoplastic Polyurethane Elastomer, J. Therm. Anal. Calorim. 148 (5) (2022) 1841-1851.

[19] J. Zhang, Z. Li, X.L. Qi, D.-Y. Wang, Recent Progress on Metal-Organic Framework and Its Derivatives as Novel Fire Retardants to Polymeric Materials, Nano-Micro Lett. 12 (2020) 1-21.

[20] J.C. Markwart, A. Battig, L. Zimmermann, M. Wagner, J. Fischer, B. Schartel, F.R. Wurm, Systematically Controlled Decomposition Mechanism in Phosphorus Flame Retardants by Precise Molecular Architecture: P-O Vs P-N, ACS Appl. Polym. Mater. 1 (5) (2019) 1118-1128.

[21] S.C. Kim, H.S. Ryou, An Experimental and Numerical Study on Fire Suppression Using a Water Mist in an Enclosure, Build. Environ. 38 (11) (2003) 1309-1316.

[22] D.T. Butry, Economic Performance of Residential Fire Sprinkler Systems, Fire Technol. 45 (1) (2008) 117-143.

[23] H. Ingason, Model Scale Tunnel Tests with Water Spray, Fire Saf. J. 43 (7) (2008) 512-528.

[24] J. Hua, K. Kumar, B. C. Khoo, H. Xue, A Numerical Study of the Interaction of Water Spray with a Fire Plume, Fire Saf. J. 37 (2002) 631-657.

[25] D.R.M. Nahid Chowdhury, A.Z.M. Ehtesham Chowdhury, Computer Vision and Smoke Sensor Based Fire Detection System, 1st International Conference on Advances in Science, Engineering and Robotics Technology 2019.

[26] X.G. Junjie Chen, Review on the Fundamentals of Polymer Combustion and Flammability Characteristics for Hybrid Propulsion, J. Polym. Biopolym. Phys. Chem. 2 (4) (2014) 78-83.

[27] D.P. A R Horrocks, Fire Retardant Materials, 2010.

[28] C.J.S. E. L. Lawton, Flame-Retardant Polyethylene Terephthalate Fibers, 1986.

[29] R. Bogue, Sensors for Fire Detection, Sens. Rev. 33 (2) (2013) 99-103.

[30] F. Khan, Z. Xu, J. Sun, F.M. Khan, A. Ahmed, Y. Zhao, Recent Advances in Sensors for Fire Detection, Sensors 22 (9) (2022) 3310.

[31] M. Chao-Ching Ho, IEEE, T.-H. Kuo, Real-Time Video-Based Smoke Detection System, In 2009 IEEE/ASME International Conference on Advanced Intelligent Mechatronics (2009) 1845-1850.

[32] A. Gaur, A. Singh, A. Kumar, A. Kumar, K. Kapoor, Video Flame and Smoke Based Fire Detection Algorithms: A Literature Review, Fire Technol. 56 (5) (2020) 1943-1980.

[33] A. Keller, Open Photoacoustic Sensor as Smoke Detector, Sens. Actuators B Chem. 104 (1) (2005) 1-7.

[34] Z. Mokhtari, S. Holé, J. Lewiner, Study of an Ionic Smoke Sensor, Meas. Sci. Technol. 24 (5) (2013) 055006.

[35] A.E. Çetin, K. Dimitropoulos, B. Gouverneur, N. Grammalidis, O. Günay, Y.H. Habiboğlu, B.U. Töreyin, S. Verstockt, Video Fire Detection - Review, Digit. Signal Process 23 (6) (2013) 1827-1843.

[36] J.i.Y. Hideaki Yamagishi, Fire Flame Detection Algorithm Using a Color Camera,1999 International Symposium On Micromechatronics And Human Science 1999.

[37] M. Chao-Ching Ho, IEEE, Tzu-Hsin Kuo, Real-Time Video-Based Smoke Detection System, 2009 IEEE/ASME International Conference on Advanced Intelligent Mechatronics, 2009, 1845-1850.

[38] J.C. Owrutsky, D.A. Steinhurst, C.P. Minor, S.L. Rose-Pehrsson, F.W. Williams, D.T. Gottuk, Long Wavelength Video Detection of Fire in Ship Compartments, Fire Saf. J. 41 (4) (2006) 315-320.

[39] C. Yu, J. Fang, J. Wang, Y. Zhang, Video Fire Smoke Detection Using Motion and Color Features,

Fire Technol. 46 (3) (2009) 651-663.

[40] J.i.Y. Hideaki Yamagishi, Fire Flame Detection Algorithm Using a Color Camera, 1999 International Symposium On Micromechatronics And Human Science 1999, 255-259.

[41] A. Enis Cetin, F. Porikli, Special Issue on Dynamic Textures in Video, Mach. Vis. Appl. 22 (5) (2011) 739-740.

[42] R.P. Dmitry Chetverikov, A Brief Survey of Dynamic Texture Description and Recognition, In Computer Recognition Systems: Proceedings of the 4th International Conference on Computer Recognition Systems CORES 05 30 (2005) 17-26.

[43] M.A. Jackson, I. Robins, Gas Sensing for Fire Detection: Measurements of CO, CO_2, H_2, O_2, and Smoke Density in European Standard Fire Tests, Fire Saf. J. 22 (2) (1994) 181-205.

[44] J. Fonollosa, A. Solórzano, J.M. Jiménez-Soto, S. Oller-Moreno, S. Marco, Gas Sensor Array for Reliable Fire Detection, Procedia Engineering 168 (2016) 444-447.

[45] J.F. A. Solórzano, L. Fernández, J. Eichmann, S. Marco, Fire Detection Using a Gas Sensor Array with Sensor Fusion Algorithms, ISOCS/IEEE International Symposium on Olfaction and Electronic Nose (ISOEN) (2017) 1-3.

[46] T. Kashiwagi, Gilman, J.W., Butler, K.M., Harris, R.H., Shields, J.R., Asano, A., Flame Retardant Mechanism of Silica Gel Cilica, Fire Saf. J. 24 (1994) 277-289.

[47] I.R. M. A. Jackson, Gas Sensing for Fire Detection Measurements of Co, Fire Saf. J. 22 (1994) 181-205.

[48] C. Wiedinmyer, J.C. Neff, Estimates of CO_2 from Fires in the United States: Implications for Carbon Management, Carbon Balance Manag. 2 (2007) 10.

[49] A.A. Stec, Fire Toxicity - the Elephant in the Room?, Fire Saf. J. 91 (2017) 79-90.

[50] C. Chen, Q.-H. Yang, Y. Yang, W. Lv, Y. Wen, P.-X. Hou, M. Wang, H.-M. Cheng, Self-Assembled Free-Standing Graphite Oxide Membrane, Adv. Mater. 21 (29) (2009) 3007-3011.

[51] D.R. Dreyer, S. Park, C.W. Bielawski, R.S. Ruoff, The Chemistry of Graphene Oxide, Chem. Soc. Rev. 39 (1) (2010) 228-240.

[52] A.K. Geim, K.S. Novoselov, The Rise of Graphene, Nat. Mater. 6 (3) (2007) 183-191.

[53] J.J. Shao, W. Lv, Q.H. Yang, Self-Assembly of Graphene Oxide at Interfaces, Adv. Mater. 26 (32) (2014) 5586-5612.

[54] J.-L.L. Hannes C. Schniepp, Michael J. McAllister, Hiroaki Sai, D.H.A. Margarita Herrera-Alonso, Robert K. Prud'homme, Roberto Car,, a.I.A.A. Dudley A. Saville, Functionalized Single Graphene Sheets Derived from Splitting Graphite Oxide, J. Phys. Chem. B (110) (2006) 8535-8539.

[55] X. Wang, L. Zhi, K. Müllen, Transparent Conductive Graphene Electrodes for Dye-Sensitized Solar Cells, Nano Lett. 1 (2008) 323-327.

[56] H. Chen, M.B. Müller, K.J. Gilmore, G.G. Wallace, D. Li, Mechanically Strong, Electrically Conductive, and Biocompatible Graphene Paper, Adv. Mater. 20 (18) (2008) 3557-3561.

[57] J. Liu, Z. Yin, X. Cao, F. Zhao, L. Wang, W. Huang, H. Zhang, Fabrication of Flexible, All-Reduced Graphene Oxide Non-Volatile Memory Devices, Adv. Mater. 25 (2) (2013) 233-238.

[58] V. Agarwal, P.B. Zetterlund, Strategies for Reduction of Graphene Oxide - a Comprehensive Review, Chem. Eng. J. 405 (2021) 127018.

[59] M.J. McAllister, Je-Luen Li, Douglas H. Adamson, Hannes C. Schniepp, Ahmed A. Abdala, Jun Liu, Margarita Herrera-Alonso, Single Sheet Functionalized Graphene by Oxidation and Thermal Expansion of Graphite, Chem. Mater. 18 (19) (2007) 4396-4404.

[60] D.C. Marcano, D.V. Kosynkin, J.M. Berlin, A. Sinitskii, Z. Sun, A. Slesarev, L.B. Alemany, W. Lu, J.M. Tour, Improved Synthesis of Graphene Oxide, ACS Nano 4 (8) (2010) 4806-4814.

[61] K.P. Loh, Q. Bao, G. Eda, M. Chhowalla, Graphene Oxide as a Chemically Tunable Platform for Optical Applications, Nat. Chem. 2 (12) (2010) 1015-1024.

[62] J.W. Burress, S. Gadipelli, J. Ford, J.M. Simmons, W. Zhou, T. Yildirim, Graphene Oxide Framework Materials: Theoretical Predictions and Experimental Results, Angew Chem. Int. Ed. Engl. 49 (47) (2010) 8902-8904.

[63] R. Furlan de Oliveira, P.A. Livio, V. Montes‐García, S. Ippolito, M. Eredia, P. Fanjul‐Bolado, M.B. González García, S. Casalini, P. Samorì, Liquid‐Gated Transistors Based on Reduced Graphene Gxide for Flexible and Wearable Electronics, Adv. Funct. Mater. 29 (46) (2019) 1905375.

[64] S.K. Kim, J.Y. Kim, S.-Y. Choi, J.Y. Lee, H.Y. Jeong, Direct Observation of Conducting Nanofilaments in Graphene-Oxide-Resistive Switching Memory, Adv. Funct. Mater. 25 (43) (2015) 6710-6715.

[65] S.K. Kim, J.Y. Kim, B.C. Jang, M.S. Cho, S.-Y. Choi, J.Y. Lee, H.Y. Jeong, Conductive Graphitic Channel in Graphene Oxide-Based Memristive Devices, Adv. Funct. Mater. 26 (41) (2016) 7406-

7414.

[66] F. Li, X. Jiang, J. Zhao, S. Zhang, Graphene Oxide: A Promising Nanomaterial for Energy and Environmental Applications, Nano Energy 16 (2015) 488-515.

[67] I. Sengupta, S. Chakraborty, M. Talukdar, S.K. Pal, S. Chakraborty, Thermal Reduction of Graphene Oxide: How Temperature Influences Purity, J. Mater. Res. 33 (23) (2018) 4113-4122.

[68] R. Larciprete, S. Fabris, T. Sun, P. Lacovig, A. Baraldi, S. Lizzit, Dual Path Mechanism in the Thermal Reduction of Graphene Oxide, J. Am. Chem. Soc. 133 (43) (2011) 17315-17321.

[69] J.J. Xingfa Gao, Shigeru Nagase, Hydrazine and Thermal Reduction of Graphene Oxide Reaction Mechanism Product Structures and Reaction Design.Pdf, J. Phys. Chem. C 114 (2010) 832-842.

[70] A. Bagri, C. Mattevi, M. Acik, Y.J. Chabal, M. Chhowalla, V.B. Shenoy, Structural Evolution During the Reduction of Chemically Derived Graphene Oxide, Nat. Chem. 2 (7) (2010) 581-587.

[71] K. Yin, H. Li, Y. Xia, H. Bi, J. Sun, Z. Liu, L. Sun, Thermodynamic and Kinetic Analysis of Low-Temperature Thermal Reduction of Graphene Oxide., Nano-micro. Lett. 3 (1) (2011) 51-55.

[72] A. Hussein, S. Sarkar, B. Kim, Low Temperature Reduction of Graphene Oxide Using Hot-Plate for Nanocomposites Applications, J. Mater. Sci. Technol. 32 (5) (2016) 411-418.

[73] Y. Liu, K. Wu, M. Lu, S. Nie, W. Chen, E. Jiao, B. Nan, L. Liang, M. Lu, Vertically Aligned Dopamine-Reduced Graphene Oxide with High Thermal Conductivity for Epoxy Nanocomposites, J. Mater. Sci. 55 (21) (2020) 8917-8929.

[74] M.J. McAllister, J.-L. Li, D.H. Adamson, H.C. Schniepp, A.A. Abdala, J. Liu, M. Herrera-Alonso, D.L. Milius, R. Car, R.K. Prud'homme, I.A. Aksay, Single Sheet Functionalized Graphene by Oxidation and Thermal Expansion of Graphite, Chem. Mater. 19 (2007) 4396-4404.

[75] J. Chen, H. Li, L. Zhang, C. Du, T. Fang, J. Hu, Direct Reduction of Graphene Oxide/Nanofibrillated Cellulose Composite Film and Its Electrical Conductivity Research, Sci. Rep. 10 (1) (2020) 3124.

[76] Z. Hu, Y. Chen, Q. Hou, R. Yin, F. Liu, H. Chen, Characterization of Graphite Oxide after Heat Treatment, New J. Chem. 36 (6) (2012) 1373-1377.

[77] M. Naguib, M. Kurtoglu, V. Presser, J. Lu, J. Niu, M. Heon, L. Hultman, Y. Gogotsi, M.W. Barsoum, Two-Dimensional Nanocrystals Produced by Exfoliation of Ti_3AlC_2, Adv. Mater. 23 (37) (2011) 4248-4253.

[78] M.W. Barsoum, The $M_{n+1}AX$ Phase a New Class of Solids Thermody Namically Stable

Nanolaminates, Frog. Solid St. Chem. 28 (2000) 201-281.

[79] Y. Gogotsi, A. Nikitin, H. Ye, W. Zhou, J.E. Fischer, B. Yi, H.C. Foley, M.W. Barsoum, Nanoporous Carbide-Derived Carbon with Tunable Pore Size, Nat. Mater. 2 (9) (2003) 591-594.

[80] A.V. Mohammadi, J. Rosen, Y. Gogotsi, The World of Two-Dimensional Carbides and Nitrides (Mxenes), Science 372 (6547) (2021) eabf1581.

[81] M. Kolodziejska, K. Jankowska, M. Klak, M. Wszola, Chitosan as an Underrated Polymer in Modern Tissue Engineering, Nanomaterials 11 (11) (2021) 3019.

[82] S.G. Kou, L. Peters, M. Mucalo, Chitosan: A Review of Molecular Structure, Bioactivities and Interactions with the Human Body and Micro-Organisms, Carbohydr. Polym. 282 (2022) 119132.

[83] P. Ramasamy, N. Subhapradha, V. Shanmugam, A. Shanmugam, Extraction, Characterization and Antioxidant Property of Chitosan from Cuttlebone Sepia Kobiensis (Hoyle 1885), Int. J. Biol. Macromol. 64 (2014) 202-212.

[84] Y. Yang, X. Wang, F. Yang, H. Shen, D. Wu, A Universal Soaking Strategy to Convert Composite Hydrogels into Extremely Tough and Rapidly Recoverable Double-Network Hydrogels, Adv. Mater. 28 (33) (2016) 7178-7184.

[85] Z. Ma, J. Zhang, L. Liu, H. Zheng, J. Dai, L.-C. Tang, P. Song, A Highly Fire-Retardant Rigid Polyurethane Foam Capable of Fire-Warning, Compos. Commun. 29 (2022) 101046.

[86] C.-F. Cao, B. Yu, B.-F. Guo, W.-J. Hu, F.-N. Sun, Z.-H. Zhang, S.-N. Li, W. Wu, L.-C. Tang, P. Song, H. Wang, Bio-Inspired, Sustainable and Mechanically Robust Graphene Oxide-Based Hybrid Networks for Efficient Fire Protection and Warning, Chem. Eng. J. 439 (2022) 134516.

[87] M. Mao, H. Xu, K.-Y. Guo, J.-W. Zhang, Q.-Q. Xia, G.-D. Zhang, L. Zhao, J.-F. Gao, L.-C. Tang, Mechanically Flexible, Super-Hydrophobic and Flame-Retardant Hybrid Nano-Silica/Graphene Oxide Wide Ribbon Decorated Sponges for Efficient Oil/Water Separation and Fire Warning Response, Compos. Part A Appl. Sci. Manuf. 140 (2021) 106191.

[88] Z. Luo, H. Ning, X. Zhou, B. Yuan, Efficient Flame-Retardant Biomass Aerogel Endowed with Graphene Oxide Interconnected Networks for Ultrasensitive Fire Warning, ACS Mater. Lett. 318 (2022) 132237.

[89] W.W. Qiu, Z.-R. Yu, L.-Y. Zhou, L.-Y. Lv, H. Chen, L.-C. Tang, Facile Fabrication of Graphene Oxide Nanoribbon-Based Nanocomposite Papers with Different Oxidation Degrees and

Morphologies for Tunable Fire-Warning Response, Nanomaterials 12 (12) (2022) 1963.

[90] K. Wang, K. Wu, Z. Qu, Y. Wu, E. Jiao, X. Zheng, J. Shi, Flame-Retardant and Alarm-Sensitive Composite Films by Covalent Modification of Mwcnt with Dopamine, Eur. Polym. J. 164 (2022) 110986.

[91] W. Wei, Y. Yi, J. Song, X. Chen, J. Li, J. Li, Tunable Graphene/Nitrocellulose Temperature Alarm Sensors, ACS Appl. Mater. Interfaces 14 (11) (2022) 13790-13800.

[92] F. Yang, H. Zhao, Y. Wang, G. Zhang, B. Yuan, Flame-Retardant AlOOH/Graphene Oxide Composite Coating with Temperature-Responsive Resistance for Efficient Early-Warning Fire Sensors, Colloids Surf. A Physicochem. Eng. Asp. 648 (2022) 129326.

[93] N.-J. Huang, Q.-Q. Xia, Z.-H. Zhang, L. Zhao, G.-D. Zhang, J.-F. Gao, L.-C. Tang, Simultaneous Improvements in Fire Resistance and Alarm Response of GO Paper Via One-Step 3-Mercaptopropyltrimethoxysilane Functionalization for Efficient Fire Safety and Prevention, Compos. Part A Appl. Sci. Manuf. 131 (2020) 105797.

[94] B. Yuan, Y. Wang, G. Chen, F. Yang, H. Zhang, C. Cao, B. Zuo, Nacre-Like Graphene Oxide Paper Bonded with Boric Acid for Fire Early-Warning Sensor, J. Hazard. Mater. 403 (2021) 123645.

[95] B. Zuo, B. Yuan, Flame‐Retardant Cellulose Nanofiber Aerogel Modified with Graphene Oxide and Sodium Montmorillonite and Its Fire‐Alarm Application, Polym Adv Technol. 32 (4) (2021) 1877-1887.

[96] C. Cao, B. Yuan, Thermally Induced Fire Early Warning Aerogel with Efficient Thermal Isolation and Flame‐Retardant Properties, Polym Adv Technol. 32 (5) (2021) 2159-2168.

[97] C.F. Cao, B. Yu, Z.Y. Chen, Y.X. Qu, Y.T. Li, Y.Q. Shi, Z.W. Ma, F.N. Sun, Q.H. Pan, L.C. Tang, P. Song, H. Wang, Fire Intumescent, High-Temperature Resistant, Mechanically Flexible Graphene Oxide Network for Exceptional Fire Shielding and Ultra-Fast Fire Warning, Nano-micro. Lett. 14 (1) (2022) 92.

[98] F.F. Chen, Y.J. Zhu, F. Chen, L.Y. Dong, R.L. Yang, Z.C. Xiong, Fire Alarm Wallpaper Based on Fire-Resistant Hydroxyapatite Nanowire Inorganic Paper and Graphene Oxide Thermosensitive Sensor, ACS Nano 12 (4) (2018) 3159-3171.

[99] W. Chen, P. Liu, Y. Liu, Q. Wang, W. Duan, A Temperature-Induced Conductive Coating Via Layer-by-Layer Assembly of Functionalized Graphene Oxide and Carbon Nanotubes for a Flexible,

Adjustable Response Time Flame Sensor, Chem. Eng. J. 353 (2018) 115-125.

[100] Z.-H. Zhang, J.-W. Zhang, C.-F. Cao, K.-Y. Guo, L. Zhao, G.-D. Zhang, J.-F. Gao, L.-C. Tang, Temperature-Responsive Resistance Sensitivity Controlled by L-Ascorbic Acid and Silane Co-Functionalization in Flame-Retardant Go Network for Efficient Fire Early-Warning Response, Chem. Eng. J. 386 (2020) 123894.

[101] Z. Zhang, D. Yang, H. Yang, Y. Li, S. Lu, R. Cai, W. Tan, A Hydrophobic Sisal Cellulose Microcrystal Film for Fire Alarm Sensors, Nano Lett. 21 (5) (2021) 2104-2110.

[102] Q. Wu, L.X. Gong, Y. Li, C.F. Cao, L.C. Tang, L. Wu, L. Zhao, G.D. Zhang, S.N. Li, J. Gao, Y. Li, Y.W. Mai, Efficient Flame Detection and Early Warning Sensors on Combustible Materials Using Hierarchical Graphene Oxide/Silicone Coatings, ACS Nano 12 (1) (2018) 416-424.

[103] K.-Y. Guo, Q. Wu, M. Mao, H. Chen, G.-D. Zhang, L. Zhao, J.-F. Gao, P. Song, L.-C. Tang, Water-Based Hybrid Coatings toward Mechanically Flexible, Super-Hydrophobic and Flame-Retardant Polyurethane Foam Nanocomposites with High-Efficiency and Reliable Fire Alarm Response, Compos. B. Eng. 193 (2020) 108017.

[104] H. Xu, Y. Li, N.J. Huang, Z.R. Yu, P.H. Wang, Z.H. Zhang, Q.Q. Xia, L.X. Gong, S.N. Li, L. Zhao, G.D. Zhang, L.C. Tang, Temperature-Triggered Sensitive Resistance Transition of Graphene Oxide Wide-Ribbons Wrapped Sponge for Fire Ultrafast Detecting and Early Warning, J. Hazard. Mater. 363 (2019) 286-294.

[105] H. He, J. Liu, Y. Wang, Y. Zhao, Y. Qin, Z. Zhu, Z. Yu, J. Wang, An Ultralight Self-Powered Fire Alarm e-Textile Based on Conductive Aerogel Fiber with Repeatable Temperature Monitoring Performance Used in Firefighting Clothing, ACS Nano 16 (2) (2022) 2953-2967.

[106] C. Jiang, J. Chen, X. Lai, H. Li, X. Zeng, Y. Zhao, Q. Zeng, J. Gao, Z. Wu, Y. Qiu, Mechanically Robust and Multifunctional Polyimide/Mxene Composite Aerogel for Smart Fire Protection, Chem. Eng. J. 434 (2022) 134630.

[107] B. Wang, X. Lai, H. Li, C. Jiang, J. Gao, X. Zeng, Multifunctional Mxene/Chitosan-Coated Cotton Fabric for Intelligent Fire Protection, ACS Appl. Mater. Interfaces 13 (19) (2021) 23020-23029.

[108] H. Xie, X. Lai, H. Li, J. Gao, X. Zeng, Skin-Inspired Thermoelectric Nanocoating for Temperature Sensing and Fire Safety, J. Colloid Interface Sci. 602 (602) (2021) 756-766.

[109] L. Xia, Y. Lv, Z. Miao, L. Luo, W. Luo, Y. Xu, C. Yuan, B. Zeng, L. Dai, A Flame Retardant Fabric

Nanocoating Based on Nanocarbon Black Particles@Polymer Composite and Its Fire-Alarm Application, Chem. Eng. J. 433 (2021) 133501.

[110] M. Zhang, M. Wang, M. Zhang, C. Yang, Y. Li, Y. Zhang, J. Hu, G. Wu, Flexible and Thermally Induced Switchable Fire Alarm Fabric Based on Layer-by-Layer Self-Assembled Silver Sheet/Fe_3O_4 Nanowire Composite, ACS Appl. Mater. Interfaces 11 (50) (2019) 47456-47467.

[111] Q. Liu, S. Yang, J. Ren, S. Ling, Flame-Retardant and Sustainable Silk Ionotronic Skin for Fire Alarm Systems, ACS Mater. Lett. 2 (7) (2020) 712-720.

[112] G. Xiao, H. Weng, L. Ge, Q. Huang, Application Status of Carbon Nanotubes in Fire Detection Sensors, Front. Mater. 7 (2020) 588521.

[113] B. Yang, N.V. Myung, T.T. Tran, 1d Metal Oxide Semiconductor Materials for Chemiresistive Gas Sensors: A Review, Adv. Funct. Mater. 7 (9) (2021) 2100271.

[114] Y. Li, G. Liu, L. Wang, J. Zhang, M. Xu, S.Q. Shi, Multifunctional Conductive Graphite/Cellulosic Microfiber-Natural Rubber Composite Sponge with Ultrasensitive Collision-Warning and Fire-Waring, Chem. Eng. J. 431 (2022) 134046.

[115] H. Chen, J. Zhou, S. Liu, S. Wang, X. Gong, A Novel Anti-Impact and Flame Retardant Gel Towards Human Protection and High-Temperature Alarm, Compos. Part A Appl. Sci. Manuf. 158 (2022) 106994.

[116] T. Zhao, D. Teng, Y. Xu, X. Zhang, Y. Li, Y. Zeng, Multi-Functional Air Filters with Excellent Flame Retardancy and Fire-Warning Capability, J. Colloid Interface Sci. 617 (2022) 236-245.

[117] A.W. Zaibudeen, J. Philip, Temperature and Ph Sensor Based on Functionalized Magnetic Nanofluid, Sens. Actuators B Chem. 268 (2018) 338-349.

[118] J. Yi, W. Chen, J. Han, D. Chen, Sensitive and Selective Detection of Plasticizer Vapors with Modified-SnO_2 Hollow Nanofibers for Electrical Fire Warning, Sens. Actuators B Chem. 287 (2019) 364-370.

[119] J. Chen, H. Xie, X. Lai, H. Li, J. Gao, X. Zeng, An Ultrasensitive Fire-Warning Chitosan/Montmorillonite/Carbon Nanotube Composite Aerogel with High Fire-Resistance, Chem. Eng. J. 399 (2020) 125729.

[120] T. Zhou, C. Wu, Y. Wang, A.P. Tomsia, M. Li, E. Saiz, S. Fang, R.H. Baughman, L. Jiang, Q. Cheng, Super-Tough Mxene-Functionalized Graphene Sheets, Nat. Commun. 11 (1) (2020) 2077.

[121] M. Mao, K.-X. Yu, C.-F. Cao, L.-X. Gong, G.-D. Zhang, L. Zhao, P. Song, J.-F. Gao, L.-C. Tang, Facile and Green Fabrication of Flame-Retardant Ti_3C_2Tx Mxene Networks for Ultrafast, Reusable and Weather-Resistant Fire Warning, Chem. Eng. J. 427 (2022) 131615.

[122] C. Zhao, Y. Wang, L. Gao, Y. Xu, Z. Fan, X. Liu, Y. Ni, S. Xuan, H. Deng, X. Gong, High-Performance Liquid Metal/Polyborosiloxane Elastomer toward Thermally Conductive Applications, ACS Appl. Mater. Interfaces 14 (18) (2022) 21564-21576.

[123] T. Fu, X. Zhao, L. Chen, W.-S. Wu, Q. Zhao, X.-L. Wang, D.-M. Guo, Y.-Z. Wang, Bioinspired Color Changing Molecular Sensor toward Early Fire Detection Based on Transformation of Phthalonitrile to Phthalocyanine, Adv. Funct. Mater. 29 (8) (2019) 1806586.

[124] Y. Xu, L. Huang, J. Long, R. Zhang, Z. Zhong, L. Yang, L. Liu, Y. Huang, Reversible Thermochromic Poss-Metal Films for Early Warning, Compos Sci. Technol. 217 (2022) 109083.

[125] L. Chen, H.-B. Zhao, Y.-P. Ni, T. Fu, W.-S. Wu, X.-L. Wang, Y.-Z. Wang, 3D Printable Robust Shape Memory Pet Copolyesters with Fire Safety Via Π Stacking and Synergistic Crosslinking, J. Mater. Chem. A 7 (2019) 17037-17045.

[126] J. Jia, N. Gao, R. Li, S. Liao, S. Lyu, Y. Wang, An “Off-to-On” Shape Memory Polymer Conductor for Early Fire Disaster Alarming, Chem. Eng. J. 437 (4) (2022) 133285.

[127] L. Zhang, Y. Huang, H. Dong, R. Xu, S. Jiang, Flame-Retardant Shape Memory Polyurethane/MXene Paper and the Application for Early Fire Alarm Sensor, Compos. B. Eng. 223 (2021) 109149.

[128] X. Wu, N. Gao, X. Zheng, X. Tao, Y. He, Z. Liu, Y. Wang, Self-Powered and Green Ionic-Type Thermoelectric Paper Chips for Early Fire Alarming, ACS Appl. Mater. Interfaces 12 (24) (2020) 27691-27699.

[129] H. Zhou, M.H. Chua, Q. Zhu, J. Xu, High-Performance Pedot: Pss-Based Thermoelectric Composites, Compos. Commun. 27 (2021) 100877.

[130] Y. Lu, Y. Ding, Y. Qiu, K. Cai, Q. Yao, H. Song, L. Tong, J. He, L. Chen, Good Performance and Flexible Pedot:Pss/Cu_2Se Nanowire Thermoelectric Composite Films, ACS Appl. Mater. Interfaces 11 (13) (2019) 12819-12829.

[131] H. Cheng, Q. Le, Z. Liu, Q. Qian, Y. Zhao, J. Ouyang, Ionic Thermoelectrics: Principles, Materials and Applications, J. Mater. Chem. C 10 (2) (2022) 433-450.

[132] J. Li, A.B. Huckleby, M. Zhang, Polymer-Based Thermoelectric Materials: A Review of Power Factor Improving Strategies, J. Materiomics 8 (1) (2022) 204-220.

[133] A. Lund, Y. Tian, S. Darabi, C. Müller, A Polymer-Based Textile Thermoelectric Generator for Wearable Energy Harvesting, J. Power Sources 480 (2020) 228836.

[134] A. Vázquez-López, J. Bartolomé, D. Maestre, A. Cremades, Gas Sensing and Thermoelectric Properties of Hybrid Composite Films Based on Pedot:Pss and Sno or SnO_2 Nanostructures, Phys. Status Solidi A (2022) 2100794.

[135] Y. Wang, L. Yang, X.L. Shi, X. Shi, L. Chen, M.S. Dargusch, J. Zou, Z.G. Chen, Flexible Thermoelectric Materials and Generators: Challenges and Innovations, Adv. Mater. 31 (29) (2019) 1807916.

[136] X. He, Y. Hao, M. He, X. Qin, L. Wang, J. Yu, Stretchable Thermoelectric-Based Self-Powered Dual-Parameter Sensors with Decoupled Temperature and Strain Sensing, ACS Appl. Mater. Interfaces 13 (50) (2021) 60498-60507.

[137] Y. Shi, Y. Wang, Y. Deng, H. Gao, Z. Lin, W. Zhu, H. Ye, A Novel Self-Powered Wireless Temperature Sensor Based on Thermoelectric Generators, Energy Convers. Manag. 80 (2014) 110-116.

[138] Y. Jia, Q. Jiang, H. Sun, P. Liu, D. Hu, Y. Pei, W. Liu, X. Crispin, S. Fabiano, Y. Ma, Y. Cao, Wearable Thermoelectric Materials and Devices for Self-Powered Electronic Systems, Adv. Mater. 33 (42) (2021) 2102990.

[139] W. Lee, S. Lee, H. Kim, Y. Kim, Organic Thermoelectric Devices with Pedot:Pss/ZnO Hybrid Composites, Chem. Eng. J. 415 (2021) 128935.

[140] M. Li, J. Chen, W. Zhong, M. Luo, W. Wang, X. Qing, Y. Lu, Q. Liu, K. Liu, Y. Wang, D. Wang, Large-Area, Wearable, Self-Powered Pressure-Temperature Sensor Based on 3D Thermoelectric Spacer Fabric, ACS Sens 5 (8) (2020) 2545-2554.

[141] Q. Zeng, Y. Zhao, X. Lai, C. Jiang, B. Wang, H. Li, X. Zeng, Z. Chen, Skin-Inspired Multifunctional MXene/Cellulose Nanocoating for Smart and Efficient Fire Protection, Chem. Eng. J. 446 (2022) 136899.

[142] J. Deng, F. Zhou, B. Shi, J.L. Torero, H. Qi, P. Liu, S. Ge, Z. Wang, C. Chen, Waste Heat Recovery, Utilization and Evaluation of Coalfield Fire Applying Heat Pipe Combined Thermoelectric

Generator in Xinjiang, China, Energy 207 (2020) 118303.

[143] K. Sornek, M. Filipowicz, M. Żoladek, R. Kot, M. Mikrut, Comparative Analysis of Selected Thermoelectric Generators Operating with Wood-Fired Stove, Energy 166 (2019) 1303-1313.

[144] Y. Pang, Y. Cao, M. Derakhshani, Y. Fang, Z.L. Wang, C. Cao, Hybrid Energy-Harvesting Systems Based on Triboelectric Nanogenerators, Matter 4 (1) (2021) 116-143.

[145] X. Chen, A. Yusuf, J.S. del Rio, D.-Y. Wang, A Facile and Robust Route to Polyvinyl Alcohol-Based Triboelectric Nanogenerator Containing Flame-Retardant Polyelectrolyte with Improved Output Performance and Fire Safety, Nano Energy 81 (2021) 105656.

[146] X. Li, J. Sánchez del Río Saez, X. Ao, B. Xu, D.-Y. Wang, Tailored P/Si-Decorated Graphene Oxide-Based Fire Sensor for Sensitive Detection at Low-Temperature Via Local and Remote Wireless Transmission, Constr. Build. Mater. 349 (2022) 128600.

[147] X. Li, J.S.d. Río Saez, X. Ao, A. Vázquez-López, X. Xu, B. Xu, D.-Y. Wang, Smart Low-Temperature Responsive Fire Alarm Based on MXene/Graphene Oxide Film with Wireless Transmission: Remote Real-Time Luminosity Detection, Colloids Surf. A Physicochem. Eng. Asp. 651 (2022) 129641.

[148] M. Mucha, A. Pawlak, Thermal Analysis of Chitosan and Its Blends, Thermochim. Acta 427 (1-2) (2005) 69-76.

[149] M. Mucha, J. Piekielna, A. Wieczorek, Characterisation and Morphology of Biodegradable Chitosan/Synthetic Polymer Blends, Macromol. Symp. 144 (1) (1999) 391-412.

[150] S.T. McKenna, N. Jones, G. Peck, K. Dickens, W. Pawelec, S. Oradei, S. Harris, A.A. Stec, T.R. Hull, Fire Behaviour of Modern Facade Materials - Understanding the Grenfell Tower Fire, J. Hazard. Mater. 368 (2019) 115-123.

[151] M. Bar, R. Alagirusamy, A. Das, Flame Retardant Polymer Composites, Fibers Polym. 16 (4) (2015) 705-717.

[152] K.J. Overholt, M.J. Gollner, J. Perricone, A.S. Rangwala, F.A. Williams, Warehouse Commodity Classification from Fundamental Principles. Part Ii: Flame Heights and Flame Spread, Fire Saf. J. 46 (6) (2011) 317-329.

[153] Y. Li, X. Wang, J. Sun, Layer-by-Layer Assembly for Rapid Fabrication of Thick Polymeric Films, Chem. Soc. Rev. 41 (18) (2012) 5998-6009.

[154] L. Wagberg, J. Erlandsson, The Use of Layer-by-Layer Self-Assembly and Nanocellulose to Prepare Advanced Functional Materials, Adv. Mater. 33 (28) (2021) 2001474.

[155] K. Ariga, Y. Yamauchi, G. Rydzek, Q. Ji, Y. Yonamine, K.C.W. Wu, J.P. Hill, Layer-by-Layer Nanoarchitectonics: Invention, Innovation, and Evolution, Chem. Lett. 43 (1) (2014) 36-68.

[156] Y.C. Li, S. Mannen, A.B. Morgan, S. Chang, Y.H. Yang, B. Condon, J.C. Grunlan, Intumescent All-Polymer Multilayer Nanocoating Capable of Extinguishing Flame on Fabric, Adv. Mater. 23 (34) (2011) 3926-3931.

[157] C. Jiang, V.V. Tsukruk, Freestanding Nanostructures Via Layer-by-Layer Assembly, Adv. Mater. 18 (7) (2006) 829-840.

[158] G. Decher, Fuzzy Nanoassemblies toward Layered Polymeric Multicomposites, Science 277 (1997) 1232-1237.

[159] P. Yao, Chen, P., Jiang, L., Zhao, H., Zhu, H., Zhou, D., Hu, W., Han, B.H. Liu, M., Electric Current Induced Reduction of Graphene Oxide and Its Application as Gap Electrodes in Organic Photoswitching Devices, Adv. Mater. 22 (44) (2010) 5008-5012.

[160] X. Qiu, Z. Li, X. Li, Z. Zhang, Flame Retardant Coatings Prepared Using Layer by Layer Assembly: A Review, Chem. Eng. J. 334 (2018) 108-122.

[161] G. Malucelli, Layer-by-Layer Nanostructured Assemblies for the Fire Protection of Fabrics, Mater. Lett. 166 (2016) 339-342.

[162] Z.-R. Yu, M. Mao, S.-N. Li, Q.-Q. Xia, C.-F. Cao, L. Zhao, G.-D. Zhang, Z.-J. Zheng, J.-F. Gao, L.-C. Tang, Facile and Green Synthesis of Mechanically Flexible and Flame-Retardant Clay/Graphene Oxide Nanoribbon Interconnected Networks for Fire Safety and Prevention, Chem. Eng. J. 405 (2021) 126620.

[163] A. Kocanalı, E. Apaydın Varol, An Experimental Study on the Electrical and Thermal Performance of Reduced Graphene Oxide Coated Cotton Fabric, Int. J. Energy Res. 45 (9) (2021) 12915-12927.

[164] M. Kim, C. Lee, J. Jang, Fabrication of Highly Flexible, Scalable, and High-Performance Supercapacitors Using Polyaniline/Reduced Graphene Oxide Film with Enhanced Electrical Conductivity and Crystallinity, Adv. Funct. Mater. 24 (17) (2014) 2489-2499.

[165] Z. Wei, D. Wang, S. Kim, S.Y. Kim, Y. Hu, M.K. Yakes, A.R. Laracuente, Z. Dai, S.R. Marder, C. Berger, W.P. King, W.A. de Heer, P.E. Sheehan, E. Riedo, Nanoscale Tunable Reduction of Graphene

Oxide for Graphene Electronics, Science 328 (5984) (2010) 1373-1376.

[166] F. Carosio, A. Di Blasio, F. Cuttica, J. Alongi, G. Malucelli, Self-Assembled Hybrid Nanoarchitectures Deposited on Poly(urethane) Foams Capable of Chemically Adapting to Extreme Heat, RSC Adv. 4 (32) (2014) 16674-16680.

[167] L. Maddalena, F. Carosio, J. Gomez, G. Saracco, A. Fina, Layer-by-Layer Assembly of Efficient Flame Retardant Coatings Based on High Aspect Ratio Graphene Oxide and Chitosan Capable of Preventing Ignition of PU Foam, Polym. Degrad. Stab. 152 (2018) 1-9.

[168] R.R. Nair, H.A. Wu, P.N. Jayaram, I.V. Grigorieva, A.K. Geim, Unimpeded Permeation of Water through Helium-Leak-Tight Graphene-Based Membranes, Science 335 (6067) (2012) 442-444.

[169] L. Song, F. Khoerunnisa, W. Gao, W. Dou, T. Hayashi, K. Kaneko, M. Endo, P.M. Ajayan, Effect of High-Temperature Thermal Treatment on the Structure and Adsorption Properties of Reduced Graphene Oxide, Carbon 52 (2013) 608-612.

[170] H.H. Huang, K.K.H. De Silva, G.R.A. Kumara, M. Yoshimura, Structural Evolution of Hydrothermally Derived Reduced Graphene Oxide, Sci. Rep. 8 (1) (2018) 6849.

[171] T. Kashiwagi1, J.W. Gilman, K.M. Butler, R.H. Harris Jr, J.R. Shields, A. Asano, Flame Retardant Mechnism of Silica Gel/Silica, Fire Mater. 24 (2000) 277-289.

[172] F. Carosio, G. Laufer, J. Alongi, G. Camino, J.C. Grunlan, Layer-by-Layer Assembly of Silica-Based Flame Retardant Thin Film on PET Fabric, Polym. Degrad. Stab. 96 (5) (2011) 745-750.

[173] P. Liu, W. Chen, S. Bai, Y. Liu, Q. Wang, Fabrication of an Ultralight Flame-Induced High Conductivity Hybrid Sponge Based on Poly (Vinyl Alcohol)/Silver Nitrate Composite, Mater. Des. 139 (2018) 96-103.

[174] D. Li, M.B. Muller, S. Gilje, R.B. Kaner, G.G. Wallace, Processable Aqueous Dispersions of Graphene Nanosheets, Nat. Nanotechnol. 3 (2) (2008) 101-105.

[175] V. Hospodarova, Singovszka, E. Stevulova, N. , Characterization of Cellulosic Fibers by Ftir Spectroscopy for Their Further Implementation to Building Materials, Am. J. Anal. Chem. 09 (06) (2018) 303-310.

[176] G. Chen, B. Yuan, Y. Wang, X. Chen, C. Huang, S. Shang, H. Tao, J. Liu, W. Sun, P. Yang, G. Shi, Nacre-Biomimetic Graphene Oxide Paper Intercalated by Phytic Acid and Its Ultrafast Fire-Alarm Application, J. Colloid Interface Sci. 578 (2020) 412-421.

[177] Y. Xue, J. Feng, S. Huo, P. Song, B. Yu, L. Liu, H. Wang, Polyphosphoramide-Intercalated Mxene for Simultaneously Enhancing Thermal Stability, Flame Retardancy and Mechanical Properties of Polylactide, Chem. Eng. J. 397 (2020) 125336.

[178] F. Niu, J. Yang, N. Wang, D. Zhang, W. Fan, J. Yang, Y. Qian, $MoSe_2$-Covered N,P-Doped Carbon Nanosheets as a Long-Life and High-Rate Anode Material for Sodium-Ion Batteries, Adv. Funct. Mater. 27 (23) (2017) 1700522.

[179] A.C. Ferrari, D.M. Basko, Raman Spectroscopy as a Versatile Tool for Studying the Properties of Graphene, Nat. Nanotechnol. 8 (4) (2013) 235-246.

[180] H. Xie, X. Lai, H. Li, J. Gao, X. Zeng, X. Huang, S. Zhang, A Sandwich-Like Flame Retardant Nanocoating for Supersensitive Fire-Warning, Chem. Eng. J. 382 (2020) 122929.

[181] L. Costes, F. Laoutid, S. Brohez, P. Dubois, Bio-Based Flame Retardants: When Nature Meets Fire Protection, Mater. Sci. Eng. R Rep. 117 (2017) 1-25.

[182] S. Cao, Rathi, P., Wu, X., Ghim, D., Jun, Y.S. Singamaneni, S., Cellulose Nanomaterials in Interfacial Evaporators for Desalination: A “Natural” Choice, Adv. Mater. 33 (28) (2020) 2000922.

[183] X. Dai, Guo, Z., The Gorgeous Transformation of Paper: From Cellulose Paper to Inorganic Paper to 2D Paper Materials with Multifunctional Properties, J. Mater. Chem. A 10 (1) (2022) 122-156.

[184] X. Li, J. Sánchez del Río Saez, X. Ao, A. Yusuf, D.-Y. Wang, Highly-Sensitive Fire Alarm System Based on Cellulose Paper with Low-Temperature Response and Wireless Signal Conversion, Chem. Eng. J. 431 (2022) 134108.

[185] A.A. D’souza, R. Shegokar., Polyethylene Glycol (PEG): A Versatile Polymer for Pharmaceutical Applications, Expert. Opin. Drug. Deliv. 13 (9) (2016) 1257-1275.

[186] J. Chen, S.K. Spear, J.G. Huddleston, R.D. Rogers, Polyethylene Glycol and Solutions of Polyethylene Glycol as Green Reaction Media, Green Chem. 7 (2) (2005) 64-82.

[187] A.R. Polu, H.-W. Rhee, Nanocomposite Solid Polymer Electrolytes Based on Poly(ethylene oxide)/POSS-PEG (n=13.3) Hybrid Nanoparticles for Lithium Ion Batteries, J. Ind. Eng. Chem. 31 (2015) 323-329.

[188] B.W. Chieng, N.A. Ibrahim, W. Md Zin Wan Yunus, M.Z. Hussein, Poly(lactic acid)/Poly(ethylene glycol) Polymer Nanocomposites: Effects of Graphene Nanoplatelets, Polymers 6 (1) (2013) 93-104.

[189] K. Shameli, M.B. Ahmad, S.D. Jazayeri, S. Sedaghat, P. Shabanzadeh, H. Jahangirian, M. Mahdavi,

Y. Abdollahi, Synthesis and Characterization of Polyethylene Glycol Mediated Silver Nanoparticles by the Green Method, Int. J. Mol. Sci. 13 (6) (2012) 6639-6650.

[190] P. Kolhe., R.M. Kannan, Improvement in Ductility of Chitosan through Blending and Copolymerization with PEG: FTIR Investigation of Molecular Interactions, Biomacromolecules 4 (2003) 173-180.

[191] A. Pawlak, M. Mucha, Thermogravimetric and Ftir Studies of Chitosan Blends, Thermochim. Acta 396 (2003) 153-166.

[192] Y. Hwang, H.-J. Park, A. Potthast, M.-J. Jeong, Evaluation of Cellulose Paper Degradation Irradiated by an Electron Beam for Conservation Treatment, Cellulose 28 (2) (2020) 1071-1083.

[193] C.J. Garvey, I.H. Parker, G.P. Simon, On the Interpretation of X-Ray Diffraction Powder Patterns in Terms of the Nanostructure of Cellulose I Fibres, Macromol. Chem. Phys 206 (15) (2005) 1568-1575.

[194] L. Dong, C. Hu, L. Song, X. Huang, N. Chen, L. Qu, A Large-Area, Flexible, and Flame-Retardant Graphene Paper, Adv. Funct. Mater. 26 (9) (2016) 1470-1476.

[195] B. Jiang, T. Zhang, L. Zhao, Y. Huang, Interfacially Reinforced Carbon Fiber Composites by Grafting Modified Methylsilicone Resin, Compos Sci. Technol. 140 (2017) 39-45.

[196] K. Krishnamoorthy, M. Veerapandian, R. Mohan, S.-J. Kim, Investigation of Raman and Photoluminescence Studies of Reduced Graphene Oxide Sheets, Appl. Phys. A 106 (3) (2011) 501-506.

[197] L. Cao, Q. Liu, J. Ren, W. Chen, Y. Pei, D.L. Kaplan, S. Ling, Electro-Blown Spun Silk/Graphene Nanoionotronic Skin for Multifunctional Fire Protection and Alarm, Adv. Mater. 33 (38) (2021) 2102500.

[198] Z. Qu, C.-A. Xu, X. Li, Y. Wu, K. Wang, X. Zheng, X. Cui, X. Wu, J. Shi, K. Wu, Facile Preparation of BP-MoS_2/GO Composite Films with Excellent Flame Retardancy and Ultrasensitive Response for Smart Fire Alarm, Chem. Eng. J. 426 (2021) 130717.

[199] Q. Liu, Li, X., Zhang, H., Ren, J., Yang, S., Cao, L., Liang, J., Ling, S., Intellisense Silk Fibroin Ionotronic Batteries for Wildfire Detection and Alarm, Nano Energy 101 (2022) 107630.

[200] J.T. Chen, Y.J. Fu, Q.F. An, S.C. Lo, S.H. Huang, W.S. Hung, C.C. Hu, K.R. Lee, J.Y. Lai, Tuning Nanostructure of Graphene Oxide/Polyelectrolyte LBL Assemblies by Controlling PH of GO

Suspension to Fabricate Transparent and Super Gas Barrier Films, Nanoscale 5 (19) (2013) 9081-9088.

[201] J.K. Wassei, R.B. Kaner, Graphene a Promising Transparent Conductor, Mater. Today 13 (3) (2010) 52-59.

[202] V.C. Tung, L.-M. Chen, Matthew J. Allen, J.K. Wassei, K. Nelson, R.B. Kaner, Y. Yang, Low-Temperaure Solution Processing of Grapheen Cnt Hybrid Materials for High-Performance Transparent Conductors, Nano Lett. 9 (5) (2009) 1949-1955.

[203] J.-K. Wu, C.-C. Ye, T. Liu, Q.-F. An, Y.-H. Song, K.-R. Lee, W.-S. Hung, C.-J. Gao, Synergistic Effects of CNT and GO on Enhancing Mechanical Properties and Separation Performance of Polyelectrolyte Complex Membranes, Mater. Des. 119 (2017) 38-46.

[204] S.K. Shukla, A.K. Mishra, O.A. Arotiba, B.B. Mamba, Chitosan-Based Nanomaterials: A State-of-the-Art Review, Int. J. Biol. Macromol. 59 (2013) 46-58.

[205] M.N.V. Ravi Kumar, A Review of Chitin and Chitosan Applications, React. Funct. Polym. 46 (1) (2000) 1-27.

[206] S.B. Aziz, O.G. Abdullah, M.A. Rasheed, H.M. Ahmed, Effect of High Salt Concentration (HSC) on Structural, Morphological, and Electrical Characteristics of Chitosan Based Solid Polymer Electrolytes, Polymers 9 (6) (2017) 187.

[207] M.B. Ahmad, M.B. Huglin, States of Water in Poly(Methyl Methacrylate-Co-N-Vinyl-2-Pyrrolidone) Hydrogels During Swelling, Polymer 35 (9) (1994) 1997-2000.

[208] H.K. No, S.H. Kim, S.H. Lee, N.Y. Park, W. Prinyawiwatkul, Stability and Antibacterial Activity of Chitosan Solutions Affected by Storage Temperature and Time, Carbohydr. Polym. 65 (2) (2006) 174-178.

[209] J. Jang, K. Kang, N. Raeis‐Hosseini, A. Ismukhanova, H. Jeong, C. Jung, B. Kim, J.Y. Lee, I. Park, J. Rho, Self‐Powered Humidity Sensor Using Chitosan‐Based Plasmonic Metal-Hydrogel-Metal Filters, Adv. Opt. Mater. 8 (9) (2020) 1901932.

[210] L.H. Chen, T. Li, C.C. Chan, R. Menon, P. Balamurali, M. Shaillender, B. Neu, X.M. Ang, P. Zu, W.C. Wong, K.C. Leong, Chitosan Based Fiber-Optic Fabry-Perot Humidity Sensor, Sens. Actuators B Chem. 169 (2012) 167-172.

[211] S. Navaratnam, K. Ramesh, S. Ramesh, A. Sanusi, W.J. Basirun, A.K. Arof, Transport Mechanism

Studies of Chitosan Electrolyte Systems, Electrochim. Acta 175 (2015) 68-73.

[212] A. El Kadib, M. Bousmina, D. Brunel, Recent Progress in Chitosan Bio-Based Soft Nanomaterials, J. Nanosci. Nanotechnol. 14 (1) (2014) 308-331.

[213] S.M. Wang, Q.Z. Huang, Q.S. Wang, Study on the Synergetic Degradation of Chitosan with Ultraviolet Light and Hydrogen Peroxide, Carbohydr. Res. 340 (6) (2005) 1143-1147.

[214] V.R. Shaumbwa, D. Liu, B. Archer, J. Li, F. Su, Preparation and Application of Magnetic Chitosan in Environmental Remediation and Other Fields: A Review, J. Appl. Polym. Sci. 138 (42) (2021) 51241.

[215] B. Li, D. Jia, Y. Zhou, Q. Hu, W. Cai, In Situ Hybridization to Chitosan/Magnetite Nanocomposite Induced by the Magnetic Field, J. Magn. Magn. Mater. 306 (2) (2006) 223-227.

[216] F. Yang, B. Yuan, Y. Wang, X. Chen, L. Wang, H. Zhang, Graphene Oxide/Chitosan Nano‐Coating with Ultrafast Fire‐Alarm Response and Flame‐Retardant Property, Polym. Adv. Technol. 33 (3) (2021) 795-803.

[217] X. Mu, J. Zhan, X. Feng, W. Cai, L. Song, Y. Hu, Exfoliation and Modification of Covalent Organic Frameworks by a Green One-Step Strategy: Enhanced Thermal, Mechanical and Flame Retardant Performances of Biopolymer Nanocomposite Film, Compos. Part A Appl. Sci. Manuf. 110 (2018) 162-171.

[218] J.R.A. Pires, V.G.L. Souza, L.A. Gomes, I.M. Coelhoso, M.H. Godinho, A.L. Fernando, Micro and Nanocellulose Extracted from Energy Crops as Reinforcement Agents in Chitosan Films, Ind. Crops. Prod. 186 (2022) 115247.

[219] H. Dai, N. Feng, J. Li, J. Zhang, W. Li, Chemiresistive Humidity Sensor Based on Chitosan/Zinc Oxide/Single-Walled Carbon Nanotube Composite Film, Sens. Actuators B Chem. 283 (2019) 786-792.

[220] S. Prateepchanachai, W. Thakhiew, S. Devahastin, S. Soponronnarit, Mechanical Properties Improvement of Chitosan Films Via the Use of Plasticizer, Charge Modifying Agent and Film Solution Homogenization, Carbohydr. Polym. 174 (2017) 253-261.

[221] S. B. Aziz, Investigation of Metallic Silver Nanoparticles through UV-Vis and Optical Micrograph Techniques, Int. J. Electrochem. Sci. 12 (2017) 363-373.

[222] C. Choi, S. Kim, P. Pak, D. Yoo, Y. Chung, Effect of N-Acylation on Structure and Properties of

Chitosan Fibers, Carbohydr. Polym. 68 (1) (2007) 122-127.

[223] F. Göktepe, S.Ü. Çelik, A. Bozkurt, Preparation and the Proton Conductivity of Chitosan/Poly(vinyl phosphonic acid) Complex Polymer Electrolytes, J. Non. Cryst. Solids 354 (30) (2008) 3637-3642.

[224] S.C. Dey, M.A.-Amin. T.U. Rashid, M.Z. Sultan, M. Ashaduzzaman, M. Sarker, S. M. Shamsuddin, Preparation Characterization and Performance Evaluation of Chitosan as an Adsorbent for Remazol Red, Int. J. Latest Eng. Res. Appl. 2 (2) (2016) 52-62.

[225] S. Saber-Samandari, O. Yilmaz, E. Yilmaz, Photoinduced Graft Copolymerization onto Chitosan under Heterogeneous Conditions, J. Macromol. Sci. A 49 (7) (2012) 591-598.

[226] M. Jaipal Reddy, P.P. Chu, Ion Pair Formation and Its Effect in Peo:Mg Solid Polymer Electrolyte System, J. Power Sources 109 (2) (2002) 340-346.

[227] S.B. Aziz, Z.H.Z. Abidin, Electrical Conduction Mechanism in Solid Polymer Electrolytes: New Concepts to Arrhenius Equation, Soft. Matter. 2013 (2013) 1-8.

[228] P.-L. Kuo, W.-J. Liang, T.-Y. Chen, Solid Polymer Electrolytes V: Microstructure and Ionic Conductivity of Epoxide-Crosslinked Polyether Networks Doped with $LiClO_4$, Polymer 44 (10) (2003) 2957-2964.

[229] S.M. Costa, D.P. Ferreira, P. Teixeira, L.F. Ballesteros, J.A. Teixeira, R. Fangueiro, Active Natural-Based Films for Food Packaging Applications: The Combined Effect of Chitosan and Nanocellulose, Int. J. Biol. Macromol. 177 (2021) 241-251.

[230] K. Okada, M. Nakanome, Y. Kameshima, T. Isobe, A. Nakajima, Water Vapor Adsorption of $CaCl_2$-Impregnated Activated Carbon, Mater. Res. Bull. 45 (11) (2010) 1549-1553.

[231] Y. Wang, G. Chen, F. Yang, Z. Luo, B. Yuan, X. Chen, L. Wang, Serendipity Discovery of Fire Early Warning Function of Chitosan Film, Carbohydr. Polym. 277 (2022) 118884.

[232] S.C. Chie, M.K.A. Wahab, Morphology and Biodegradability of Microcrystalline Cellulose / Chitosan Films, IOP Conference Series: Materials Science and Engineering 701 (1) (2019) 012053.

[233] X. Qu, A. Wirsén, A.C. Albertsson, Novel PH-Sensitive Chitosan Hydrogels: Swelling Behavior and States of Water, Polymer 41 (12) (2000) 4589-4598.

[234] S.B. Aziz, Z.H.Z. Abidin, M.F.Z. Kadir, Innovative Method to Avoid the Reduction of Silver Ions to Silver Nanoparticles (Ag^+ - Ag^o) in Silver Ion Conducting Based Polymer Electrolytes, Phys. Scr.

90 (3) (2015) 035808.

[235] S.B. Aziz, Z.H.Z. Abidin, A.K. Arof, Effect of Silver Nanoparticles on the DC Conductivity in Chitosan-Silver Triflate Polymer Electrolyte, Physica B: Condensed Matter 405 (21) (2010) 4429-4433.

[236] X.Y. Dong, J.H. Wang, S.S. Liu, Z. Han, Q.J. Tang, F.F. Li, S.Q. Zang, Synergy between Isomorphous Acid and Basic Metal-Organic Frameworks for Anhydrous Proton Conduction of Low-Cost Hybrid Membranes at High Temperatures, ACS Appl. Mater. Interfaces 10 (44) (2018) 38209-38216.

[237] E. Prokhorov, G. Luna-Bárcenas, J.B. González-Campos, Y. Kovalenko, Z.Y. García-Carvajal, J. Mota-Morales, Proton Conductivity and Relaxation Properties of Chitosan-Acetate Films, Electrochim. Acta 215 (2016) 600-608.

[238] M. Wu, X. Zhang, Y. Zhao, C. Yang, S. Jing, Q. Wu, A. Brozena, J.T. Miller, N.J. Libretto, T. Wu, S. Bhattacharyya, M.N. Garaga, Y. Zhang, Y. Qi, S.G. Greenbaum, R.M. Briber, Y. Yan, L. Hu, A High-Performance Hydroxide Exchange Membrane Enabled by Cu^{2+}-Crosslinked Chitosan, Nat. Nanotechnol. 17 (6) (2022) 629-636.

[239] Z. Duan, Q. Zhao, S. Wang, Q. Huang, Z. Yuan, Y. Zhang, Y. Jiang, H. Tai, Halloysite Nanotubes: Natural, Environmental-Friendly and Low-Cost Nanomaterials for High-Performance Humidity Sensor, Sens. Actuators B Chem. 317 (2020).

[240] H. Ding, X. Liang, Q. Wang, M. Wang, Z. Li, G. Sun, A Semi-Interpenetrating Network Ionic Composite Hydrogel with Low Modulus, Fast Self-Recoverability and High Conductivity as Flexible Sensor, Carbohydr. Polym. 248 (2020) 116797.